"PLURONIC POLYMER FUNCTIONALIZED POLYMERIC NANOPARTICLES LOADED CAPECITABINE AND THYMOQUINONE FOR TARGETING COLORECTAL CANCER: AN EXPERIMENTAL STUDY"

Thesis Submitted to

The KLE Academy of Higher Education and Research, Belagavi

(Deemed-to-be -University)

[Declared as Deemed-to-be-University u/s 3 of the UGC Act, 1956 vide Govt. of India Notification No.F.9-19/2000-U.3 (A)]

(Accredited 'A++' Grade by NAAC) (3rd Cycle)

[Placed in Category 'A' by MoE (GoI)]

For the award of the degree of Doctor of Philosophy in the Faculty of Pharmacy

By

Ms. Prasiddhi R. Raikar M. Pharm.

(Registration No: KLEU/Ph.D./19-20/DO1219015)

Under the Guidance of

Prof. (Dr.) Panchaxari M. Dandagi Ph.D.

Professor,

KLE COLLEGE OF PHARMACY BELAGAVI

KLE ACADEMY OF HIGHER EDUCATION AND RESEARCH

BELAGAVI – 590010

2023

UNDERTAKING

I, **Ms. Prasiddhi R. Raikar** hereby declare that the information and the data mentioned in my thesis entitled **"Pluronic Polymer functionalized polymeric nanoparticles loaded Capecitabine and Thymoquinone for targeting colorectal cancer: an experimental study"** belongs to me and is original.

I am aware of the definition of plagiarism as detailed below:

- An act or instance of using or closely imitating the language and thoughts of another author without authorization and the representation of that author's work as one's own, as by not crediting the original author.
- A piece of writing or other work reflecting such unauthorized use or imitation.
- The deliberate or reckless representation of another's words, thoughts or ideas as one's own without attribution in connection with submission of academic work, whether graded or otherwise.

I hereby declare that the thesis prepared by me is original-one and does not involve plagiarism anywhere. In case at a later stage it is found that I have indulged in plagiarism, then I am solely responsible for the same and the Institution is at liberty to take any disciplinary action against me including cancellation of dissertation or any other penalties imposed by the University.

Place: Belagavi
Date: 09/11/23

Signature
Ms. Prasiddhi R. Raikar
Full Time Ph.D. Research Scholar
Reg. No: DO1219015
KAHER Belagavi - 590010

PLAGIARISM CERTIFICATE

KLE ACADEMY OF HIGHER EDUCATION AND RESEARCH
(Formerly known as KLE University)
(Deemed-to-be-University established u/s 3 of the UGC Act, 1956)
Accredited 'A' Grade by NAAC (3rd Cycle) Placed in Category '1' by MoE (GoI)
JNMC Campus, Nehru Nagar, Belagavi-590 010, Karnataka State, India
☎: 0831-2444444 Web: http://www.kledeemeduniversity.edu.in E-mail: info@kledeemeduniversity.edu.in

Ref. No. KAHER/AA/23-24/D- 377 25th September 2023

Madam,

The soft copy of Ph.D. research thesis of **Ms. Prasiddhi R Raikar, Faculty of Pharmacy, KAHER, Belagavi** has been submitted for anti-plagiarism check at the office of the undersigned through "Turn-it-in" package. The scan has been carried out and the scanned output reveals a match percentage of **4%** which is within the acceptable limit of 10%.

To obtain the comprehensive report of the plagiarism test, research scholar can send a mail to **diracademic@kledeemeduniversity.edu.in** along with the Registration Number, Name of the Scholar, Name of Guide/Co-guide and title of the thesis.

DIRECTOR ACADEMIC AFFAIRS Deemed-to-be University

Dr.(Mrs.) Roopa M. Bellad
Director, Academic Affairs

To,

Ms. Prasiddhi R. Raikar
Full-Time Ph.D. Scholar,
2019-20 Batch
KLE College of Pharmacy,
Faculty of Pharmacy, KAHER
Belagavi.

Cc to :

1. The Principal, KLE College of Pharmacy, Belagavi
2. Dr. P. M. Dandagi, Professor, KLE College of Pharmacy, KAHER, Belagavi - Guide

KLE ACADEMY OF HIGHER EDUCATION AND RESEARCH

(Deemed-to-be-University)

[Declared as Deemed-to-be-University u/s 3 of the UGC Act, 1956 vide Govt. of India Notification No.F.9-19/2000-U.3 (A)]

(Accredited 'A^{+}' Grade by NAAC) (3rd Cycle)

[Placed in Category 'A' by MoE (GoI)]

Copyright Declaration

We hereby declare that **KLE ACADEMY OF HIGHER EDUCATION AND RESEARCH, BELAGAVI, KARNATAKA,** *shall have the rights to preserve, use and disseminate this thesis in print or electronic format for academic/research purpose.*

Signature

Ms. Prasiddhi R. Raikar

Full Time Ph.D. Research Scholar

Reg. No: DO1219015

KAHER Belagavi - 590010

Place: Belagavi

Date: 09/11/23

Signature

Prof. (Dr.) Panchaxari M. Dandagi

Professor, KLE College of Pharmacy

KAHER, Belagavi – 590010

Place: Belagavi

Date: 09/11/23

KLE ACADEMY OF HIGHER EDUCATION AND RESEARCH

(Deemed-to-be-University)

[Declared as Deemed-to-be-University u/s 3 of the UGC Act, 1956 vide Govt. of India Notification No.F.9-19/2000-U.3 (A)]

(Accredited 'A^{+}' Grade by NAAC) (3rd Cycle)

[Placed in Category 'A' by MoE (GoI)]

KLE
EMPOWERING PROFESSIONALS

Declaration

I hereby declare that the thesis entitled **"PLURONIC POLYMER FUNCTIONALIZED POLYMERIC NANOPARTICLES LOADED CAPECITABINE AND THYMOQUINONE FOR TARGETING COLORECTAL CANCER: AN EXPERIMENTAL STUDY"** is a bonafide and original research carried out by me under the guidance of **Prof. (Dr.) Panchaxari M. Dandagi,** *Professor, KLE College of Pharmacy, Belagavi- 590010. The thesis or any part thereof has not formed the basis for the award of any degree/fellowship or similar title to any candidate of any University.*

Place: Belagavi
Date: 09/11/23

Signature
Ms. Prasiddhi R. Raikar
Full Time Ph.D. Research Scholar
Reg. No: DO1219015
KAHER Belagavi - 590010

KLE ACADEMY OF HIGHER EDUCATION AND RESEARCH

(Deemed-to-be-University)

[Declared as Deemed-to-be-University u/s 3 of the UGC Act, 1956 vide Govt. of India Notification No.F.9-19/2000-U.3 (A)]

(Accredited 'A^{+}' Grade by NAAC) (3rd Cycle)

[Placed in Category 'A' by MoE (GoI)]

KLE
EMPOWERING PROFESSIONALS

Certificate

This is to certify that the thesis entitled **"PLURONIC POLYMER FUNCTIONALIZED POLYMERIC NANOPARTICLES LOADED CAPECITABINE AND THYMOQUINONE FOR TARGETING COLORECTAL CANCER: AN EXPERIMENTAL STUDY"** is a bonafide and genuine research carried out by **Ms. Prasiddhi R. Raikar** under the guidance of **Prof. (Dr.) Panchaxari M. Dandagi,** *Professor, KLE College of Pharmacy, Belagavi- 590010.*

Place: Belagavi
Date: 09/11/23

Signature
Prof. (Dr.) M. S. Ganachari
Dean - Faculty of Pharmacy
KAHER, Belagavi - 590010

KLE ACADEMY OF HIGHER EDUCATION AND RESEARCH

(Deemed-to-be-University)

[Declared as Deemed-to-be-University u/s 3 of the UGC Act, 1956 vide Govt. of India Notification No.F.9-19/2000-U.3 (A)]

(Accredited 'A^{+}' Grade by NAAC) (3rd Cycle)

[Placed in Category 'A' by MoE (GoI)]

KLE

EMPOWERING PROFESSIONALS

Certificate

This is to certify that the thesis entitled **"PLURONIC POLYMER FUNCTIONALIZED POLYMERIC NANOPARTICLES LOADED CAPECITABINE AND THYMOQUINONE FOR TARGETING COLORECTAL CANCER: AN EXPERIMENTAL STUDY"** is a bonafide and genuine research carried out by **Ms. Prasiddhi R. Raikar** under the guidance of **Prof. (Dr.) Panchaxari M. Dandagi,** *Professor, KLE College of Pharmacy, Belagavi- 590010.*

Place: Belagavi

Date:

Signature

Prof. (Dr.) Sunil S. Jalalpure

Principal,

KLE College of Pharmacy,

KAHER, Belagavi, Karnataka

KLE ACADEMY OF HIGHER EDUCATION AND RESEARCH

(Deemed-to-be-University)

[Declared as Deemed-to-be-University u/s 3 of the UGC Act, 1956 vide Govt. of India Notification No.F.9-19/2000-U.3 (A)]

(Accredited 'A^{+}' Grade by NAAC) (3rd Cycle)

[Placed in Category 'A' by MoE (GoI)]

KLE
EMPOWERING PROFESSIONALS

Certificate

This is to certify that the thesis entitled **"PLURONIC POLYMER FUNCTIONALIZED POLYMERIC NANOPARTICLES LOADED CAPECITABINE AND THYMOQUINONE FOR TARGETING COLORECTAL CANCER: AN EXPERIMENTAL STUDY"** is a bonafide record of original research carried out by **Ms. Prasiddhi R. Raikar** under the guidance of **Prof. (Dr.) Panchaxari M. Dandagi,** *Professor, KLE College of Pharmacy, Belagavi- 590010.*

Place: Belagavi

Date: 09/11/23

Signature Guide P. M. Dandagi

Prof. (Dr.) Panchaxari M. Dandagi

Professor, KLE College of Pharmacy

KAHER, Belagavi - 590010

ACKNOWLEDGMENT

I would like to thank the great almighty, my Kamakshi Aai, who is everything to me, and all the people whose blessings, unceasing love, and enthusiasm kept my vision alive throughout this fantastic Ph.D. journey.

First and foremost, I would like to convey my heartfelt gratitude and appreciation to my research mentor, (Prof.) Dr. Panchaxari M. Dandagi, for his persistent advice and cooperation during my dissertation study. From the initial stages of refining my research proposal to the final submission of my thesis, his unwavering presence and wealth of wisdom have been instrumental in shaping my academic growth. I couldn't have asked for a greater advisor and mentor for my doctoral studies. I am grateful to him for believing in me and pointing me in the proper direction when I most needed it.

I am deeply indebted to our Chancellor Dr. Prabhakar B. Kore and Vice-Chancellor Prof. (Dr.) Nitin Gangane for giving me an opportunity and providing state-of-the-art facilities to join and complete the Ph.D. course as Full Time research scholar. Also, I am deeply grateful to our Honorable Principal Prof. (Dr.) Sunil Jalalpure and Prof. (Dr.) Rajashree Masareddy, HOD of pharmaceutical sciences, KLE Academy of Higher Education and Research, Belagavi, for being available to help whenever needed.

I appreciate the generous support from the KLE Academy of Higher Education and Research, Belagavi for funding my research and my deep sense of gratitude to the entire staff at KLE College of Pharmacy, Belagavi, and Dr. Prabhakar Kore Basic Science Research Center for providing all necessary support required during study.

I would like to offer my heartfelt appreciation to Dr. Daksha Dixit, previous Director of Academic Affairs, and esteemed Director of Academic Affairs, Dr. Roopa Bellad for their valuable support. I would like to extend my sincere thanks to Prof. (Dr.) Ramesh Paranjape, for sharing his knowledge and expertise, and for helping me brainstorm and troubleshoot when I encountered challenges.

A special thanks to Mrs. Swati Samuel for all of her assistance and support during my PhD tenure. A special appreciation goes to my colleagues *and juniors who have guided and supported me since the beginning of my research. Mr. Taufik Kazi, Ms. Shivani Tendulkar, Mr. Tukaram Kedar, and Dr. Niraj Gokhale for their valuable support.*

I want to express my deepest gratitude to my loving husband, Mr. Gautam Naik for always being my rock, and accompanying me through the highs and lows of this academic journey. I would also like to thank my in-laws, who have been my biggest cheerleader throughout this journey, and I cannot thank you enough for your love and support.

Lastly, I express my immense gratitude and love to my greatest source of inspiration, my Parents and family whose encouragement played an integral role in my accomplishments. To my mom, dad, and sister: Thank you for everything. I dedicate this PhD thesis to you.

Place: Belagavi
Date:

Signature
Ms. Prasiddhi R. Raikar
Full Time Ph.D. Research Scholar
Reg. No: DO1219015
KAHER Belagavi - 590010

LIST OF ABBREVIATIONS USED

AA	:	Anisamide
ACF	:	Aberrant crypt foci
ANOVA	:	Analysis of variance
BBD	:	Box-Behnken Design
CAP	:	Capecitabine
CO_2	:	Carbon-dioxide
CPCSEA	:	The Committee for the Purpose of Control and Supervision of Experiments on Animals
CRC	:	Colorectal cancer
CTDDS	:	Colon Targeted Drug Delivery System
DAPI	:	4',6-Diamidino-2-phenylindole
DCF	:	Dichlorofluorescein
DCFH-DA	:	Dichloro-dihydro-fluorescein
DLS	:	Dynamic light scattering
DMEM	:	Dulbecco's Modified Eagle Medium
DMH	:	Dimethyl hydrazine
DNA	:	Deoxyribonucleic acid
DSC	:	Differential scanning calorimetry
EE	:	Entrapment efficiency
EGF	:	Epidermal growth factor
EO	:	Ethylene oxide
Eud-CAP-TQ-Gal-PLGANP	:	Eudragit-Coated Capecitabine and Thymoquinone loaded galactosylated PLGA nanoparticle
FBS	:	Fetal bovine serum

Gal-PLGA	:	Galactosylated PLGA
GC	:	Galactosylated Chitosan
GI_{50}	:	Half-maximal growth inhibitory concentration
HLB	:	Hydrophilic lipophilic balance
H-NMR	:	Proton Nuclear Magnetic Resonance spectroscopy
IAEC	:	Institutional Animal Ethics Committee
IC_{50}	:	Half maximal inhibitory concentration
KBR	:	Potassium bromide
kV	:	Kilovolts
LOD	:	Limit of Detection
LOQ	:	Limit of Quantification
LV	:	Leucovorin
Mg	:	Milligram
mL	:	Milliliter
MLT	:	Melatonin
mm	:	millimeter
MMP	:	Mitochondrial membrane potential
MP	:	Macrophage
MTD	:	Maximum tolerated dose
NaOH	:	Sodium hydroxide
NF	:	Nanoformulation
nm	:	Nanometer
NP	:	Nanoparticle
OECD	:	Organization for Economic Cooperation and Development
P	:	Probability

PALS	:	Phase analysis light scattering
PBS	:	Phosphate buffer
PDI	:	Polydispersity index
PEG	:	Polyethylene glycol
PFC	:	Perfluorocarbon
PF-127	:	Pluronic F-127
PLA	:	Polylactide
PLGA	:	Poly Lactic-co-Glycolic Acid
PNP	:	Polymeric nanoparticle
PO	:	Propylene oxide
PS	:	Particle size
PVA	:	Polyvinyl alcohol
RES	:	Reticuloendothelial system
RNA	:	Ribonucleic acid
ROS	:	Reactive oxygen species
RP-HPLC	:	Reverse phase High-performance liquid chromatography
RSD	:	Relative standard deviation
R2	:	Correlation coeffient
SD	:	Standard deviation
SEM	:	Scanning electron microscope
TEM	:	Transmission electron microscope
T-NF	:	Targeted Nanoformulation
NT-NF	:	Non-Targeted Nanoformulation
TQ	:	Thymoquinone
UV	:	Ultraviolet

w/v	:	Weight by volume
ZP	:	Zeta potential
5-DFUR	:	5′-Deoxy-5-fluorouridine
5-FDUMP	:	5-Fluoro-2-deoxyuridine monophosphate
5-FU	:	5- Fluorouracil
5-FUTP	:	5- Fuorouridine triphosphate
µg	:	Microgram
µL	:	Microliter
µm	:	Micrometer
°C	:	Degree Celsius
%	:	Percent
<	:	Less than
>	:	Greater than

ABSTRACT

Colorectal cancer (CRC), often known as colon cancer, typically originates as a benign polyp in the colon or rectum and spreads slowly over 10–20 years. About 9.4% of cancer-related deaths in 2020 were caused by CRC. Survival rates from CRC are significantly affected by both recurrence and metastasis. In systemic therapy, the problem of non-targeted drug dispersion is of paramount importance. The main worries and key grounds for chemotherapy failure are side effects and resistance to medicines, both of which are caused by this lack of specificity. To tackle these challenges, polymeric nanoparticles (PNP) were developed as transporter devices for CRC therapy, with the ability to encapsulate diverse medications, shield therapeutic molecules, and give numerous advantages above their counterparts in bulk. To the extent of our information this is the first work to demonstrate that functionalized Polymeric nanoparticle loaded CAP and TQ can effectively be used as a synergistic combination to induce apoptosis, which could be used to kill off cancer cells.

Aim

This research aims to formulate a Nano-based drug delivery system targeting colorectal cancer. The objectives of the study are:

1. To formulate, optimize, and evaluate pluronic polymer functionalized nanocarrier system loaded Capecitabine and Thymoquinone.
2. To assess the anticancer activity of optimized formulation by conducting *in vitro and in vivo* studies.

Methodology

To begin, polymer functionalization was used to synthesize galactosylated PLGA. Then, using the double emulsion solvent evaporation process, CAP and TQ-loaded Galactosylated PLGA NP were created. Eudragit-S100 was employed as a coating polymer to deliver the medicine to the desired spot at the appropriate pH. Optimization was done using Design-Expert® software utilizing Box-Behnken design. Entrapment efficiency, particle size, shape, and zeta potential were all measured for the developed PNP. The optimized coated nanoformulation was tested in vitro for drug release and cell culture investigations were carried out on Targeted nanoformulation (T-NF) in comparison to Non-targeted nanoformulation (NT-NF) and pure CAP+TQ utilizing HT- 29 Colorectal cancer cell lines. Cytocompatibility, cytotoxicity, and cell uptake studies were carried out. T-NF was tested in vivo for pharmacological effect in DMH-induced colorectal cancer-bearing male Wistar rats.

Results

The spherical-shaped nanoparticles optimized (PNP9) batch had a mean particle size (PS) and zeta potential (ZP) of 161nm and +47.30 mV, respectively. After coating with Eudragit S-100 the PS and ZP changed to 183 nm and -25.2 mV respectively. The effectiveness of CAP and TQ entrapped inside the PNP was 84.92% and 87.01%, respectively. Eudragit-coated NP showed no drug release in an acidic medium whereas uncoated drug-loaded NP began to release the drug in the same. T-NF (Eud-coated CAP and TQ-loaded Galactosylated PLGANP) showed better anticancer activity in HT-29 cell lines compared to non-targeted nanoformulation (Eud-coated CAP and TQ-loaded PLGANP). At a concentration of 3.125µg/mL, the T-NF exhibited a cell survival rate of 57%, while NT-NF and pure CAP+TQ demonstrated comparable efficacy with survival rates of 64% and 75% respectively.

When compared to the control (non-treated) a pharmacodynamic examination demonstrated a significant reduction in tumor growth and a considerable gain in body weight in T-NF-treated-CRC-bearing male Wistar rats. Histopathological study of cancer tissues from male Wistar rats revealed a substantial decrease in aberrant crypt foci in the same after treatment with T-NF. The findings of in vitro and in vivo experiments suggest that Eudragit-coated CAP and TQ-loaded Galactosylated-PLGANP is a potential drug delivery technology for CRC treatment by oral administration.

Conclusion

These findings indicated that the developed Targeted Nano delivery can effectively target colon cancer. Fundamentally, the application of an intricately crafted PNP system exhibits substantial potential in the domain of averting and managing CRC through the utilization of TQ, which has demonstrated encouraging synergistic outcomes with CAP.

Keywords: Capecitabine; Thymoquinone; Colorectal cancer; PLGA; Polymeric nanoparticles; Galactosylation; Eudragit; Targeted Nanoformulation

TABLE OF CONTENTS

Sl. No.	Particulars	Page No.
1.	**INTRODUCTION**	**1-24**
1.1	Background	
1.2	Literature Review	
1.3	Justification	
1.4	Objective and Plan of work	
2.	**MATERIAL AND METHODS**	**25-39**
3.	**STATISTICAL ANALYSIS**	**40**
4.	**RESULTS**	**41-71**
5.	**DISCUSSION**	**72-82**
6.	**SUMMARY**	**83-84**
7.	**CONCLUSION**	**85-86**
8.	**BIBLIOGRAPHY**	**87-97**
9.	**ANNEXURES**	**98-153**
	a. Animal Ethical Clearance letter	
	b. Publications and Poster Certificates	

LIST OF TABLES

Sl. No.	Particulars	Page No.
1	List of Equipment, Instruments, and Devices used	**25**
2	List of Chemicals, API's, Reagents, Polymers and solvents used	**26**
3	The Protocol for the in-vivo anticancer research	**39**
4	CAP-TQ-Gal-PLGANP's Box-Behnken experimental runs	**45**
5	ANOVA table for Responses 1 and 2	**48**
6	PS, PDI, and ZP values of coated and uncoated NF	**51**
7	Histological findings score	**70**

LIST OF FIGURES

Sl. No.	Particulars	Page No.
1	Chemical structure of Thymoquinone	**4**
2	Thymoquinone's Biological Effects	**5**
3	Chemical structure of Capecitabine	**7**
4	Chemical structure of Pluronic	**12**
5	NP delivery systems via passive and active targeting	**14**
6	Polymeric Nanoparticle Preparation Strategies	**16**
7	Medical applications of PNP	**16**
8	UV–Vis isosbestic absorption spectra	**42**
9	CAP and TQ HPLC chromatograms in methanolic (A) and PNP (B)	**42**
10	Capecitabine (CAP) and Thymoquinone (TQ) chromatogram linearity	**43**
11	Spectra via H-NMR of Gal-PLGA	**44**
12	Perbutation plots demonstrating the effects of independent factors on responses; A: particle size, B: entrapment efficiency(CAP) C: entrapment efficiency(TQ)	**49**
13	Contour plots showing the desirability of factor optimization	**50**
14	Optimized PNP9's particle size distribution (A) and ZP (B)	**51**
15	FTIR spectra: CAP (A), TQ (B), PF-127 (C), Gal-PLGA (D) and CAP-TQ-Gal-PLGANP (E)	**53**

16	DSC thermograms: CAP, TQ, PF-127, Gal-PLGA and Eud-CAP-TQ-Gal-PLGANP	**54**
17	TEM and SEM study of coated and uncoated nanoformulation	**55**
18	Drug release characteristics of coated and uncoated nanoformulation in vitro	**56**
19	Stability data of Eudragit S100 coated CAP and TQ loaded Galactosylated PLGANP	**57**
20	HT-29 cell cytotoxicity when exposed to pure drug CAP+TQ, Non-targeted NF, Targeted NF, Pure CAP, pure TQ, and doxorubicin; significant levels of probability are defined as follows: p*, p$, p# <.05; p**, p$$, p## <.01 and p***, p$$$, p## < .001 across groups	**58**
21	ROS study demonstrating effect in pure CAP+TQ, targeted and non-targeted nanoformulation; p$<.05, p** <.01, p## <.001	**59**
22	MMP study of pure CAP+TQ, targeted and non-targeted nanoformulation; p$$<.01, p** <.01, p## <.001	**60**
23	Caspase-3-expression of pure CAP+TQ, targeted and non-targeted nanoformulation; p$$<.01, p*** <.001, p### <.001	**61**
24	DAPI assay where condensed chromatin and nuclear attrition/fragmentation are shown by the direction of the arrow; blebbed nuclei and apoptotic bodies are depicted by circles in respective groups	**62**
25	Apoptosis study in pure CAP+TQ, targeted and non-targeted NF; p$$$<.001, p*** <.001, p### <.001	**63**

26	Dissected rat colon of (A) normal control, (B) CRC-induced, (C) treated with targeted nanoformulation, (D) treated with non-targeted nanoformulation, (E) treated with marketed CAP tablet, and (F) dissected CRC-induced rat. Red Arrows represent tumors.	**65**
27	Normal crypts and ACF at 40× in the colonic mucosa, viewed topographically: (A) normal crypts, (B) DMH-treated, treated with (C) non-targeted nanoformulation (NT-NF), (D) targeted nanoformulation(T-NF), and (E) marketed CAP tablet	**66**
28	Wistar rat survival rates were evaluated in five groups: (i) normal saline, DMH-induced CRC treated with (ii) non-targeted nanoformulation (NT), (iii) targeted nanoformulation (TN), (iv) commercialized CAP tablet, and (v) comparison with published data	**67**
29	Images showing characteristics of hematoxylin and eosin staining of cancer tissues from the male Wistar rat CRC model in (A) normal control, (B) CRC-induced where yellow, (C) treated with targeted nanoformulation, (D) treated with non-targeted nanoformulation, (E) treated with marketed CAP tablet. Arrows represent: lymphnode metastasis (White); lymphoid follicles (Black); high-grade dysplasia (Yellow); ACF (Orange); mucosal ulcers (Blue)	**69**
30	Hematological parameters measured before and after treatment; p*** <.001(T-NF vs NT-NF), p### <.001(T-NF vs marketed CAP tablet), p$$$<.001(T-NF vs marketed CAP tablet)	**71**

1. INTRODUCTION

1.1 BACKGROUND

Colorectal cancer:

Colorectal cancer (CRC), often known as colon cancer, typically originates as a benign polyp in the colon or rectum and spreads slowly over 10–20 years to become the third most common and second deadliest form of the disease. About 9.4% of cancer-related deaths in 2020 were caused by CRC. Survival rates from CRC are significantly affected by both recurrence and metastasis. Chemotherapy persists as one of the frequently employed and effective approaches for managing CRC (1,2). In systemic therapy, the problem of non-targeted drug dispersion is of paramount importance. To attain therapeutic levels of an anticancer agent in cancer tissue, chemotherapy often results in widespread infection throughout the body. The main worries and key grounds for chemotherapy failure are side effects and resistance to medicines, both of which are caused by this lack of specificity (3).

To tackle these challenges, polymeric nanoparticles (PNPs), were developed as transporter devices for CRC therapy, with the ability to encapsulate diverse medications, shield therapeutic molecules, and give numerous advantages above their counterparts in bulk. Modern methods are focused on slowing down the removal process by modifying the nanocarrier surface by incorporating hydrophilic surface features, rendering them invisible to the reticuloendothelial system (RES) cells. These characteristics make polymeric NPs a potentially more attractive therapeutic option than standard cancer treatments (4). Improved in vivo navigation and extended release of anticancer drugs are two additional benefits of surface modification using targeted

ligands like Poly Lactic-co-Glycolic Acid (PLGA). For sustained drug administration with little nanoparticle (NP) bioaccumulation, certain amphiphilic polymers like poloxamer boast desirable functional properties such as biodegradability and hydrophilic/hydrophobic domains.

Given the propensity of numerous medications to exhibit dose-limiting toxicity or inadequate selectivity towards the intended organ or tissue, the administration of drugs poses a formidable challenge in the realm of clinical advancement. Given the remarkable ability of NPs to traverse blood vessels and cell membranes, it is evident that they possess considerable promise as carriers for therapeutic agents. To achieve both selectivity and efficiency, one may consider the prospect of designing moieties containing NP structures that possess the capacity to be duly recognized by proteins expressed within specific target cells. The incorporation of numerous pharmaceutical agents for synergistic treatment or a wide array of therapeutic approaches represents one of the myriad advantages stemming from the utilization of NP-based drug targeting (5).

Furthermore, the NPs for drug targeting not only enhance the therapeutic index of the drug but also encompass the myriad advantages associated with drug carrier systems. These advantages encompass the amalgamation of multiple drugs for combination therapy or diverse therapeutic modalities, meticulous administration of medication, the ability to accommodate hydrophobic drugs, safeguarding against drug degradation, and mitigating systemic toxicity by impeding the drugs' accessibility within the bloodstream. Henceforth, the principle research goal was to devise a novel form of NP possessing augmented targeting specificity towards colorectal cancer, employing the utilization of pluronic polymers. The study's hypotheses were substantiated by both in vitro and in vivo investigations.

THYMOQUINONE

The botanical specimen known as black cumin, scientifically referred to as Nigella sativa, harbors within its composition a phytochemical entity denoted as Thymoquinone (TQ), which is the abbreviated form of 2-methyl-5-isopropyl-1,4-benzoquinone, as visually represented in Figure 1. Throughout the annals of history, this particular molecular entity has been harnessed for its therapeutic properties, serving as a cornerstone in the realm of medicinal practices for countless generations. The compound known as TQ exhibits a plethora of remarkable attributes, including but not limited to its anti-oxidative, anti-inflammatory, hepatoprotective, neuroprotective, anti-carcinogenic, anti-ulcerative, and various other therapeutic properties (6). Through the stimulation of reactive oxygen species (ROS) generation, infliction of Deoxyribonucleic acid (DNA) harm, immunomodulation, regulation of signaling pathways, inhibition of nuclear factor kappa B (NF-B) activation, and initiation of autophagy, TQ effectively instigates apoptosis in malignant cells (7). The demonstrated properties of TQ encompass its anti-oxidant and chemopreventive attributes, which have been observed in normal cellular contexts. The observed similarities in the efficacy of TQ and 5-fluorouracil (5-FU) in terms of their cytotoxicity against SW-626 human colon cancer cells and their capacity to disrupt intercellular metabolic pathways are noteworthy. Moreover, it has been observed that TQ exhibits a propensity to augment the apoptotic efficacy of 5-FU in gastric cancer cells both in laboratory settings *in vitro* and *in vivo*. Upon subjecting the SK-OV-3 ovarian cancer cell line to rigorous examination, it was observed that the amalgamation of TQ, 5-FU, and epigallocatechin-3-gallate exhibited the most potent anticancer properties (8). The synergistic integration of TQ in a cell-line-specific fashion amplifies the anticancer potency of the

chemotherapeutic agent doxorubicin (9). The synergistic utilization of cisplatin and TQ has demonstrated remarkable efficacy in surmounting cisplatin resistance, particularly in the context of non-small cell lung cancer (NSCLC) cell lines and the mice xenograft model (10). The compound known as TQ exhibits a plethora of biological properties, including but not limited to its role as an antioxidant, antibacterial agent, anti-cancer agent, and nephroprotective agent (Figure 2).

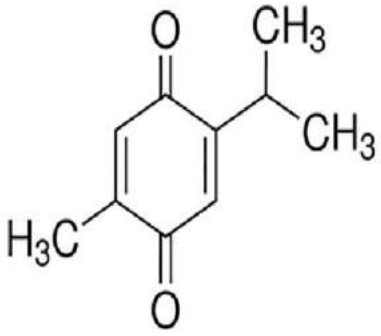

Figure 1: Chemical structure of Thymoquinone

The chemical properties of TQ and its limited ability to penetrate cellular membranes impose constraints on its potential utilization in human contexts. The hydrophobic nature of this chemical compound serves to diminish its solubility and bioavailability. A remarkable novel approach to the distribution of TQ has surfaced with the introduction of NPs; this particular strategy holds the promise of substantially enhancing bioavailability. The findings of the study revealed the presence of stability, enhanced bioavailability, and sustained anticancer efficacy in liposomes loaded with TQ, as well as in liposomes loaded with TQ and modified with Triton X-100 (11). The anti-proliferative, anti-inflammatory, and chemosensitizing properties of TQ are significantly enhanced when it is encapsulated within NPs, achieving an impressive efficiency rate of 97.5%. This encapsulation is achieved using a biodegradable nanoparticulate formulation that is

primarily composed of PLGA, a polymer, and is further stabilized with polyethylene glycol (PEG)-5000 (12). The synergistic potential of TQ in conjunction with other chemotherapeutic agents has been demonstrated to enhance its anticancer properties. Due to its limited solubility, susceptibility to thermal and photonic influences, as well as its diminished systemic bioavailability, the utilization of TQ in the realm of cancer therapy remains relatively infrequent. Nevertheless, this particular approach holds the potential to surmount the aforementioned impediments (13).

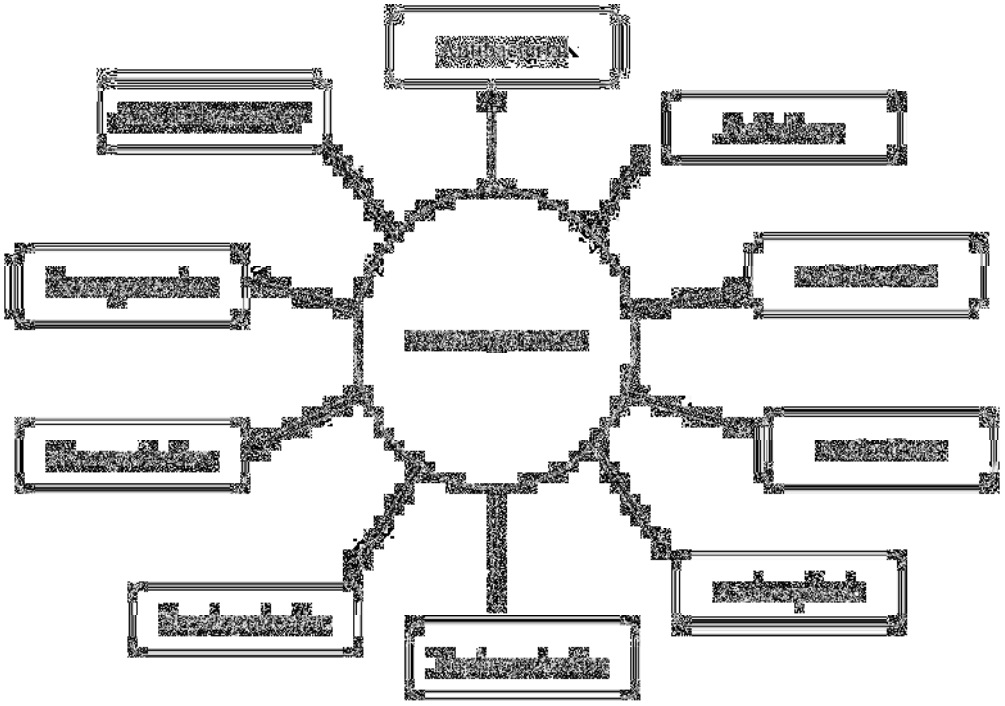

Figure 2: Thymoquinone's Biological Effects

CAPECITABINE

The anticancer agent Capecitabine (CAP), is a hydrophobic fluoropyrimidine carbamate (Figure 3). It functions as a precursor to both 5′-deoxy-5-fluorouridine (5′-DFUR) and 5-FU. It was devised and developed specifically to overcome some of 5-FU's deficiencies and to mimic the infusional administration of 5-FU without the complexity. After being taken in whole, CAP undergoes a series of enzymatic reactions to become its active metabolite. In addition to 5-fluoro-2-deoxyuridine monophosphate (FdUMP), 5-fluorouridine triphosphate (FUTP) is also an active metabolite of 5-fluorouridine. Thymidine phosphorylase, an enzyme necessary for the final step, has been demonstrated to be present in more concentrations in cancer tissue than in normal tissue, which might provide tumor selectivity (14). There are two potential mechanisms for cellular damage:

- The N5-10 methylenetetrahydrofolate, which serves as a vital cofactor for the enzymatic activity of thymidylate synthase, becomes covalently linked to the FdUMP molecule. This intricate mechanism impedes the transformation of uracil into thymidylate. Thymidylate plays an indispensable role in the process of DNA synthesis, as it undergoes a crucial conversion into thymidine triphosphate. The process of cell proliferation can indeed be effectively suppressed through strategic interference with the said procedure.

- The replacement of FUTP with uridine triphosphate in Ribonucleic acid (RNA) molecules induces a disturbance in the intricate processes of ribosomal and messenger RNA processing within the nucleus, thereby impeding cellular proliferation.

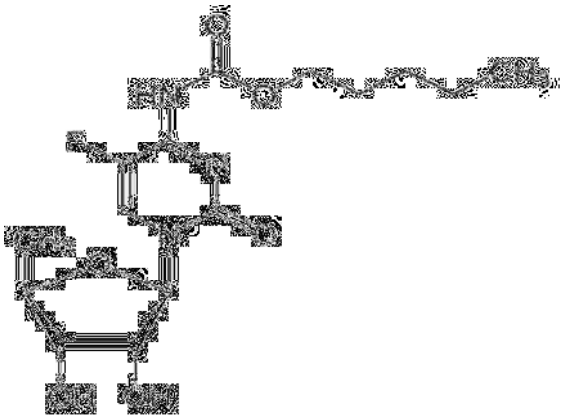

Figure 3: Chemical structure of Capecitabine

Furthermore, the aforementioned pharmaceutical substance has been duly sanctioned for administration as a solitary therapeutic agent in individuals afflicted with metastatic breast carcinoma, who have exhibited a diminished response to treatment regimens involving both anthracycline and paclitaxel. Additionally, it is authorized for employment in conjunction with docetaxel after an unsuccessful course of antecedent chemotherapy reliant on anthracycline. Patients diagnosed with prostate, pancreatic, renal cell, and ovarian cancer have also experienced favorable outcomes through the utilization of both single-agent and combination therapeutic regimens. This is primarily attributed to its enhanced tolerability and comparable efficacy when compared to the conventional combination of FU/leucovorin (LV) and its oral administration route. Nevertheless, to maintain the desired concentration, it is imperative to administer a high dosage of 1250 mg/m2 b.i.d., owing to the compound's notably brief half-life of 0.51 hours. Frequently, it becomes imperative to interrupt the course of treatment owing to the emergence of side effects stemming from the administration of a substantial dosage, including but not limited to dermatitis and hand-foot syndrome (15,16). The strategies elucidated in the research will enable you to surmount these challenges.

Colon-targeted drug delivery system (CTDDS)

The utilization of the colon as a means for the administration of medication can be employed for either local or systemic purposes. Nevertheless, it is plausible to mitigate systemic adverse effects and enhance therapeutic efficacy through targeted administration of medications specifically to the colon. To safeguard the integrity of the bioactive agent until it reaches the colon, it is imperative for CTDDS to effectively impede the absorption of the drug within the stomach and small intestine. The controlled liberation and subsequent assimilation of the bioactive agent ought to transpire solely upon the attainment of the colonic region by the system. In recent times, there has been a notable surge in the significance attributed to oral colon-targeted drug delivery systems, which have emerged as a pivotal means of administering a diverse array of therapeutic medications (17,18).

When orally administered, medications are strategically directed towards the colon, thereby circumventing the processes of degradation and release that typically occur within the confines of the stomach and small intestine. Furthermore, it ensures the prompt or gradual dissemination of medication within the proximal region of the gastrointestinal tract. Numerous drug delivery systems have been devised, each exhibiting the capacity to administer a predetermined dosage of medication to the colon, subsequently initiating the controlled liberation of the therapeutic compound. Colonic microflora diligently synthesizes a multitude of intestinal enzymes, which are then strategically utilized to initiate the controlled liberation of medication at distinct junctures within the intricate gastrointestinal milieu. To liberate a pharmaceutical agent from its prodrug form, specific enzymes are employed to catalyze the hydrolysis of chemical linkages connecting an inactive carrier molecule

with the biologically active constituent (19,20).

Maximizing the proximity of the medication to the intended sites of physiological action, while ensuring its structural integrity, serves to mitigate the incidence of untoward secondary effects. Moreover, the potential to reduce the customary dosage represents merely one of the manifold therapeutic advantages associated with the targeted delivery of pharmaceutical agents to the colon. The utilization of prodrug synthesis, pH-responsive polymer coatings, biodegradable polymer coatings, polysaccharide-based formulations, sustained-release mechanisms, pressure-regulated drug delivery systems, and osmotic pressure-controlled systems exemplify a plethora of approaches and methodologies accessible to achieve targeted drug delivery to the colon (21,22). This investigation has primarily centered around two distinct methodologies: the prodrug strategy and the implementation of pH-sensitive polymer coatings. CAP is a prodrug necessitating conversion into its active moiety, 5FU. This approach, commonly referred to as the prodrug methodology, has already been expounded upon. The fabrication of coatings was achieved through the utilization of a polymer with pH-responsive properties, commonly referred to as Eudragit-S100. The utilization of a pH gradient spanning from the gastric region (1.5-3.5) to the duodenum (5.5-6.8) and subsequently extending to the colon (6.4-7.0) is being harnessed in this context. By encapsulating the pharmaceutical compound within the eudragit-S100 polymer, which exhibits selective degradation solely within the colonic region, the bioactive substance can be effectively conveyed to the colon while evading absorption within the proximal segments of the gastrointestinal tract (23–25).

Polymer functionalization (Galactosylation)

The biocompatibility and uptake efficiency of these nanotechnologies is believed to be primarily influenced by their physicochemical characteristics, including surface composition, superficial charge, size, and shape. Given the inherent modifiability of the physicochemical properties of NPs, it is plausible to assert that the surface of NPs can be subjected to functionalization processes. Such functionalization endeavors aim to enhance the biocompatibility of NPs and augment their efficiency in terms of cellular uptake. Given that the toxicity and absorption of NPs are significantly impacted by the surface composition of said NPs, it becomes evident that altering the surface of these particles presents a formidable approach to tackle these issues. Surface functionalization is a transformative procedure that enhances the suitability of NPs for medicinal applications. Various techniques exist for the modification of NP surfaces, encompassing both non-covalent and covalent conjugation methods (26,27). PEG and PLGA are widely recognized as two of the most prominent compounds employed for surface functionalization of NPs in both in vitro and in vivo applications. The synthesis of galactosylated PLGA NPs was conducted in a prior investigation to facilitate the oral administration of resveratrol. The findings of the study revealed a substantial enhancement in oral bioavailability upon administration, primarily attributed to the augmented permeability of these NPs within the intestinal region (28). The process of synthesizing galactosylated polymer entails the covalent linkage of D-galactose units to a polymer substrate, a chemical transformation commonly referred to as Galactosylation. The benefits of Galactosylation are outlined in further detail below (29).

- Directing the drug to a certain organ and boosting its biodistribution throughout the body.
- Facilitating increased transmembrane penetration.
- Lowering clearance rates and improving metabolic stability.
- The high specificity for target cells and the high productivity for standardization make this a promising strategy for cell-selective targeting.
- Keeping the drug's physicochemical qualities stable.
- Better solubility in water and mucoadhesion.
- Reduced systemic toxicity and cell compatibility
- Galactose-mediated endocytosis is used for delivering the medication.

Pluronics®

Poly (ethylene oxide) (PEO) and poly (propylene oxide) (PPO) block copolymers, colloquially referred to as Pluronic® and Poloxamers (Figure 4), exhibit amphiphilic properties and possess advantageous association and adsorption capabilities. One of the notable advantages conferred by these structures lies in their capacity to engage in interactions with hydrophobic substances and biological membranes. Due to its inherent low toxicity and the myriad of desirable physiological attributes, these substances prove to be highly advantageous across a diverse range of applications (30,31). Poloxamers of varying proportions of EO (x) to PO (y) moieties exhibit discernible HLB (hydrophilic-lipophilic balance) characteristics (32). Given the wide array of commercially accessible variants and the notable instances of regulatory endorsement for pharmaceutical utilization, formulators possess the capacity to

seamlessly transition from rudimentary investigative endeavors to the realm of therapeutic applications (33). The utilization of Pluronic F127 (PF-127) in the current experimental investigation stems from its status as a nonionic polymer surfactant that possesses both safety and efficacy. Due to its potential as a viable medium for the targeted transportation of therapeutic agents to combat a diverse array of ailments, it has garnered considerable attention (33). The benefits of poloxamer are as follows (34,35).

- Due to their amphiphilic architectures and surfactant behavior, they can increase the solubility of hydrophobic surfaces in water.
- In addition, compounds of varying hydrophobicity can be made more miscible.
- They are employed as suspension stabilizers, solubilizers for hydrophobic medications, and emulsifiers.
- These chemicals are not immunogenic and have a low toxicity profile.
- By altering the surface of hydrophobic drug carriers, "stealth" particles can be created that are undetectable by macrophages (MPs) and so extend the carriers' limited lifetime.

Figure 4: Chemical structure of Pluronic

POLYMERIC NANOPARTICLES (PNP)

Highly Porous NPs can be categorized based on their morphology, size, composition, and physicochemical attributes. While they are technically defined as having a size of less than 100 nm, it is worth noting that structures up to 300 nm in size are commonly encompassed within this classification. Polymers, being versatile macromolecules, can manifest in two distinct forms: natural or synthetic. These entities, in their essence, assume the guise of colloidal systems, thereby exhibiting intriguing properties and behaviors. In contrast to alternative nanocarriers such as liposomes, micelles, and inorganic nanosystems, they offer a plethora of advantageous attributes. The colloidal entities known as biodegradable PNPs encompass a genetic material of significance encapsulated within a biodegradable polymer matrix (36,37). These NPs are fashioned from biocompatible and biodegradable polymers such as PLGA or polylactide (PLA), both of which have obtained the sanction of the esteemed Food and Drug Administration (38).

PLGA represents a distinguished polyester copolymer synthesized through the amalgamation of polylactic acid and polyglycolic acid. Regarding the administration of pharmaceutical substances, it can be asserted that this particular biomaterial currently holds the most comprehensive and precise characterization within the existing market. PLGA has garnered considerable attention within the scientific community owing to its extensive investigation as a biodegradable copolymer (39,40). This copolymer, upon degradation, transforms into innocuous entities, namely water and carbon dioxide, which are naturally expelled from the human body. These mechanisms can impede the degradation of drug moieties,

thereby facilitating a more consistent and controlled release of the medication. Cytotoxicity may also be elicited by PLGA NPs, which, after endocytosis, localize within the lysosomes. Within this intracellular compartment, they have the potential to inflict harm upon the lysosomal membrane and incite its activation. The intricate networks of cellular communication govern the process of apoptosis (41,42).

There are numerous strategies available through which biodegradable PNPs can effectively accomplish anti-cancer targeting. This encompasses the intricate process of employing ligand-mediated targeting mechanisms, facilitating the transportation of therapeutic agents across the endothelial barrier to the tumor site, and subsequently administering them directly to the neoplastic cells within the circulatory system (43). Figure 5 exemplifies the significance of both passive and active targeting mechanisms in facilitating the efficient delivery of NPs to cancerous sites.

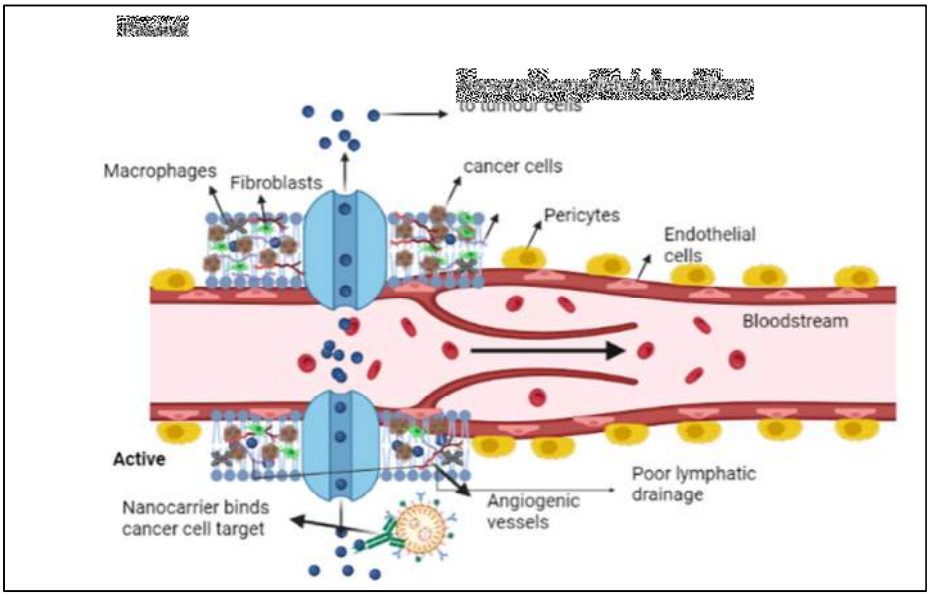

Figure 5: NP delivery systems via passive and active targeting

PNPs exhibit remarkable characteristics, such as exceptional stability in biological fluids, a wide array of available polymers, the potential for surface functionalization, and the ability to regulate polymer degradation and controlled release of encapsulated substances in response to various stimuli. In pursuit of augmenting the antitumor efficacy, inhibiting metastasis, and mitigating the effective dosage and untoward consequences, numerous chemotherapeutic agents have been integrated within polymeric delivery systems (44). The distinctive characteristics of biodegradable PNP systems include diminished systemic toxicity and a predilection for altering drug-release kinetics. These systems typically undergo fragmentation into oligomers and monomers before being metabolized and eliminated from the body through regular physiological pathways. The loading and entrapment efficiency (EE) of therapeutic agents within the NP core is influenced by various factors, including the properties of the drug and polymer, the choice of solvent, and the specific encapsulation process employed (45,46). Figure 6 exhibits a multitude of PNP preparatory methodologies, while Figure 7 elucidates the application of PNP within the realm of medicine.

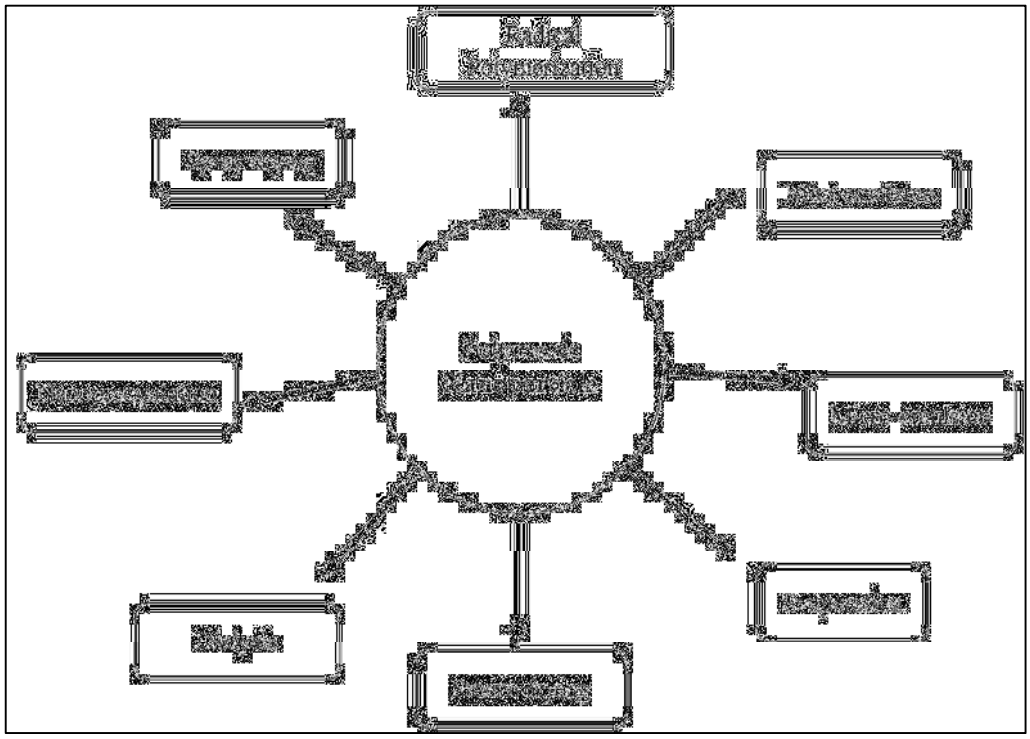

Figure 6: Polymeric Nanoparticle Preparation Strategies

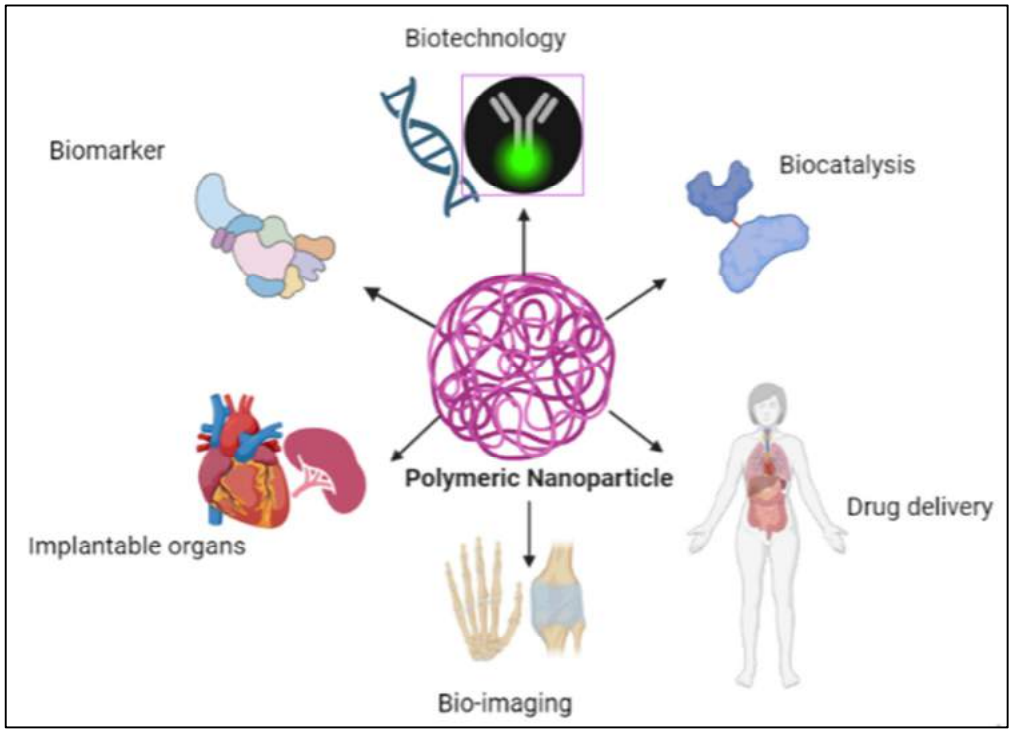

Figure 7: Medical applications of PNP

Biodegradable PNPs' advantages:

- Due to their high loading efficiency, increases their ability to target tumors.
- Increased antitumor efficacy is achieved through triggered release inside tumors.
- Also has a shielding effect, preventing the medications from being quickly cleared by the liver, kidney, and reticuloendothelial system.
- This keeps the pharmaceuticals stable and increases their specificity for their intended targets.
- Have superior biodegradability and biocompatibility to other drug delivery systems while also being non-toxic, non-immunogenic, easily synthesizable, inexpensive, water-soluble, and safe.
- With excellent stability, pinpoint accuracy, a large drug-carrying capacity, and the ability to modulate drug release.

1.2 LITERATURE REVIEW

Hirsch et al., (2011) focused on CAP for several off-label uses, such as in the treatment of rectal cancer as a neoadjuvant therapy and in the management of advanced or metastatic colorectal cancer. In sum, researchers found that CAP is a promising first step towards replacing infusion therapies with oral ones for CRC and other malignancies. Also examined current CRC screening and treatment methods, with a primary emphasis on the theranostic strategy of nanotechnology for CRC therapy along with its potential. The purpose of this review was twofold: first, to inform readers about the progress of nanotechnology in CRC, and second, to get them thinking about new methods of therapy that could make use of nanotechnology (47).

Thiruppathi et al., (2016) analysis revealed that Via surface modification, functionalization improves the qualities and attributes of NPs, allowing them to play a significant role in the medical area. High-contrast, high-quality functional pictures are essential for molecular imaging due to the importance of correct distinction. This paper looks at how functionalization improves molecular imaging and makes multimodal imaging possible, allowing for the creation of images that combine the capabilities of different imaging modalities. This also explains how functionalizing NPs with molecules enables them to specifically target the cells of interest through molecular-level interactions (26).

Chu et al., (2017) The biocompatibility and liver-targeting efficacy of SDF-1-loaded galactosylated chitosan (GC) NPs synthesized through the electro spraying method were tested. After injection, GC NPs accumulated significantly in liver tissue, demonstrating uniform distribution, strong biocompatibility, and a liver targeting

effect that hinted at the delivery system's potential (48).

Raikar et al., (2022) define pluronic as a medical polymer and provide a more in-depth discussion of the present pluronic drug delivery mechanisms. Based on pluronic formulations, this review also has explained the hydrophobic payload formulations and updated, tailored dispersion methods (35).

Zhang et al., (2016) looked into how TQ affects colon cancer cells and the underlying molecular mechanisms. Treatment with TQ dramatically lowered cell viability in COLO205 and HCT116 cells in a dose-dependent fashion, as measured by a Cell Counting Kit-8 test (49).

Odeh et al., (2018) examined the efficacy of TQ in conjunction with melatonin (MLT) against a mouse model of breast cancer. TQ and MLT together have a synergistic effect and potent anticancer action (13).

Ramzy et al., (2020) examined the task of fabricating polymeric nanocapsules, both anisamide (AA) conjugated and non-conjugated, that were loaded with TQ to specifically target colon cancer. Eudragit-S100 was employed in the synthesis process. The results demonstrated that (AA) conjugated nanocapsules exhibited a greater degree of cytotoxicity against HT-29 cells after a 48-hour incubation period, in comparison to the non-conjugated counterparts and free TQ inferring that the utilization of these nanocapsules could potentially enhance the efficacy of treatment (49).

Siu et al., (2018) To boost the bioavailability and pharmacological efficacy of Resveratrol (RES), the present study used nanocarriers in combination with ligand (galactose) anchoring for oral delivery. The bioavailability of galactosylated NP was

shown to be improved by their capacity to be taken up by cells and delivered into the enterocytes (50).

Wu et al., (2020) engineered PLGA NPs with epidermal growth factor (EGF) functionalization and co-loaded them with 5Fu and perfluorocarbon (PFC) to treat colon cancer selectively. Histopathological examination added further proof that EGF-targeted NPs slowed tumor development more effectively than conventional therapies. PFC's ability to bring oxygen to tumors is what allowed for the considerable improvement in treatment outcomes seen in this study (51).

Jenna et al., (2022) studied the delivery of Cap-loaded PLGA NPs in HT-29 cell lines boosting anticancer activity. Increased bioavailability and markedly increased cytotoxic capability were seen in the optimized PLGA-based NPs compared to the pure drug (52).

Rahman et al., (2017) conducted a comprehensive investigation into the intricate interplay between pharmacokinetics and pharmacodynamics in the context of 5-FU-loaded Eudragit-S100 encapsulated colon-specific sodium alginate microspheres in a rat model. The findings of this study led to the compelling conclusion that these microspheres effectively facilitated the targeted delivery of 5-FU to colonic tissues, while simultaneously mitigating the occurrence of undesirable systemic side effects (53).

1.3 JUSTIFICATION

The administration of medication via parenteral routes and the utilization of chemotherapeutic agents have established methodologies in the management of colorectal cancer. However, it is important to acknowledge that these approaches are not without their limitations, as they are associated with dose-dependent toxicities and undesirable adverse reactions. There has been a surge of contemporary scholarly attention towards the utilization of the colon as a prime locus for pharmaceutical conveyance, owing to its perceived potential as a highly auspicious alternative avenue of drug administration utilizing NPs which presents a multitude of benefits when compared to conventional methodologies. These advantages encompass enhanced stability and specificity, augmented capacity for drug transportation, regulated release, diverse administration routes, and the capability to convey both hydrophilic and hydrophobic pharmaceutical agents.

Despite the considerable efficacy of the two anticancer agents, namely TQ and CAP, their administration is beset by a myriad of complexities. These complexities arise from various factors, such as the hydrophobic nature of the drugs, their susceptibility to light and thermal instability, and the notably brief half-life of CAP. The latter necessitates the administration of a high dosage, thereby engendering dose-dependent toxicities. The conventional administration of CAP has been associated with myelosuppression and liver dysfunction due to the drug's susceptibility to normal tissue. Consequently, it is imperative to develop an optimal Nano carrier system that specifically targets the colon, thereby enhancing the bioavailability of therapeutic agents, minimizing undesirable side effects, and fostering enhanced adherence among patients.

The primary objective of this study was to ascertain a methodology for augmenting the pharmacological efficacy of both medications, while concurrently mitigating the probability of drug resistance. This was achieved by devising a strategy involving the utilization of polymer-functionalized Pluronic NPs as carriers, which exhibited remarkable proficiency in precisely targeting the colon. The therapeutic efficacy of the medication will be augmented as a result of the utilization of polymeric NPs, which will facilitate the targeted delivery of the pharmaceutical agent to the desired anatomical site.

The incorporation of Pluronic into the nanoformulation (NF) will confer enhanced hydrophilicity to the medications. One of the advantages conferred by these shapes is their capacity to engage in interactions with hydrophobic compounds and biological membranes. Furthermore, the incorporation of the galactosylated polymer enhances the biodistribution within various tissues, facilitating the targeted delivery of therapeutic agents to activated colonic macrophages through the process of galactose receptor-mediated endocytosis. This mechanism not only ensures efficient drug uptake but also contributes to the preservation of the physicochemical stability of the drug formulation. Pluronics, in addition, will facilitate the concurrent administration of both pharmaceutical agents, thereby enabling a synergistic impact employing precise localization within cells or tissues.

1.4 OBJECTIVES AND PLAN OF WORK

AIM

To formulate a Nano-based drug delivery system targeting colorectal cancer.

OBJECTIVE

1. To formulate, optimize, and evaluate pluronic polymer functionalized nanocarrier system loaded Capecitabine and Thymoquinone.
2. To assess the anticancer activity of optimized formulation by conducting *in vitro and in vivo* studies.

STUDY PLAN

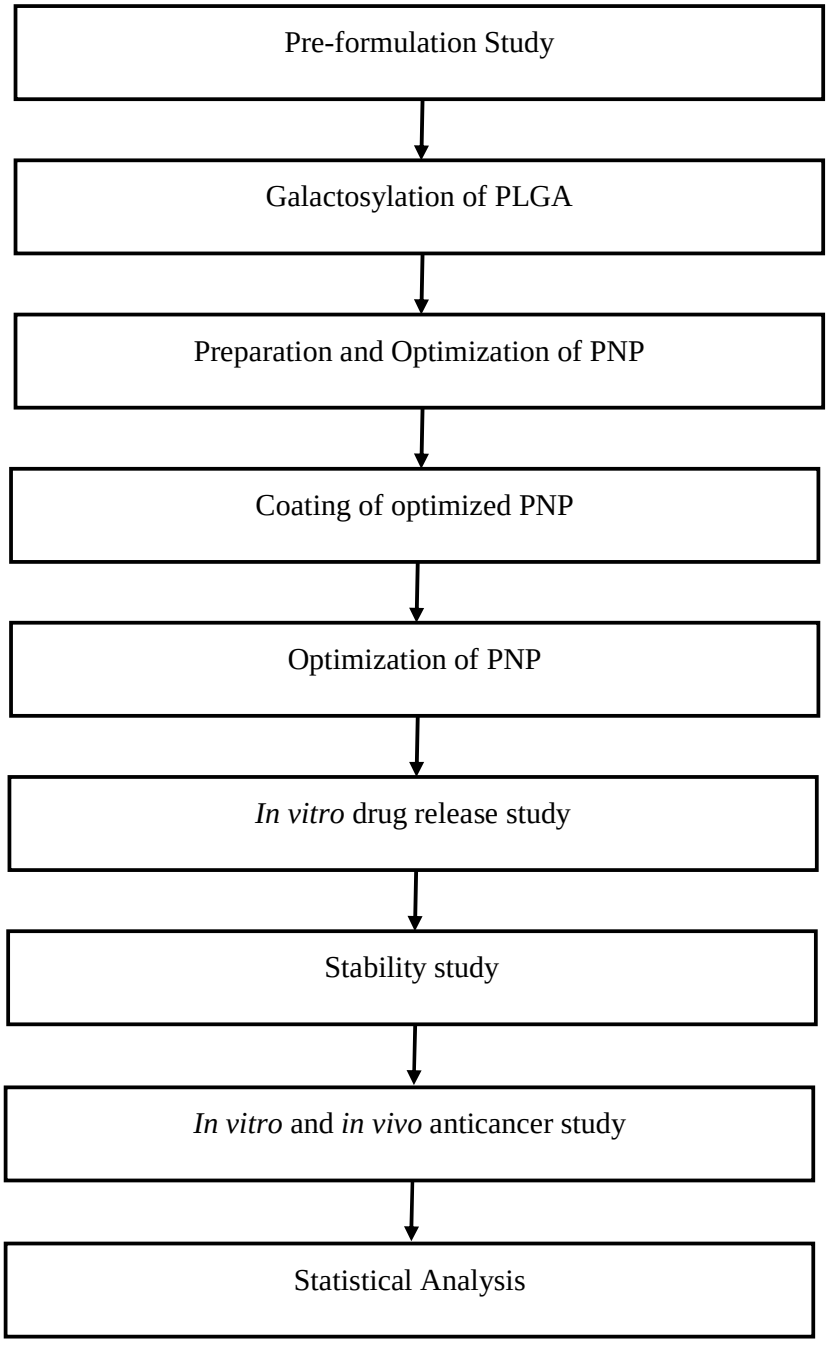
Pre-formulation Study
Galactosylation of PLGA
Preparation and Optimization of PNP
Coating of optimized PNP
Optimization of PNP
In vitro drug release study
Stability study
In vitro and *in vivo* anticancer study
Statistical Analysis

2. MATERIALS AND METHOD

Table 1: List of Equipment, Instruments, and Devices used

Sr.No.	Name	Model	Make
1	Electronic balance	AUW 220D	Shimadzu
2	Magnetic stirrer	RCT Basic	IKA
3	FTIR	IR Affinity-1S	Shimadzu
4	Differential scanning calorimetry	DSC-60	Shimadzu
5	High-performance liquid chromatography	LC-20AD Prominence	Shimadzu
6	pH meter	Cyber Scan pH 510	Eutech
7	Homogenizer	T25 digital Ultra Turax	IKA
8	Probe sonicator	Rivotek™ Ultrasonic sonicator	Riviera Glass Pvt. Ltd
9	Bath sonicator	CPX 1800 H-E	Branson
10	Stability chamber	REMI U-tech	R A scientific instruments
11	High resolution-transmission electron microscope	TEM, 2100	Jeol
12	Zetasizer	Nano ZS	Malvern instruments
13	High-speed refrigerated Centrifuge	Floor model 7000	Kubota
14	Homogenizer	RQT-127A	Remi Laboratory Instruments
15	Fluorescence microscope	BX41	Olympus
16	Ultra-low temperature freezer	U410-86	New Brunswick
17	Freeze dryer	Alpha 1-2 LD plus	Christ
18	CO_2 incubator	Galaxy 170R	New Brunswick
19	Microliter plate reader	Lisa Plus	Rapid Diagnostic Pvt. Ltd.
20	Microcentrifuge	Spinwin MC-02	Tarson

Table 2: List of Chemicals, APIs, Reagents, Polymers and solvents used

Sr.No.	Name	Purpose	Supplier
1	Capecitabine	Formulation API	Sigma, Aldrich, Bangalore, India
2	Thymoquinone	Formulation API	Sigma, Aldrich, Bangalore, India
3	PLGA	Polymer	Sigma, Aldrich, Bangalore, India
4	Pluronic F-127	polymer	Sigma Aldrich, USA
5	Potassium dihydrogen phosphate	chemical	Merck, India
6	Galactose	polymer	Innovative, India
7	Sodium hydroxide	chemical	Merck, India
8	Doxorubicin	API as standard for cell line study	Sigma Aldrich, USA
9	Mannitol	cryoprotectant	Himedia Laboratories, India
10	3-(4,5-dimethylthiazol-2-yl)-2,5-diphenyl tetrazolium bromide (MTT)	Cell line assay	Sigma Aldrich, USA
11	Ethidium bromide	Chemical for cell line study	Sisco Research Laboratories Pvt. Ltd, India
12	Acridine orange	Chemical for cell line study	Himedia Laboratories, India
13	4',6-Diamidino-2-phenylindole (DAPI)	Cell line study	Sigma Aldrich, USA
14	Dimethyl sulfoxide	Cell line study	Qualigens, India
15	Methane Sulphonic acid	Chemical	Visso Trading Co. India
16	N, N dimethylformamide	chemical	Visso Trading Co. India
17	Acetonitrile	solvent	Fisher Scientific, India
18	Methanol	solvent	Fisher Scientific, India
19	Chloroform	chemical	Fisher Scientific, India
20	Eudragit-S100	coating	Himedia Laboratories, India
21	Paraformaldehyde	chemical	Himedia Laboratories, India
22	Fetal bovine serum	Cell line study	Gibco, USA
23	Dulbecco's modified Eagle's medium (DMEM)	Cell line study	Gibco, USA
24	Ethyl acetate	solvent	Himedia Laboratories, India

2.1 An Innovative Reverse Phase High-Performance Liquid Chromatography (RP-HPLC) Approach to Quantifying CAP and TQ simultaneously

The experimental protocol, known as the chromatographic procedure CTO-10AS, was meticulously devised employing sophisticated equipment including a binary pump LC-20 AD, a degasser DGU20A5, a UV-Vis detector, and a column oven CTO-10AS. These instruments were integrated into a Shimadzu Prominence HPLC-20 AT system, which was operated using the LC Solution 1.25 program. This comprehensive setup was employed to unravel and scrutinize the obtained data. The process of chromatographic separation and subsequent analysis was carried out utilizing the analytical column known as Luna C18, which possessed dimensions of 250× 4.60 mm and a particle size of 5 µm. A nylon filter, possessing a membrane thickness measuring 0.22 microns, was employed to filter the mobile phase. The utilization of an Ultrasonic Bath Sonicator was employed to degas the mobile phase.

The direct-Q3 water purification system manufactured by Millipore Corporation utilizes Milli-Q water of analytical grade, specifically the Millex HV® variant, sourced from the United States. The experiment was verified using Design-Expert® software version 13, developed by Stat-Ease Inc. in Minneapolis, USA.2.1.1

2.1.1 API standard solution development

By employing a bath sonicator, a quantity of 10 mg of drug samples was effectively solubilized in a solution of methanol measuring 10 mL. This process was carried out for 5 minutes, resulting in the formation of a standard stock solution with a concentration of 1000 µg/mL. The generation of standard solutions with concentrations ranging from 0.25 µg/mL to 16 µg/mL was achieved through the

process of diluting the drug's standard stock solution in the meticulously produced mobile phase (54).

2.1.2 Validation studies

System appropriateness, linearity, LOD, LOQ, precision, accuracy, and robustness were used to validate the method according to ICH recommendations. Triplicate CAP and TQ standards (0.25-16 μg/ml) were tested for linearity. Precision analysis was performed at low, medium, and high concentrations on the same day and throughout three days. Inaccuracy (recovery) studies, CAP and TQ were spiked to their pre-analyzed sample and their % recovery was calculated by comparing the original and measured concentrations. LOD and LOQ are the analyses' lowest detectable and measurable concentrations, giving signal-to-noise ratios of 3:1 and 10:1 respectively. LOD and LOQ were determined from intercept slope and SD, such as [LOD=3.3 (SD/slope)] and [LOQ=10 (SD/slope) (55,56)].

2.2 Design-Expert® experimental design

In the present inquiry, the NP formulations were refined utilizing the 3^2-factor Box-Behnken Design (BBD) technique, to attain a steadfast amalgamation of auxiliary substances, thereby circumventing the necessity for protracted and laborious experimentation. The experimental setup involves the utilization of Gal-PLGA(A) at concentrations ranging from 2% to 4% w/v, PF127(B) at concentrations from 1% to 3% w/v, and a sonication period(C) lasting between 15 and 25 minutes. The investigation encompassed an analysis of the impact of particle size (X1) and entrapment efficiency (X2) on the three distinct variables. The selection of the optimized PNP was conducted utilizing the point prediction methodology, taking into consideration various criteria such as the attainment of minimal particle size (PS) and

Polydispersity index (PDI) values, while simultaneously maximizing Entrapment efficiency (EE). The quantification of indifference was achieved by employing rigorous statistical analysis (57,58).

2.3 Galactosylation of PLGA

The process of Galactosylation was executed through the establishment of a linkage between the glucose moiety and a specifically chosen polymer via the mechanism of cross-linking (59,60). Expeditiously, galactose was solubilized in N, N-dimethylformamide (10 mL). Upon the introduction of methane sulfonic acid, PLGA was subsequently incorporated. The reaction was subjected to thermal treatment and mechanical agitation at a temperature of 80°C for 48 hours. The precipitation process involved the utilization of chilled distilled water. The PLGA-galactose conjugate materialized as a pristine white powder, painstakingly acquired through the meticulous processes of filtration, thorough washing, and subsequent desiccation of the precipitate. The Galactose-PLGA(Gal-PLGA) compound underwent verification through the utilization of Proton Nuclear Magnetic Resonance spectroscopy, specifically the H-NMR technique (60).

2.4 Synthesis of CAP and TQ-loaded Pluronic Functionalized PNP (CAP-TQ-Gal-PLGANP) and Eudragit-S 100 coating

The adoption of the double emulsion-solvent evaporation technique has yielded the creation of pluronic functionalized PNP. The organic phase consisted of a 0.5 mL volume of ethyl acetate, which contained a solution of Gal-PLGA and medicines (CAP+TQ). On the other hand, the aqueous phase was composed of 2 mL of double-distilled water, in which PF 127 had been dissolved. The aqueous phase was subjected to the incorporation of the organic phase, subsequently undergoing

sonication. The solvent is subjected to the process of evaporation through the use of centrifugal force at a speed of 12000 revolutions per minute for 15 minutes. Upon completing the rinsing process with cold water, the supernatant, which contained a significant concentration of NPs, was meticulously gathered (51,61,62).

The formulation of the enteric coating solution involved the dissolution of Eudragit polymer within a composite solution comprising polyvinyl alcohol (PVA), methanol, and NaOH. Gradually, the recuperated NP was incorporated into the enteric coating solution. The ultimate suspension underwent sonication for 5 minutes. The cryogenic preservation of the nanosuspension at temperatures of -20°C and -80°C was followed by the lyophilization process, wherein mannitol was employed as a cryoprotectant. A hermetically sealed receptacle was employed to maintain the desiccation of the powder pending subsequent analysis (63).

2.5 Evaluation of Eudragit S-100 coated CAP and TQ loaded Gal-PLGANP (Eud-CAP-TQ-Gal-PLGANP)

2.5.1 Chemical and Physical Analysis (64,65)

A) Particle size (PS), polydispersibility index (PDI), and zeta potential (ZP)

The Zetasizer instrument was employed to conduct a comprehensive physicochemical analysis of Eud-CAP-TQ-Gal-PLGANP. This involved the determination of various parameters such as the average size of particles, the distribution of particle sizes, and the values of ZP. These measurements were carried out using advanced techniques, namely dynamic light scattering (DLS) and M3-phase analysis light scattering (PALS).

B) Fourier-transform infrared (FTIR) spectroscopy

The FTIR spectrophotometer was adopted to conduct an analysis of various substances including pure CAP, TQ, Gal-PLGA, PF-127, and Eud-CAP-TQ-Gal-PLGANP. This analysis was carried out using the KBr pellet technique, which covers a spectral range of 4000–400 cm-1.

C) Differential scanning calorimetry (DSC)

The thermal behavior of drugs and their mixtures was determined by DSC analysis of pure CAP, TQ, Gal-PLGA, PF-127, and Eud-CAP-TQ-Gal-PLGANP by heating the aluminum pans containing the samples (30-350 ^{o}C at 5^{o}C/min under constant Nitrogen supply).

2.5.2 Entrapment Efficiency (EE)

The quantification of CAP and TQ encapsulated within the NPs was ascertained through the process of separating the drug-laden NPs from the suspension that contained unbound CAP and TQ, employing the technique of centrifugation.

The suspension acquired after the process of solvent evaporation was subjected to centrifugation, wherein the aim was to separate the components based on their density. Subsequently, the quantity of unbound pharmaceutical substances present in the resulting liquid portion, known as the supernatant, was determined through the utilization of HPLC analysis. The quantification of drug encapsulation within NPs was determined by subtracting the number of drugs employed for the formulation from the number of drugs present in the supernatant. The calculation of entrapment efficiency was derived through the subsequent formula:

$$\%EE = \frac{A - B}{A} * 100$$

A - is the sum of the CAP and TQ contributions in the PNP, and B is the sum of the CAP and TQ contributions in the supernatant.

2.5.3 Transmission electron microscopy (TEM) and Scanning electron microscope (SEM)

Both coated (Eud-CAP-TQ-Gal-PLGANP) and uncoated (CAP-TQ-Gal-PLGANP) np's were phosphotungstic acid-coated for TEM analysis of their surface morphology, then viewed at 40000X magnification under a microscope. In the SEM study, a sputter coater was used to apply a thin layer of gold-palladium alloy to the np. For 90 seconds, a 15 kV accelerating voltage was used with the coater, and the specimens were examined using a respective electron microscope.

2.5.4 *In vitro* release from coated and uncoated NF

The drug release characteristics of eudragit coated Gal-PLGANP and eudragit uncoated Gal-PLGANP were compared in simulated fluids of varying pH: (a)1-2 hours, pH of 1.2; (b) 3-4 hours, pH 4.5; (c) 5-6 hours, pH 6.8; (d) 7-24 hours, pH 7.0+30% fetal bovine serum (FBS). The released volume (5mL) was removed and replaced at predetermined intervals. Drug concentrations were determined by filtering, diluting, and analyzing the obtained samples using an HPLC detector set at 271 nm (66).

2.5.5 Colloidal stability

The Eud-CAP-TQ-Gal-PLGANP samples were subjected to lyophilization and subsequently stored for 6 months under three distinct temperature conditions: -20°C, 4°C, and 25°C, respectively. Subsequently, an assessment was conducted to gauge the stability of the samples by closely examining the alterations in their PS and EE as time progressed.

2.6 Targeting CRC using *in vitro* Assays

The National Centre of Cell Sciences, Pune, India, supplied HT-29 human colorectal cancer cell lines. In a CO_2 incubator at 37 °C and 95% humidity, cells were cultured in Dulbecco's Modified Eagle Medium (DMEM),10% FBS, with 1% pen-step antibiotics.

2.6.1 *In vitro* cytotoxicity assay

The study evaluated various formulations, including pure CAP, pure TQ, pure CAP+TQ, targeted nanoformulation (T-NF; Eud-CAP-TQ-Gal-PLGANP), and non-targeted nanoformulation (NT-NF; Eud-CAP-TQ-PLGANP), to assess their cytotoxicity on HT-29 cancer cell lines. The MTT assay, utilizing 3-[4,5-dimethylthiazol-2-yl]-2,5-diphenyltetrazolium bromide, was employed for this purpose. In this experimental setup, HT-29 cells were seeded a day prior and subsequently subjected to incubation periods of 24 and 48 hours. Subsequently, a medium with 20 µL, MTT, and 5 mg/mL phosphate-buffered saline (PBS) was introduced to the cellular milieu, wherein they were subjected to a conducive environment within a CO_2 incubator for 4 hours. The formazan crystal that was produced was effectively dissolved in dimethyl sulfoxide (DMSO) at a volume of 150

µL per well. The absorbance at 570 nm was quantified using a microplate reader. The IC_{50} values of all formulations were also subjected to comparison with the standard agent, Doxorubicin (40).

2.6.2 Intracellular Reactive Oxygen Species (ROS) Measurement

The intracellular assessment of ROS was conducted using non-fluorescent Dichloro-dihydro-fluorescein (DCFH-DA). This compound possesses the ability to effortlessly penetrate the intracellular matrix of cells. Upon exposure to ROS, DCFH-DA undergoes oxidation, resulting in the production of fluorescent dichlorofluorescein (DCF). Upon introducing the cells into a 24-well flat-bottom microplate, accompanied by the placement of coverslips, the aforementioned assembly was subjected to an environment of controlled carbon dioxide concentration within an incubator set at 37°C. This arrangement was allowed to persist throughout an entire night. A volume of 200 µl/mL was allocated to each sample, encompassing both the targeted (Eud-CAP-TQ-Gal-PLGANP) and non-targeted (Eud-CAP-TQ-PLGANP) nanoformulation, as well as the pure CAP+TQ. These samples were subjected to an 8-hour treatment period. After the designated period of incubation, the cellular entities were subjected to fixation using a 4% paraformaldehyde solution for 30 minutes. Subsequently, the specimens were subjected to two rounds of washing with PBS, 7.4, and were subsequently subjected to analysis via a fluorescence microscope.

2.6.3 Mitochondrial Membrane Potential (MMP) measurement

During the night, the cellular entities were maintained at 37°C within a controlled environment known as a CO_2 incubator. This was done after the act of introducing said cells into a 24-well micro plate possessing a flat bottom, which was

further equipped with coverslips. Every individual specimen, namely Eud-CAP-TQ-Gal-PLGANP, Eud-CAP-TQ-PLGANP, and CAP+TQ, was subjected to a concentration of 200 µL/mL and exposed to a treatment duration of 8 hours. Subsequently, these samples were given a respite period and immersed in Rh-123 dye for 30 minutes. The cellular specimens were subjected to fixation using a 4% solution of paraformaldehyde for 30 minutes after a thorough rinsing with PBS (7.4). Following this preparatory step, the samples were subjected to analysis adopting a fluorescence microscope.

2.6.4 Caspase-3-activity assay

The efficacy of the medication was assessed through the utilization of a Caspase-3-activity assay. The cellular specimens were subjected to staining using the reagent following the prescribed guidelines provided by the manufacturer, promptly after the administration of Autocrine motility factor (AMF). Subsequently, the specimens were allowed to undergo incubation for 30 minutes, adhering to the intracellular methodology elucidated earlier. Flow cytometry was employed to scrutinize the cellular entities after their incubation period. The quantification of field exposure effects was conducted through a comparative analysis of the average fluorescence intensity exhibited by samples subjected to the AMF and those that remained within the controlled environment of the incubator.

2.6.5 4',6-diamidino-2-phenylindole (DAPI) study

During the night, the cellular entities were subjected to a controlled environment with a temperature of 37°C, within the confines of a CO_2 incubation apparatus, after their initial placement within a 24-well microplate. Following 48 hours, an assessment was conducted on the efficacy of pure CAP+TQ, both in

targeted and non-targeted nanoformulation, which were administered at a concentration of 200 µl/mL for therapeutic purposes. After the incubation period, the cellular entities were fixed in a 4% paraformaldehyde solution for 30 minutes, followed by two subsequent washes with PBS. Upon subjecting a volume of 20 µL of DAPI to an incubation process at ambient temperature for 5 minutes, while ensuring the absence of any light exposure, the resultant sample was subsequently visualized utilizing a fluorescence microscope. The enumeration of cells that have undergone apoptosis was conducted through microscopic observation (67).

2.6.6 Apoptosis assay

Cells were cultured in six-well plates. Following a 24-hour incubation period, the cells were subjected to treatment with the concentrations of the samples (Eud-CAP-TQ-Gal-PLGANP, Eud-CAP-TQ-PLGANP, CAP+TQ) that corresponded to the half-maximal growth inhibitory (GI_{50}) levels. Following the collection of the cellular specimens, a duration of 15 minutes was allocated at ambient temperature to apply Annexin V-fluorescein Isothiocyanate and Propidium iodide staining to the aforementioned cells. The specimens were subjected to analysis employing a flow cytometer, while the study itself employed the FlowJo X 10.0.7 software (68).

2.7 Evaluating the developed PNP *in Vivo*

The Institutional Animal Ethics Committee (IAEC) of the esteemed KLE College of Pharmacy, situated in Belagavi, India, has granted its esteemed approval (approval No: 221/Po/Re/S/2000/CPCSEA) to the animal experimental protocol. This protocol has also been duly sanctioned by The Committee for Control and Supervision of Experiments on Animals (CPCSEA). To conduct investigations about acute oral toxicity and anticancer properties, male Wistar rats weighing between 250

and 300 gm were utilized. The fauna was confined within enclosures subject to a diurnal rhythm of 12 hours of illumination followed by 12 hours of darkness. Additionally, they were granted unrestricted availability to a nourishing pellet-based sustenance, maintained at an ambient temperature of 25± 3℃, and a relative humidity ranging from 30% to 70%.

2.7.1 Acute Oral Toxicity Test

Under The Organization for Economic Cooperation and Development (OECD) standards 423, the effects of an acute oral dose on healthy male Wistar rats were investigated. The LD50 was calculated by randomly assigning 12 healthy rats to each of four groups (n=3). Doses of CAP+TQ containing NF were chosen based on oral toxicity data (2000mg/kg) and were suspended in normal saline (10ml/kg). In the current investigation, the high, medium, and low doses were respectively 1/5th, 1/10th, and 1/20th of the maximum tolerated dose (MTD). At 1, 2, 4, and 6 hours post-injection, visual observations, skin/fur/eye alterations, The subjects' breathing, heart rate, blood pressure, autonomic nervous system, somatic motor, and behavioral patterns were recorded. were documented. After 48 hours, and again after 14 days of once-a-day monitoring, the total number of survivors was tallied (69,70).

2.7.2 *In vivo* anticancer research

Following a period of acclimation spanning seven days within the laboratory setting, the rats were subsequently allocated into five distinct groups through a process of randomization. These groups were then subjected to a series of experiments as outlined below: The experimental conditions encompassed in this study include a control group, wherein tumor induction was not administered. Additionally, disease control was implemented with the induction of CRC.

Furthermore, the study explored the effects of CRC induction in combination with non-targeted therapy, targeted therapy, and a commercially available tablet. Rats in group I were administered a saline solution for an equivalent duration. To ascertain the induction of CRC, two rats belonging to Group II were subjected to sacrifice while under the influence of profound ether anesthesia after the final administration of 1, 2 dimethyl hydrazine (DMH). Table 3 presents a comprehensive delineation of the optimal courses of action to be pursued for the diverse subsets of patients. Following the administration of DMH, subjects belonging to group III and group IV were subsequently administered NT-NF and T-NF formulations, respectively, at equipotent dosages of 200 mg/kg CAP and 30 mg/kg TQ, administered orally twice daily via gavage for two weeks. Group V was administered the commercially obtainable CAP tablet (XELODA, which is equivalent to a dosage of 500 mg/ kg). The experimental procedure involved the intraperitoneal administration of DMH, a chemical compound, weekly over 20 weeks. This was done to induce CRC in the subjects. The weight of the subjects' bodies was consistently documented weekly throughout the treatment, while simultaneously observing and tracking their consumption of food and water. Following the prescribed treatment regimen, a rat from each experimental group was selected for sacrifice. The colons of these rats were meticulously excised and subjected to thorough examination to identify any discernible macroscopic tumors. The colon was immersed in a solution containing 10% formalin, after which the number of aberrant crypt foci (ACF) was quantified via optical microscopy. The quantification of hematological parameters was conducted to assess the effectiveness of the therapeutic intervention that was administered (53,71–74).

Table 3: The Protocol for the in-vivo anticancer research

Group	Treatment	No. of animals	Total no. of animals
I: Normal control	Normal saline	6	38
II: Disease control	DMH (15mg/kg) i.p. once a week for 20 weeks	8	
III: Non-targeted Nanoformulation (NT-NF)	DMH-induced +NT-NF orally twice daily for 14 days	8	
IV: Targeted Nanoformulation (T-NF)	DMH-induced +T-NF orally twice daily for 14 days	8	
V: Marketed CAP tablet	DMH-induced + CAP tablet orally twice daily for 14 days	8	

2.7.3 Histopathological study

The neoplastic tissues were procured from the entirety of the male Wistar rodents and subsequently conserved in a solution containing 10% formaldehyde upon the humane termination of the mice at the twenty-third week. Upon careful examination using a microscope, sections of cancerous tissues that had been treated with the hematoxylin and eosin (H & E) staining technique were scrutinized. The quantification of histopathological toxicity was accomplished through a scoring system. A numerical value of (+) denotes a state of stasis, (++) signifies a marginal alteration, (+++) represents a substantial metamorphosis, and (+++++) denotes a profound and radical transformation (75).

3. STATISTICAL ANALYSIS

Using Design-Expert® software, the developed NF was optimized. The data is presented in the form of the mean value along with the standard deviation (SD), which has been calculated based on a minimum of three independent experiments. The model and its terms were confirmed to be statistically significant using analysis of variance (ANOVA). GraphPad Prism (GraphPad Software Inc., CA, USA) was used *in vitro* and *in vivo* statistical study where experiments were carried out employing a statistical methodology known as confidence intervals, specifically at a confidence level of 95%. Through this rigorous analysis, notable disparities were observed and deemed statistically significant when the level of significance fell below the threshold of 0.05 ($P < 0.05$).

4. RESULTS

4.1 CAP and TQ HPLC Method Development

In the UV spectra of 10 µg/ml methanolic drug solutions, maximal absorption was seen for CAP at 305 nm and for TQ at 254 nm. The detection wavelength of 271 nm, where maximal absorption is seen for both medications, was chosen as the isosbestic point based on the UV spectra (Figure 8). The retention time of CAP and TQ, measured in min at 271 nm using HPLC, were determined to be 4.87 and 9.43, respectively. Figure 9 displays the HPLC chromatogram for CAP and TQ in methanolic solution and the PNP. It was determined that the system's appropriateness parameters, including the relative standard deviation of the peak area (%RSD <2.0%), the tailing factor (T <2.0), and the number of theoretical components (N >2000), all fell within the acceptable ranges. Over a concentration range of 0.25 µg/mL –16.0 µg/mL, a linear relationship can be seen between CAP and TQ concentrations in the calibration curve. The value of the correlation coefficient (R2) was determined to be 0.998 (Figure 10). The limits for detecting and quantifying CAP were 0.05 µg/mL and 0.16 µg/mL, respectively, while the limits for TQ were 0.12 µg/mL and 0.38 µg/mL, and 97–100% recovery was achieved in plain drug solution and 100–102% in PNP.

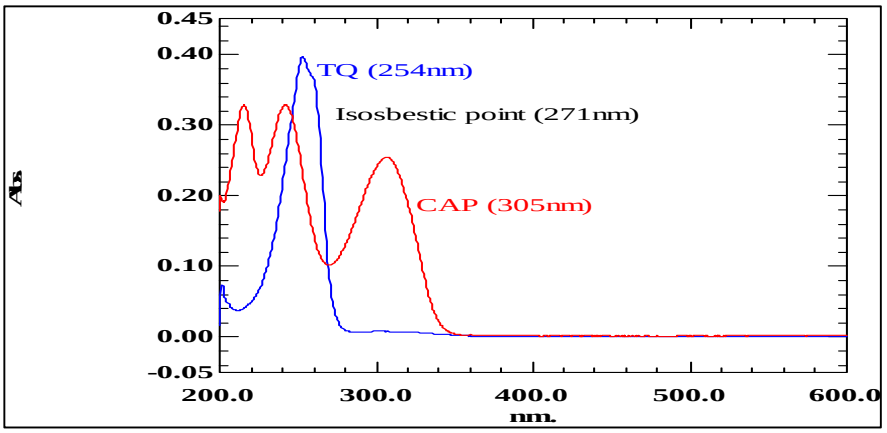

Figure 8: UV–Vis isosbestic absorption spectra

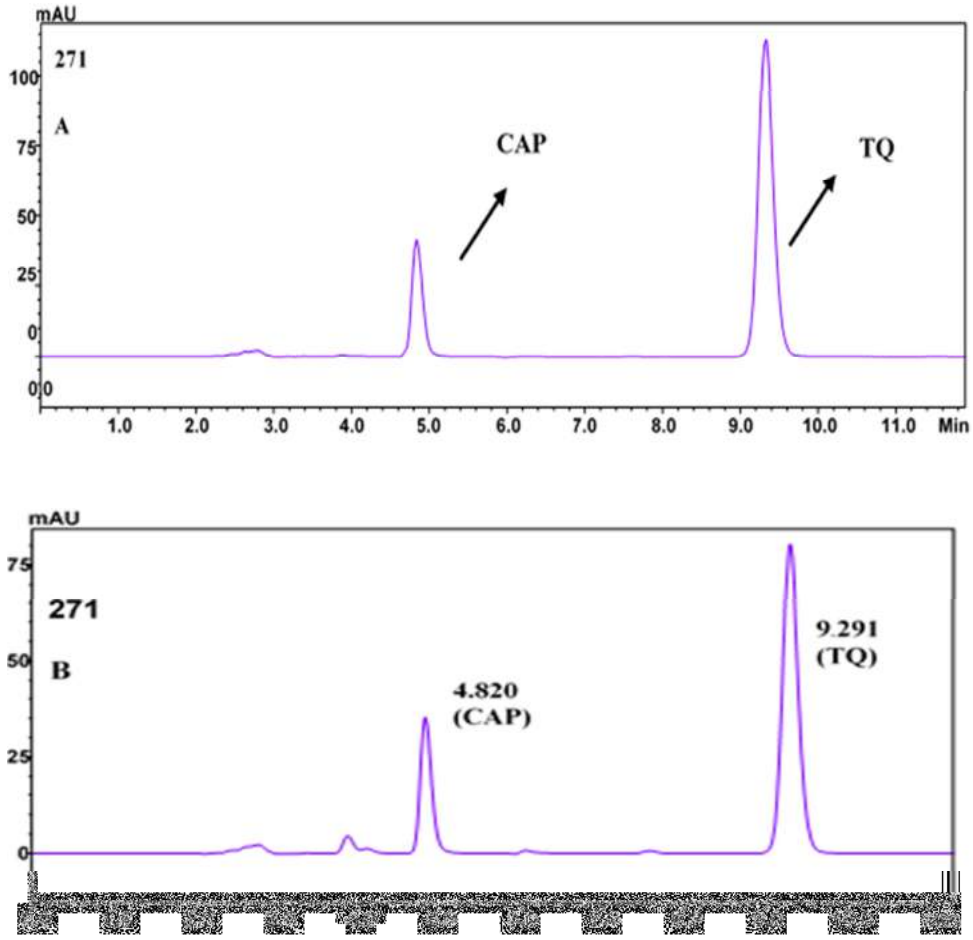

Figure 9: CAP and TQ HPLC chromatograms in methanolic (A) and PNP (B)

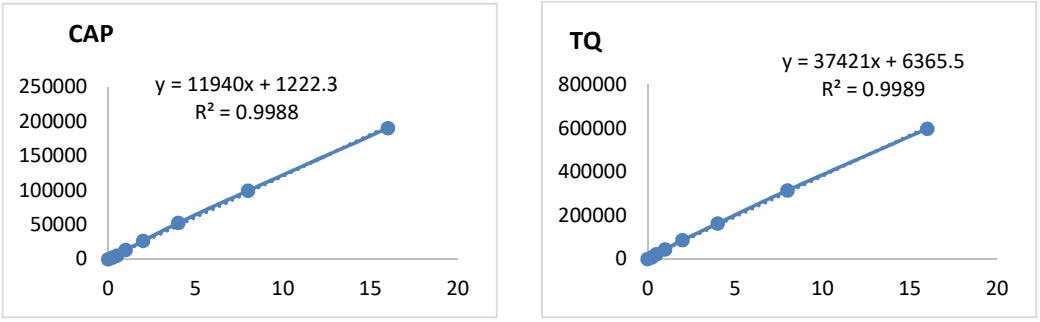

Figure 10: Capecitabine (CAP) and Thymoquinone (TQ) chromatogram linearity

4.2 Polymer functionalization, Preparation, optimization, and characterization of PNP

H-NMR spectroscopy has effectively confirmed the existence of Gal-PLGA, an altered iteration of PLGA that has been synthesized through the process of crosslinking the glucose molecule with PLGA. The H-NMR spectra of PLGA exhibited chemical shifts at 1.55-1.59 ppm (3H, -CH3), 4.8 ppm (2H, -CH2), and 5.2 ppm (1H, -CH). These shifts were also observed in the Gal-PLGA spectra, with the inclusion of an additional shift at 4.3 ppm attributed to the presence of galactose. Consequently, this substantiates the successful synthesis of Gal-PLGA, as evidenced by the data presented in Figure 11.

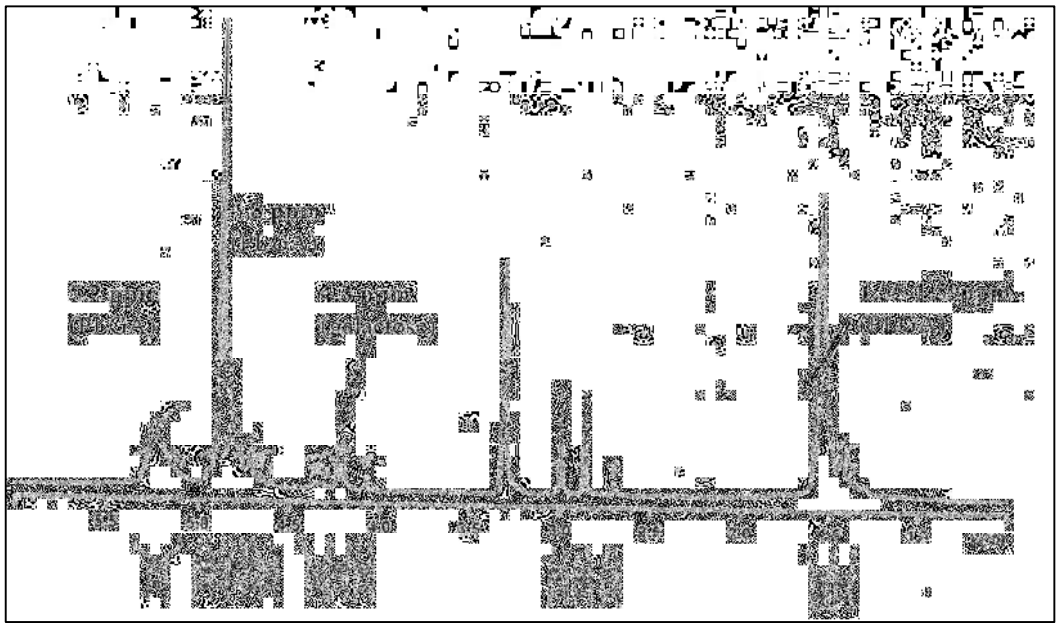

Figure 11: Spectra via H-NMR of Gal-PLGA

The fabrication of PNP was achieved through the process of solvent evaporation. The performance characteristics of PNP, particularly in terms of PS and energy % EE, are predominantly influenced by the concentration of Gal-PLGA and stabilizers. The optimal formulation was attained through the BBD. The tabular representation denoted as Table 4 showcases the amalgamation of factors within the formulation batches, alongside their corresponding performance attributes.

Table 4: CAP-TQ-Gal-PLGANP's Box-Behnken experimental runs

	Dependent Factors			Independent Factors*		
NF batches	A; Gal-PLGA (%)	B; PF127 (%)	C; Sonication time (min)	X1;particle size (nm)	X2; Entrapment efficiency (%)	
					CAP	TQ
PNP1	4	3	20	148±1.12	81.10±0.21	71.88±1.66
PNP2	3	1	25	178±1.57	74.23±0.36	82.69±1.54
PNP3	2	2	25	190±0.81	58.12±0.20	63.00±1.50
PNP4	3	3	15	177±2.65	73.00±0.18	76.18±1.23
PNP5	2	3	20	189±1.54	65.83±1.23	69.14±1.23
PNP6	4	2	25	148±2.69	86.10±1.55	81.14±1.66
PNP7	2	2	20	164±2.65	83.12±0.36	86.32±0.23
PNP8	4	1	20	147±1.23	83.02±0.98	81.13±0.12
PNP9	**3**	**2**	**20**	**161±1.91**	**84.92±0.98**	**87.01±0.11**
PNP10	4	2	15	139±0.77	83.78±1.21	79.67±1.99
PNP11	3	1	15	192±0.36	72.20±1.21	76.99±1.52
PNP12	2	1	20	218±1.32	58.33±0.32	63.02±1.10
PNP13	3	3	25	168±1.66	81.72±1.41	78.31±1.21
PNP14	3	2	15	165±3.68	81.01±0.73	89.36±0.41
PNP15	2	2	15	198±1.10	57.37±0.11	61.78±0.74

*Values shown are average ±SD (n=3)

4.2.1 PS (X1) responses to A, B and C

The synthesized PNP exhibited a mean particle size ranging from 139 to 218 nm. The polynomial equation 1 provided by Design-Expert® Software elucidates the intricate relationship between various factors and their impact on the size of particles. As the concentration of PLGA (A) decreased, a concomitant reduction in the levels of PS (X1) was observed. The discernible manifestation of the inverse relationship between PF-127 and PS was evident. The experimental findings (observed value) exhibited a statistically significant alignment with the anticipated outcomes, as evidenced by the data presented in Table 5. The Perbutation plot effectively elucidates the individual contributions of factors A, B, and C to the overarching depiction, as visually depicted in Figure 12.

$$X1 = 163.33 - 26.63A - 6.63B - 2.75C + 7.50AB + 4.25AC + 1.25BC + 1.08A^2 + 11.08B^2 + 4.33C^2 \text{-------(1)}$$

4.2.2 %EE of CAP and TQ (X2) responses to A, B, C

Table 6 displays that the EE for CAP and TQ are within the ranges of 57.37-86.10% and 61.781-89.36%, respectively. Both the EE of CAP and TQ are affected by external factors, as shown by polynomial equations 2 and 3.

$$X2(CAP) = 85 + 12.62A + 1.62B + 2.50C - 2.25AB - 1.00AC + 1.50BC - 9.37A^2 - 3.87B^2 - 6.13C^2 \text{-------(2)}$$

$$X2(TQ) = 87.67 + 7.00A - 1.00B + 1.50C - 4.00AB - 0.0000AC - 1.00BC - 11.83A^2 - 4.83B^2 - 4.83C^2 \text{-------(3)}$$

Figure 12 exhibits the profound influence exerted by factors A, B, and C upon the overall energy efficiency of both the CAP and TQ systems. Gal-PLGA and PF-127 demonstrated a noteworthy influence on the EE of CAP and TQ. Conversely, the duration of sonication exhibited only a minimal effect on the aforementioned outcome. The quadratic model has been determined to be the most optimal model, as per the data presented in Table 4. The quadratic formula model has yielded exceedingly elevated values for a diverse range of correlation indices, specifically the coefficient of determination (R2). Contour plots exhibit the aesthetic and anticipated magnitudes of desirability and projected values, as illustrated in Figure 13. The measurement of the signal-to-noise ratio was conducted using ANOVA. The results obtained for the recommended quadratic model demonstrated a commendable level of precision, with values of 21.48 for PS, 12.46 for % EE of CAP, and 12.06 for % EE of TQ. It is worth noting that values exceeding 4 are considered preferable in this context.

Table 5: ANOVA table for Responses 1 and 2

Best suit Models	SD	R^2	Adjusted R^2	Predicted R^2	Press	P-value	Remark
Response 1: Particle size							
Quadratic	4.31	0.9867	0.9627	0.8961	1422.5	0.0004	Significant
Response 2: Entrapment efficiency of CAP							
Quadratic	3.11	0.9745	0.9285	0.7059	744.50	0.0018	Significant
Response 2: Entrapment efficiency of TQ							
Quadratic	2.71	0.9680	0.9104	0.7902	550	0.0031	Significant

	Actual values	Point prediction values	
PS (nm)	161±1.91	161.95	Model suggested
EE of CAP (%)	84.92±0.98	84.09	
EE of TQ (%)	87.01±0.11	86.02	

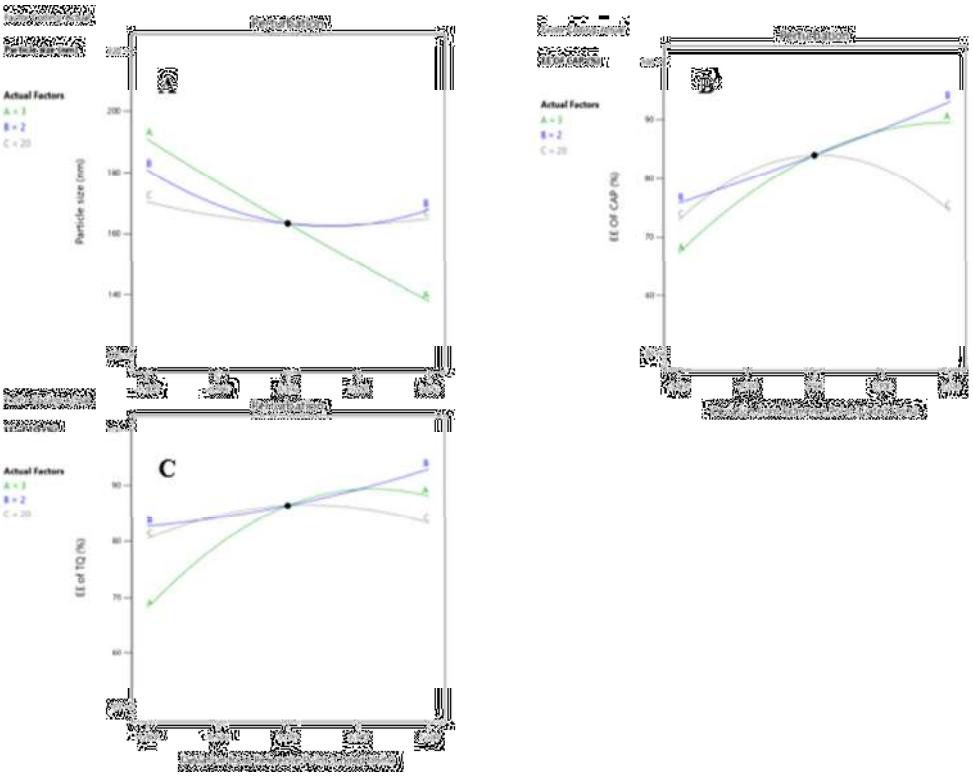

Figure 12: Perbutation plots demonstrating the effects of independent factors on responses; A: particle size, B: entrapment efficiency(CAP) C: entrapment efficiency(TQ)

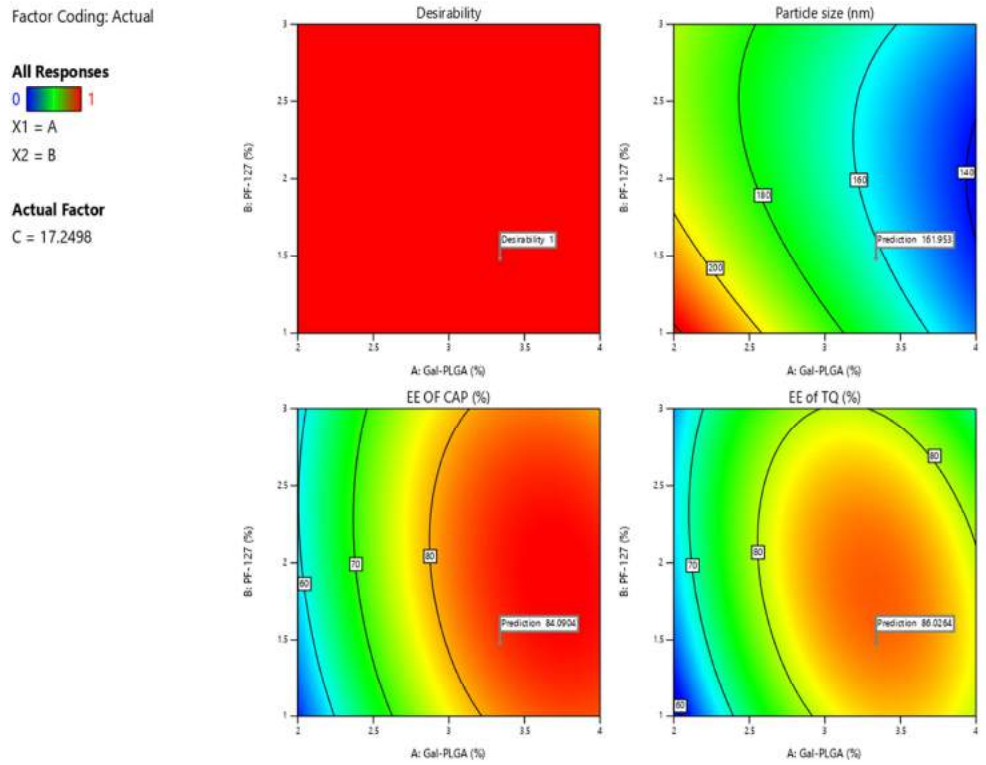

Figure 13: Contour plots showing the desirability of factor optimization

4.2.3 Optimized PNP nanoformulation selection

After careful consideration of the imperative to achieve optimal entrapment efficacy while minimizing particle size, the selection process led to the identification of the most refined PNP batch from a pool of 15 alternative formulations. The selection of the PNP9 batch, which comprises Gal-PLGA at a concentration of 3% w/w and PF-127 at a concentration of 2% w/w, was made to conduct subsequent assessment investigations. This particular batch exhibits the most noteworthy EE (84.92% for CAP and 87.01% for TQ, respectively) and possesses the smallest particle size, measuring 163 nm. A comprehensive analysis was undertaken on the PNP9 batch, encompassing the application of Eudragit-S100 coating and subsequent evaluation investigations.

4.3 Characterization

4.3.1 PS, ZP, and PDI

Table 6 displays the PS, ZP, and PDI values for both coated (Eud-CAP-TQ-Gal-PLGANP) and uncoated (CAP-TQ-Gal-PLGANP) NF. Figure 14 displays the ZP and particle size distribution of the optimized PNP9 batch. All of the generated NPs showed homogenous particle size distribution, with 0.15- 0.37 PDI and, the ZP as -15.37 to -25.71mV.

Table 6: PS, PDI, and ZP values of coated and uncoated NF

NF batches	PS (nm)	PDI	ZP (mV)
Eud-CAP-TQ-Gal-PLGANP(coated)	**183±1.78**	**0.33±1.27**	**-25.2±0.31**
CAP-TQ-Gal-PLGANP (uncoated)	**161±1.91**	**0.21±1.05**	**+47.30±0.14**

Values shown are average ±SD (n=3)

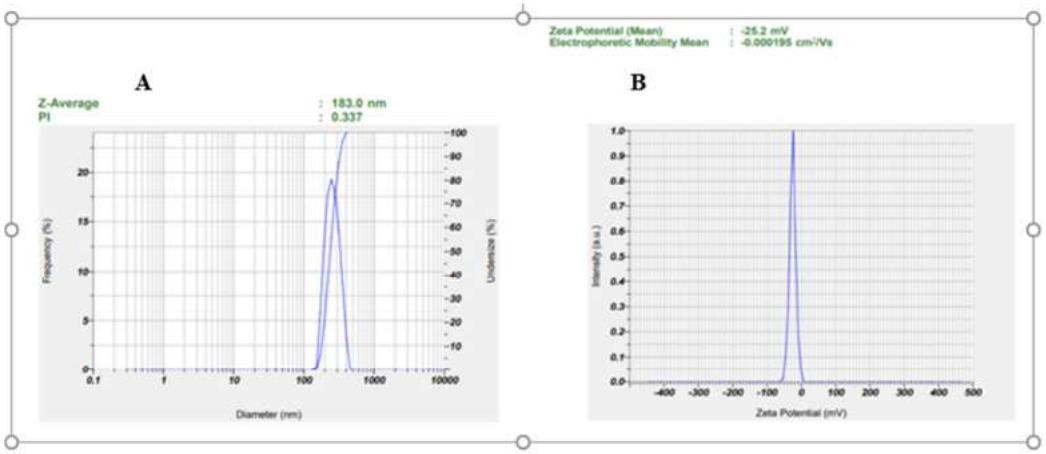

Figure 14: Optimized PNP9's particle size distribution (A) and ZP (B)

4.3.2 FTIR study

CAP's FTIR peak values appeared at 1612,1775, 2956, 3195, and 3212 cm-1, correlated to the C=C, C=O, C-H, N-H, and O-H functional groups respectively, while TQ's appeared at 1711, 2877,2969 and 3040 cm^{-1}, corresponding to the C=O, CH_3, C-H, and CH in =C-H functional groups respectively. The ester group of PLGA polymer is responsible for the presence of a characteristic peak at 1637 cm^{-1} in the FT-IR spectrum of Gal-PLGA. The distinctive peaks of the OH group of galactose at 3338 cm-1 in the spectrum are also visible, demonstrating that the Gal-PLGA polymer structure was effectively synthesized. The C=O and C=C functional groups in PF-127 were located at 1465 and 1342, cm^{-1} respectively. All the key characteristic peaks were seen in the FTIR spectra of PNP9, with only minimal shifting for Gal-PLGA and PF-127 indicating no interaction between the RV and PI and these excipients. Similarly, the typical peaks of CAP and TQ were slightly displaced but diminished in the spectra of PNP9, indicating that both were trapped in the PNP (Figure 15).

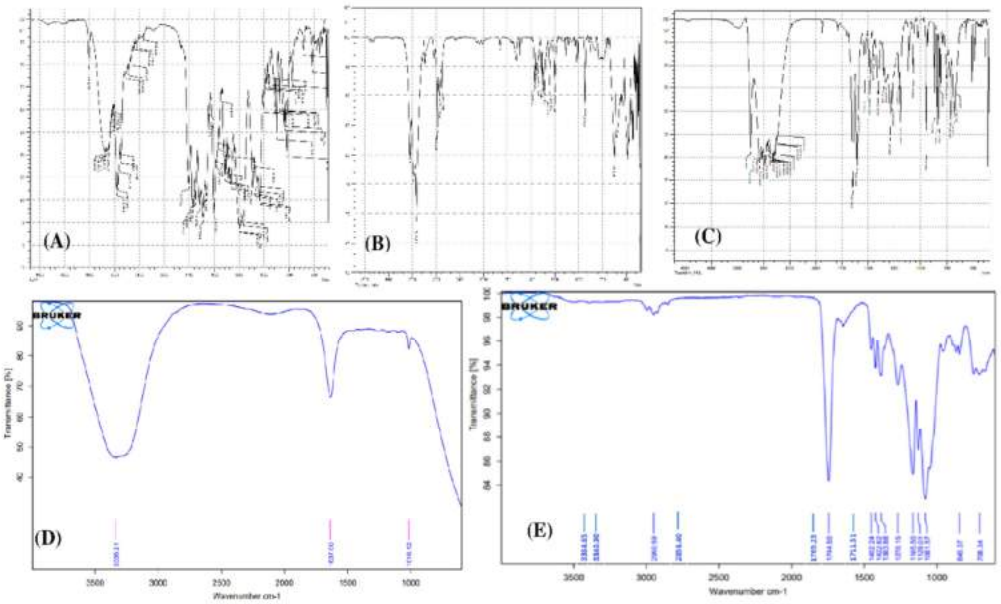

Figure 15: FTIR spectra: CAP (A), TQ (B), PF-127 (C), Gal-PLGA (D) and CAP-TQ-Gal-PLGANP (E)

4.3.3 DSC study

The DSC thermograms (Figure 16) indicate that both pure CAP and TQ possess crystalline properties, as evidenced by the presence of well-defined endothermic peaks at temperatures of 121.39 °C and 49.50 °C, respectively. These peaks correspond to the melting temperatures of the respective substances. An endothermic peak is observed at a temperature of 289 °C for the Gal-PLGA compound. Similarly, PF-127 exhibits an endothermic peak at a slightly lower temperature of 185 °C. The conspicuous absence of the distinguished CAP and TQ peaks observed in the differential scanning calorimetry (DSC) thermograms of PNP9 serves as compelling evidence of its transformation from a crystalline state to an amorphous state. The aforementioned findings suggest a molecular encapsulation phenomenon wherein the CAP and TQ are contained within the PNP structure.

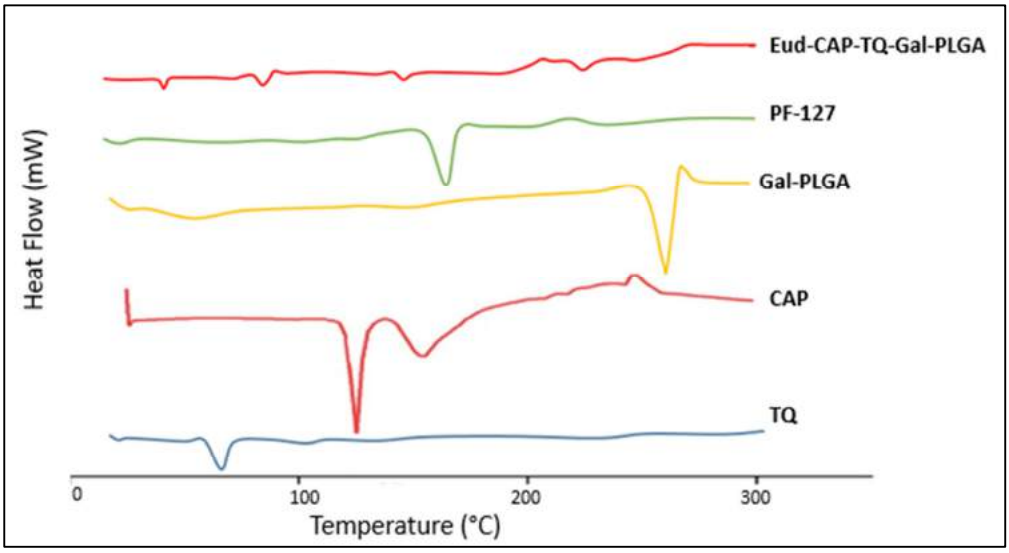

Figure 16: DSC thermograms: CAP, TQ, PF-127, Gal-PLGA and Eud-CAP-TQ-Gal-PLGANP

4.3.4 TEM and SEM

The samples, which were coated in a random manner, namely Eud-CAP-TQ-Gal-PLGANPs, underwent analysis employing both a Transmission Electron Microscope (TEM) and a Scanning Electron Microscope (SEM) at a suitable level of magnification. The observation of a diminished PS is noted in the case of uncoated CAP-TQ-Gal-PLGANPs in contrast to their coated counterparts, as confirmed through TEM. The uncoated NPs exhibited a spherical morphology with a sleek outer surface, while the Eud-CAP-TQ-Gal-PLGANP displayed roughness, as depicted in Figure 17.

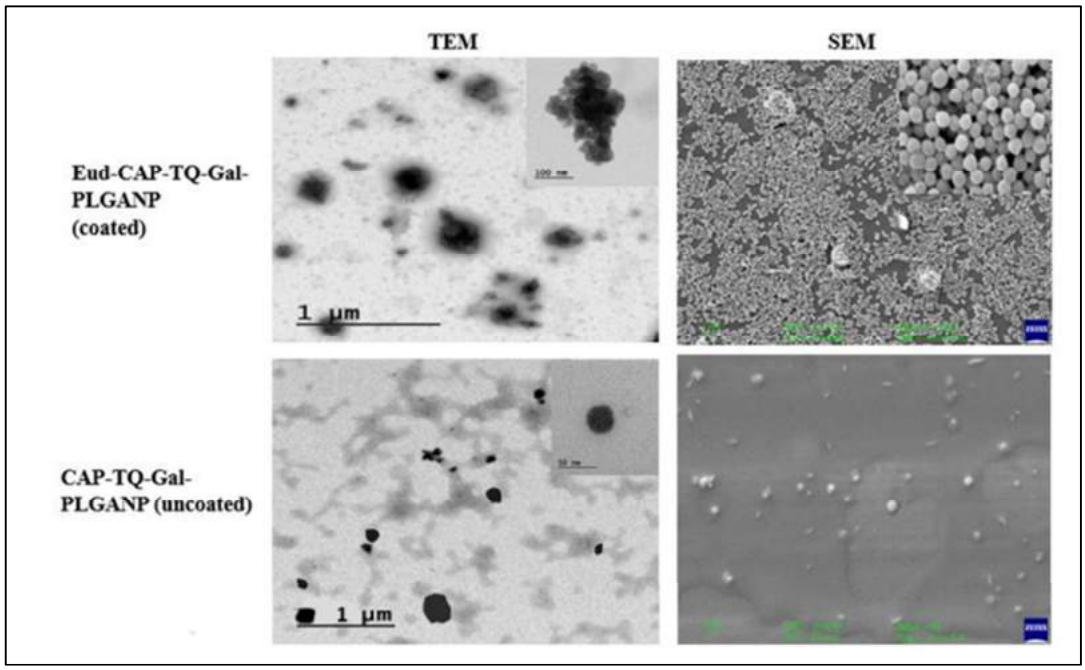

Figure 17: TEM and SEM study of coated and uncoated nanoformulation

4.3.5 Analysis of Drug Release

There were two separate iterations of the nanoformulation, one featuring a coating and the other lacking it. The objective of making use of a fluid simulator to replicate a traversal from the oral cavity to the colon was to enhance the level of realism. The findings indicate that drug release from uncoated NF is initiated in an acidic environment. Specifically, 60% of the drug was released after 8 hours, 70% after 10 hours, and 75% after 24 hours. The rate of release increased as the pH level increased. There was no significant medication leakage observed from the coated NF after 6 hours. However, the release of the drug commenced at a pH level of 7. After 8 hours, only 22.69% of the drug was observed to have been released. The drug release percentage after 24 hours was observed to be 86.40 ± 2.36% (Figure 18). The research findings for the dissolution of coated NF were analyzed using various release kinetic models.

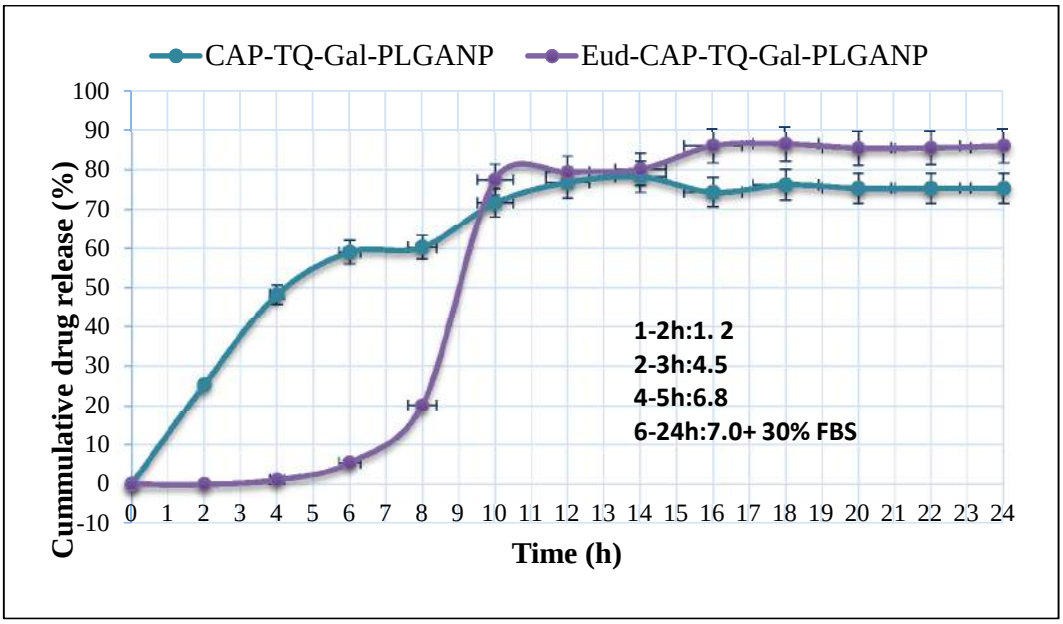

Figure 18: Drug release characteristics of coated and uncoated nanoformulation in vitro

4.3.6 Colloidal stability

Six months' worth of stable Eud-CAP-TQ-Gal-PLGANP was characterized for PS and % EE, at -20°C, 4°C, and 25°C. At ambient temperature, the parameter PS exhibited an increase to 254nm, whereas the parameter EE experienced a decrease of 38%. Conversely, when subjected to temperatures of 4 degrees and – 20 degrees, no noteworthy alterations were observed in either PS or EE. The stability of the developed PNP compound was observed under refrigerated conditions, exhibiting a pressure of 183 PS and an EE of 81%. Similarly, under freeze conditions, the compound displayed a pressure of 185 PS and an EE of 83%. The main takeaways from the analysis are depicted in Figure 19.

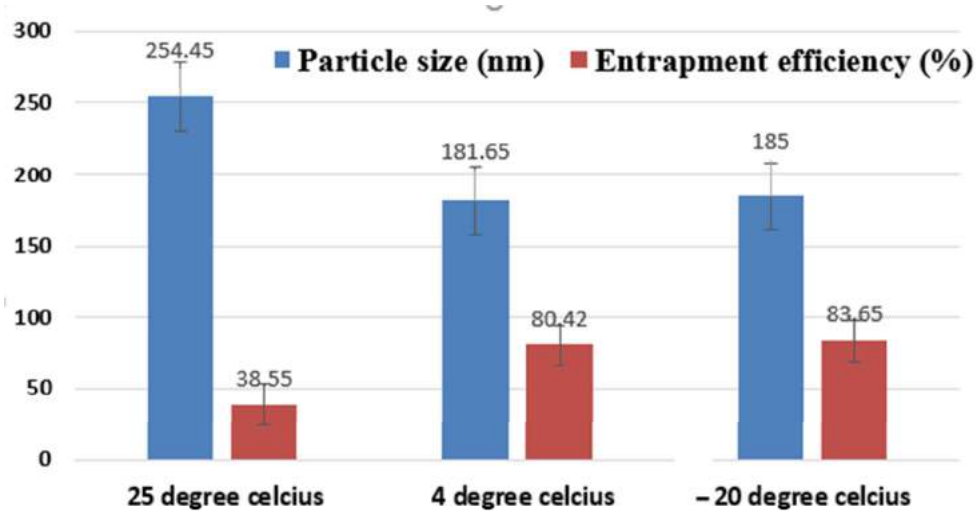

Figure 19: Stability data of Eudragit-S100 coated CAP and TQ loaded Galactosylated PLGANP

4.4 Targeting CRC using *in vitro* Assays

4.4.1 In-vitro cytotoxicity research

A range of concentrations (2.5-100µg/mL) of pure CAP, pure TQ, pure CAP+TQ, targeted nanoformulation (T-NF; Eud-CAP-TQ-Gal-PLGANP), and non-targeted nanoformulation (NT-NF; Eud-CAP-TQ-PLGANP) were adopted in an MTT experiment to ascertain their individual half maximal inhibitory concentration (IC_{50}) values. The IC_{50} values for the solutions of pure CAP, pure TQ, and pure CAP+TQ were determined to be 20.95, 25.30, and 12.0, respectively. In comparison to the standard drug doxorubicin (IC_{50}-5.31), the NT-NF exhibited an IC_{50} value of 8.81. On the other hand, the T-NF demonstrated an IC_{50} value of 4.87 and displayed a cell survival rate of 57% at an extremely low concentration of 3.215µg/mL (Figure 20).

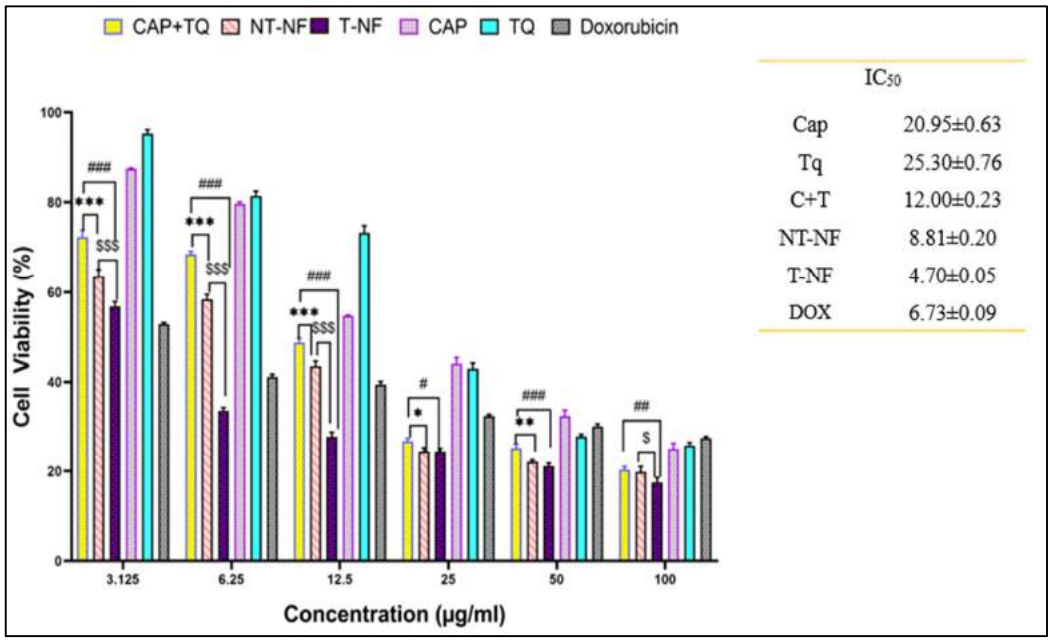

Figure 20: HT-29 cell cytotoxicity when exposed to pure drug CAP+TQ, Non-targeted NF, Targeted NF, Pure CAP, pure TQ, and doxorubicin; significant levels of probability are defined as follows: p^{*}, $p^{\$}$, $p^{\#}$ <.05; p^{**}, $p^{\$\$,}$ $p^{\#\#}$ <.01 and p^{***}, $p^{\$\$\$,}$ $p^{\#\#}$ < .001 across groups

4.4.2 ROS measurement

Figure 21 illustrates the intracellular level of ROS in various experimental conditions, including the control group; negative control(NC), the group treated with Pure CAP+TQ, the group treated with NT-NF, and the group treated with T-NF. The green fluorescence, a discernible marker denoting the existence of ROS within the cellular milieu, was employed as a means to investigate the level of activity. Both the NT-NF and T-NF groups exhibit heightened levels of reactive oxygen species. Nevertheless, it was observed that the green fluorescence exhibited amplification in the context of T-NF, thereby suggesting that the Eud-CAP-TQ-Gal-PLGANP had indeed triggered the process of apoptosis.

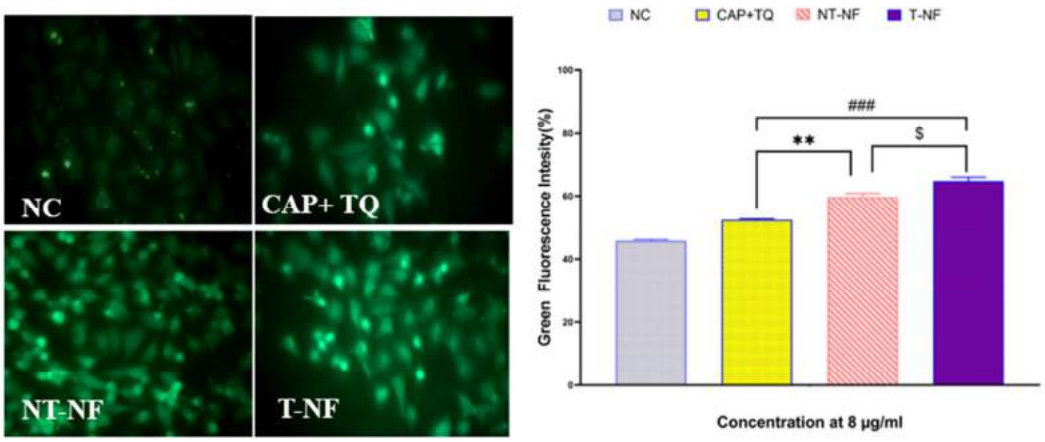

Figure 21: ROS study demonstrating effect in pure CAP+TQ, targeted and non-targeted nanoformulation; $p^{\$}<.05$, $p^{**}<.01$, $p^{\#\#}<.001$

4.4.3 MMP study

The decline in MMP after the process of apoptosis holds significant implications as it emerges as a pivotal indicator of mitochondrial functionality within the realm of cancer cells. The Rho-123 dye facilitated the identification of alterations in MMP levels within the treated cellular specimens. The observed diminishment in MMP expression, as indicated by the relatively subdued green fluorescence intensity in T-NF in comparison to the other groups, implies a concomitant acceleration of apoptosis, as depicted in Figure 22.

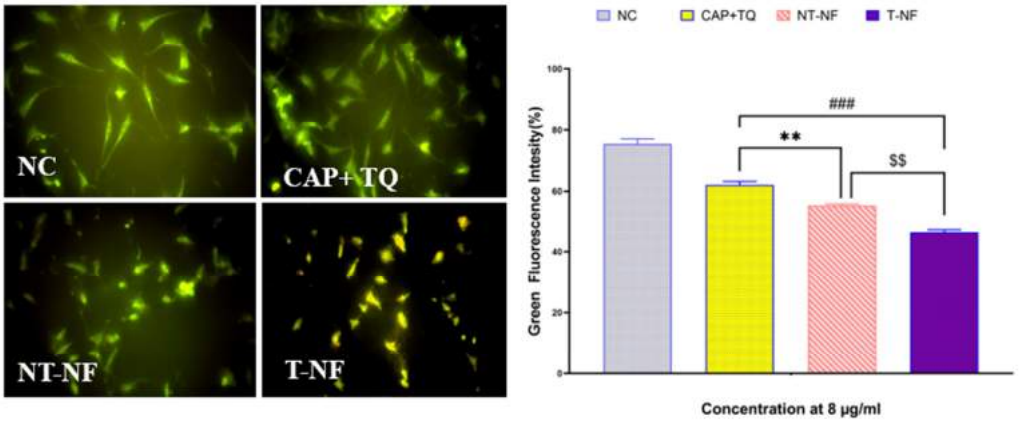

Figure 22: MMP study of pure CAP+TQ, targeted and non-targeted nanoformulation; $p^{\$\$}$<.01, p^{**} <.01, $p^{\#\#}$ <.001

4.4.4 Caspase-3-activity

Caspase-3 assumes a pivotal role as a vital biomarker in the intricate process of apoptosis. It emerges as the preeminent protease that exhibits heightened activity during cellular demise, thereby orchestrating the reduction in cell size, the compaction of chromatin, and the fragmentation of the nucleus, alongside various other distinctive features characteristic of apoptosis. The results of the study revealed that apoptosis was induced in T-NF, as demonstrated by the heightened expression of caspase-3 in comparison to the other experimental groups (Figure 23).

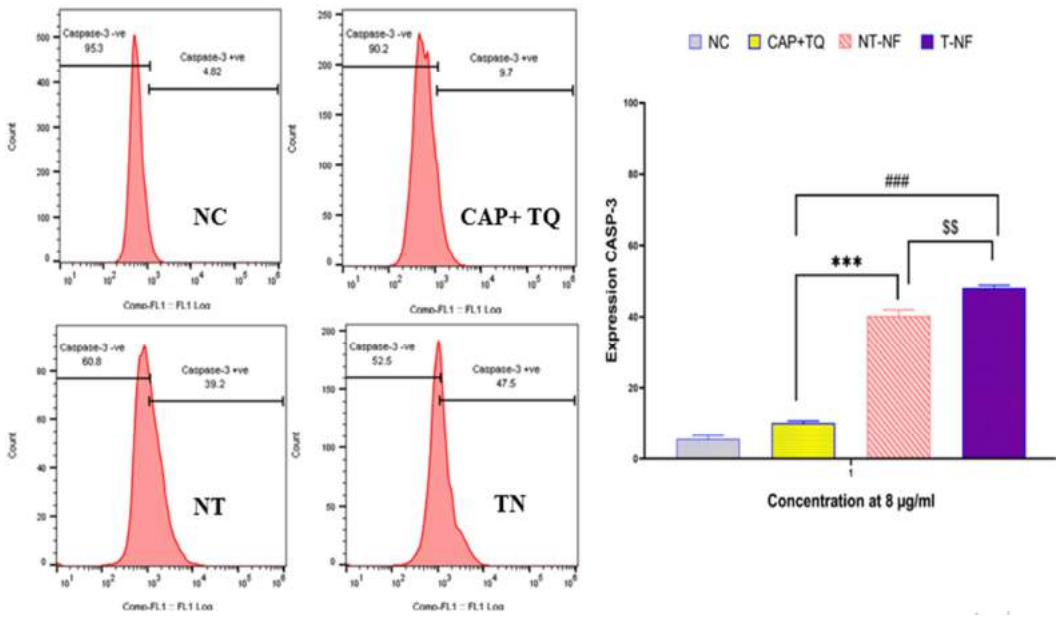

Figure 23: Caspase-3-expression of pure CAP+TQ, targeted and non-targeted nanoformulation; $p^{\$\$}$<.01, p^{***} <.001, $p^{\#\#\#}$ <.001

4.4.5 DAPI study

The distinctive morphology of apoptotic cell nuclei was unveiled through the application of DAPI staining. In the experimental group denoted as the negative control (NC), the cellular nuclei exhibited an intact morphology and displayed a subtle azure hue upon staining. The NT-NF and T-NF groups exhibited a higher degree of blue staining intensity when compared to the pure CAP+TQ group. Apoptosis is distinguished by the phenomenon of chromatin condensation, nuclear fragmentation, and the generation of apoptotic bodies, all of which were conspicuously observed in T-NF cells (as depicted in Figure 24).

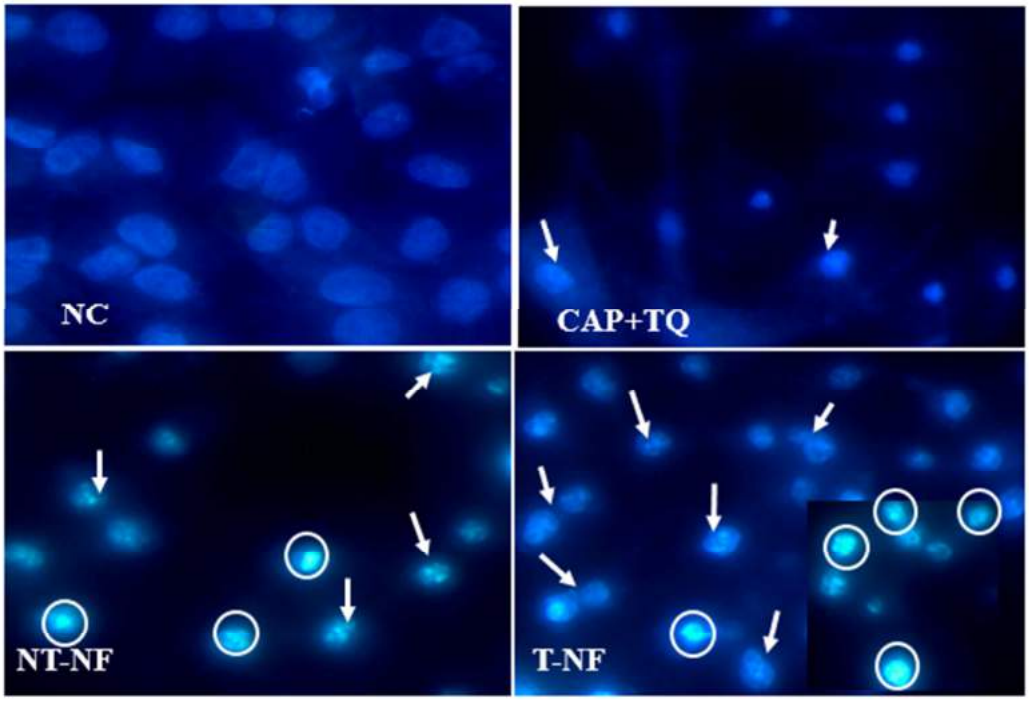

Figure 24: DAPI assay where condensed chromatin and nuclear attrition/fragmentation are shown by the direction of the arrow; blebbed nuclei and apoptotic bodies are depicted by circles in respective groups

4.4.6 Apoptosis Assay

Tumorigenesis occurs as a consequence of cellular resistance to apoptosis, an intricate mechanism of programmed cell death aimed at eliminating aberrant or impaired cells. The untreated cells in North Carolina exhibited a remarkable survival rate of 99.2%, with a mere 0.4% undergoing early apoptosis and a mere 0.17% undergoing late apoptosis. The cellular specimens subjected to NT-NF exhibited a survival rate of 86.7 percent, in contrast to the specimens treated with Pure CAP+TQ, which displayed a survival rate of 90.3%. With the escalation of early apoptosis (23.1%) and late apoptosis (2.4%), there was a discernible decline in cell viability, settling at 73.2%. This observation serves as a clear indication of the initiation of cell death induced by apoptosis in the T-NF group, as depicted in Figure 25.

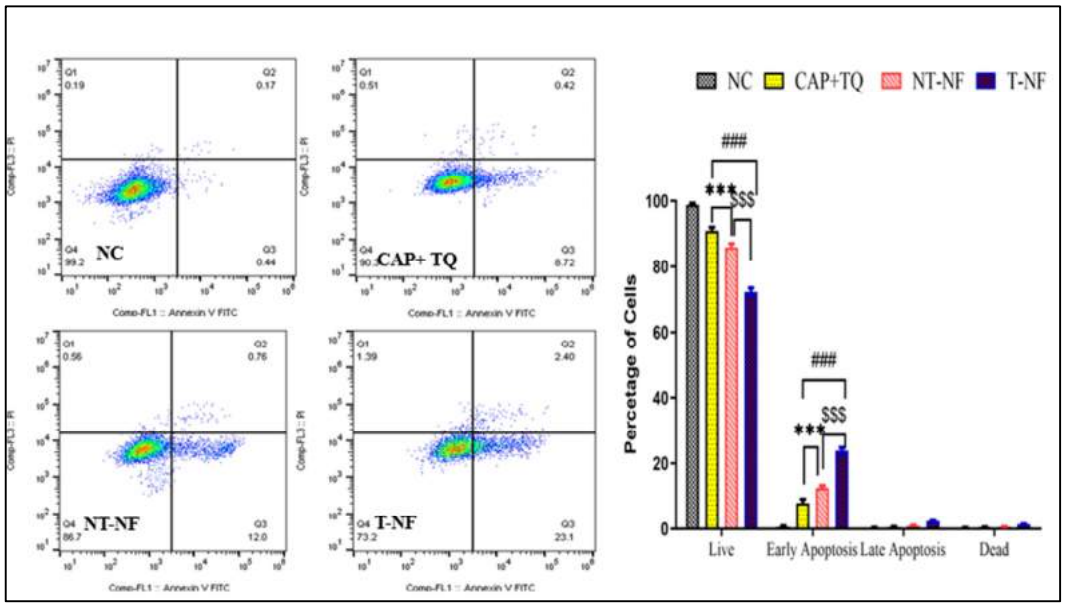

Figure 25: Apoptosis study in pure CAP+TQ, targeted and non-targeted NF;

$p^{\$\$\$}$<.001, p^{***} <.001, $p^{\#\#\#}$ <.001

4.5 *In-vivo* study

4.5.1 Acute Oral Toxicity Study

Phosphate buffer saline was administered orally once to a control group. This research aimed to assess the safety of a single oral dose of CAP+TQ in NF for 14 days. The NF was given orally at doses equal to 1/20th, 1/10th, and 1/5th of the MTD. No deaths, abnormalities in motor functions, or malignancies were found at any of the three dose levels tested.

4.5.2 *In vivo* anticancer study

Indications of CRC progression encompass manifestations such as rectal hemorrhaging and abdominal discomfort. The observed disparity in body mass index between the cohort of rats afflicted with colon cancer and the control group was

evident. The body weights of the rats in the normal control group exhibited a consistent and gradual increase throughout the trial. Although the groups subjected to DMH treatment exhibited an initial increase in weight, this phenomenon was not sustained beyond the 12-week threshold, thereby rendering comparisons with the normal control group arduous. In contrast to the control group administered with DMH, the rats belonging to groups 3 and 4, which underwent the formulation intervention, exhibited a notable increase in weight throughout the treatment. The colons of the DMH rats, which were induced to develop CRC, exhibited a substantial quantity of sizable and numerous minuscule tumors, as depicted in Figure 26.

The ACF, which serves as a pivotal metric for the identification of colon cancer, was discerned and enumerated. Upon comparing groups 3, 4, and 5 with the DMH control, a significant reduction in the quantity of ACFs (Figure 27). The ACF numbers, nonetheless, exhibited no substantial variation between the T-NF and NT-NF cohorts. Mortality rates were meticulously monitored across all cohorts under investigation, save for the standard control group, and subsequently juxtaposed against previously conducted scholarly inquiries (Figure 28).

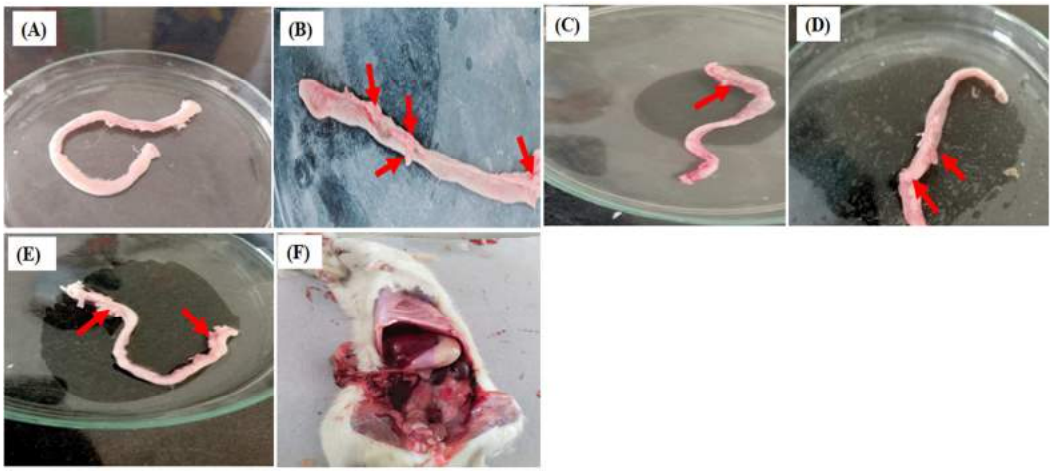

Figure 26: Dissected rat colon of (A) normal control, (B) CRC-induced, (C) treated with targeted nanoformulation, (D) treated with non-targeted nanoformulation, (E) treated with marketed CAP tablet, and (F) dissected CRC-induced rat; Red Arrows represent tumors.

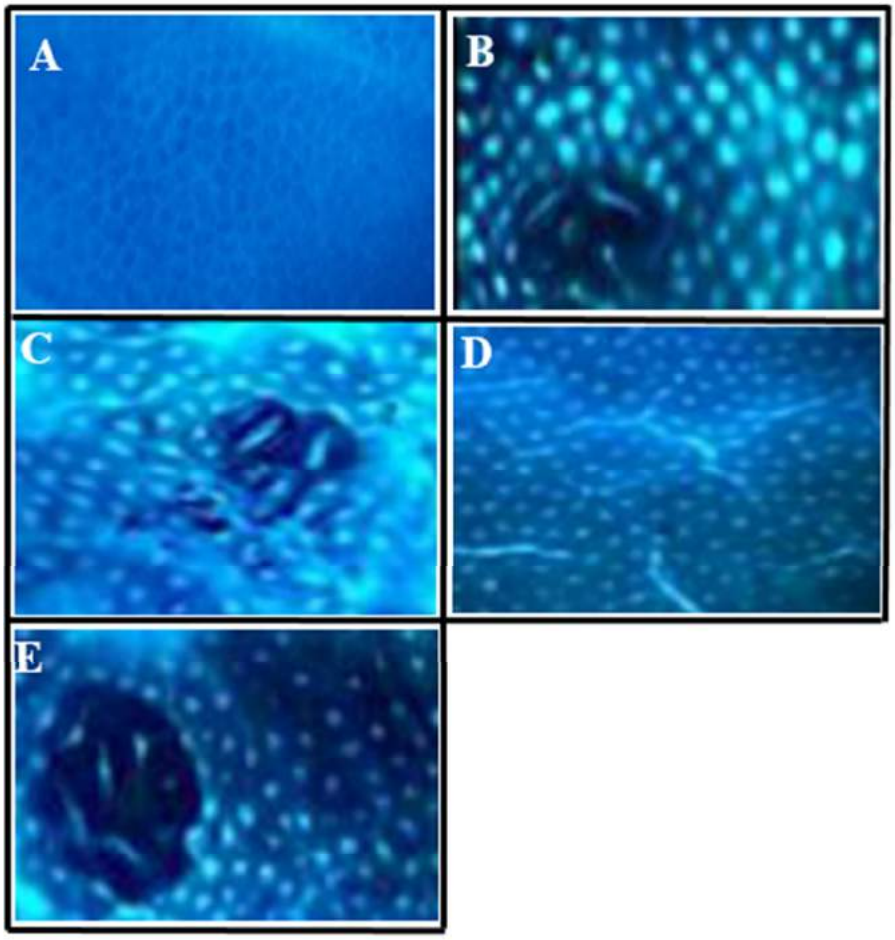

Figure 27: Normal crypts and ACF at 40× in the colonic mucosa, viewed topographically: (A) normal crypts, (B) DMH-treated, treated with (C) non-targeted nanoformulation (NT-NF), (D) targeted nanoformulation (T-NF), and (E) marketed CAP tablet

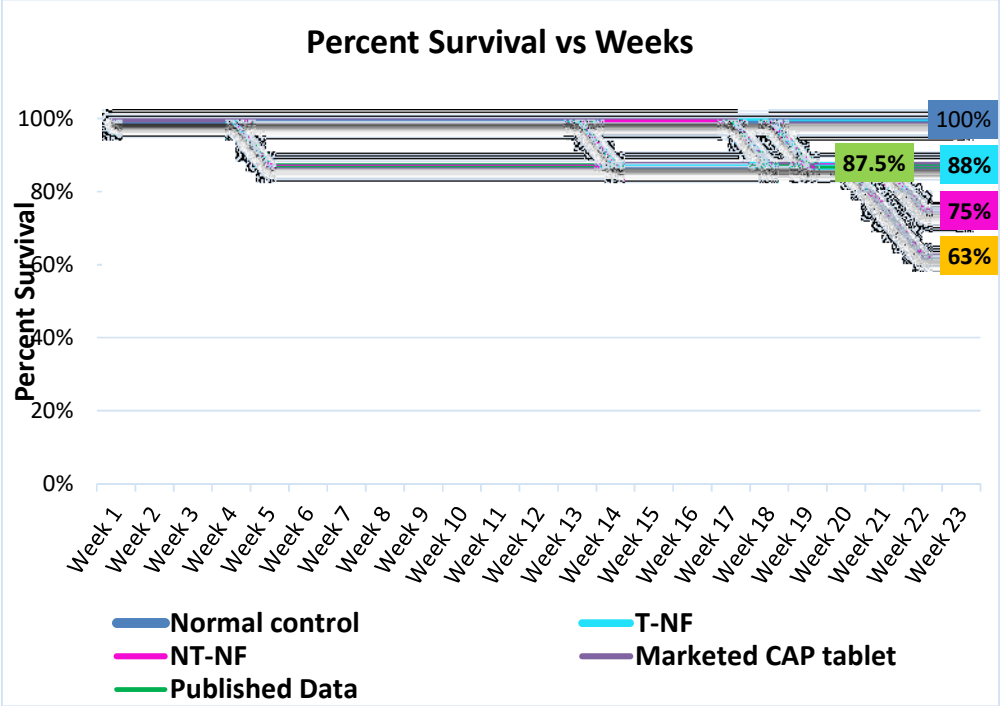

Figure 28: Wistar rat survival rates were evaluated in five groups: (i) normal saline, DMH-induced CRC treated with (ii) non-targeted nanoformulation (NT), (iii) targeted nanoformulation (TN), (iv) commercialized CAP tablet, and (v) comparison with published data

4.5.3 Histopathological and Hematological Findings

The animals belonging to Group II, upon administration of DMH, exhibited the manifestation of mucosal adenocarcinoma, characterized by a well-differentiated and non-invasive nature, as depicted in Figure 29B. The cellular entities that were found to be close to the glandular structures within the cancerous tissues exhibited a notable increase in size and intensified chromaticity. The occlusion of multiple glandular orifices was observed. The extent of lymphocytic infiltration was confined to a restricted scope, manifesting solely in isolated clusters. The level of lymphocytic infiltration within the tumor was found to be low in group III rats that were treated

with NT-NF, as depicted in Figure 29C. Following a fortnight of therapeutic intervention, it was observed that animals administered with T-NF (group IV) exhibited diminished tumor growth and lymph node metastasis in comparison to those administered with NT-NF (group III) and a tablet that is commercially obtainable (group V), as depicted in Figure 29 D and E. Whilst there existed a certain degree of lymphocytic infiltration within the mucosa surrounding the malignant glands, it did not manifest in a significant or widespread manner. The score served as a means of elucidating histopathological toxicity, as evidenced by its inclusion in Table 7. The evaluation of hematological parameters was conducted both before and after the treatment, as depicted in Figure 30. The administration of DMH to the experimental rats resulted in a notable augmentation in white blood cells, platelets, and granulocytes, while concurrently leading to a reduction in red blood cells, lymphocytes, and hemoglobin levels. In the current investigation, the implementation of Targeted NF exhibited a notable enhancement in the blood parameters in comparison to the DMH-induced group, thereby suggesting a substantial decrease in the number of tumors. These findings strongly imply a reduction in tumor burden. T-NF, on the other hand, exhibited a more favorable performance.

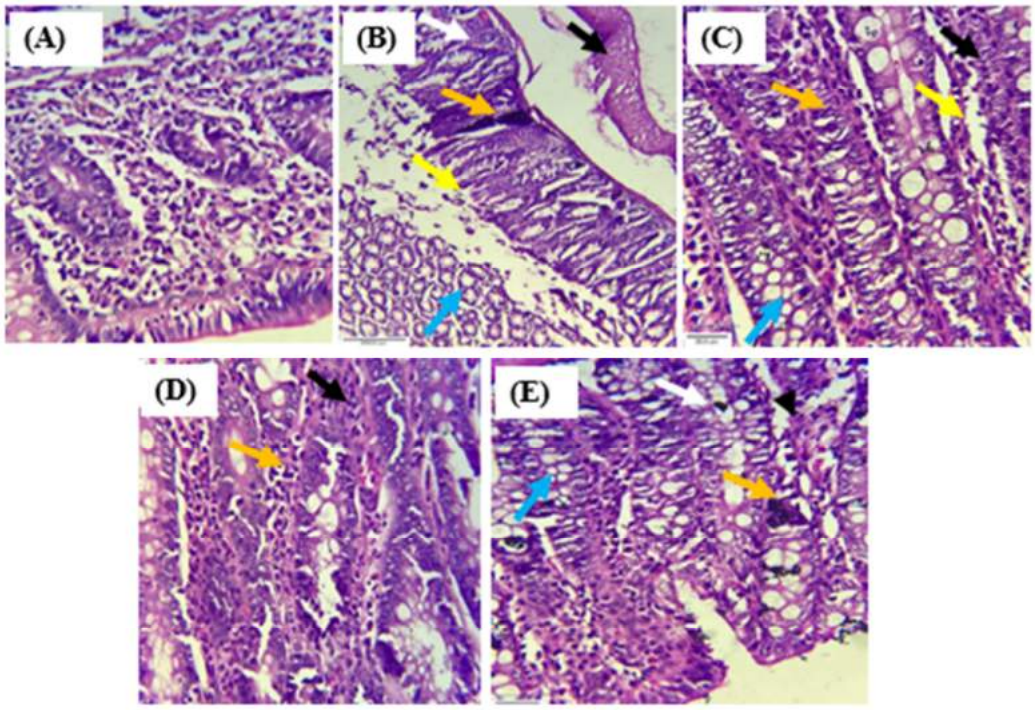

Figure 29: Images showing characteristics of hematoxylin and eosin staining of cancer tissues from the male Wistar rat CRC model in (A) normal control, (B) CRC-induced where yellow, (C) treated with targeted nanoformulation, (D) treated with non-targeted nanoformulation, (E) treated with marketed CAP tablet. Arrows represent: lymphnode metastasis (White); lymphoid follicles (Black); high-grade dysplasia (Yellow); ACF (Orange); mucosal ulcers (Blue)

Table 7: Histological findings score

Microscopy	Disease Control	Targeted Nano Formulation	Non-Targeted Nano Formulation	Marketed Tablet
Congestion	+++	+	+	++
Odema	+++	+	+	+
Hemorrhage	+++	-	+	+
Inflammation	+++	+	++	+
Loss of Intestinal Glands	+++	+	++	+
Mucosal Ulcer	+++	+	+	++
Dysplasia	+++	+	+	+
ACF	+++	+	+	+
Lymph node metastasis	+++	+	+	++
Cancer	++	+	+	+

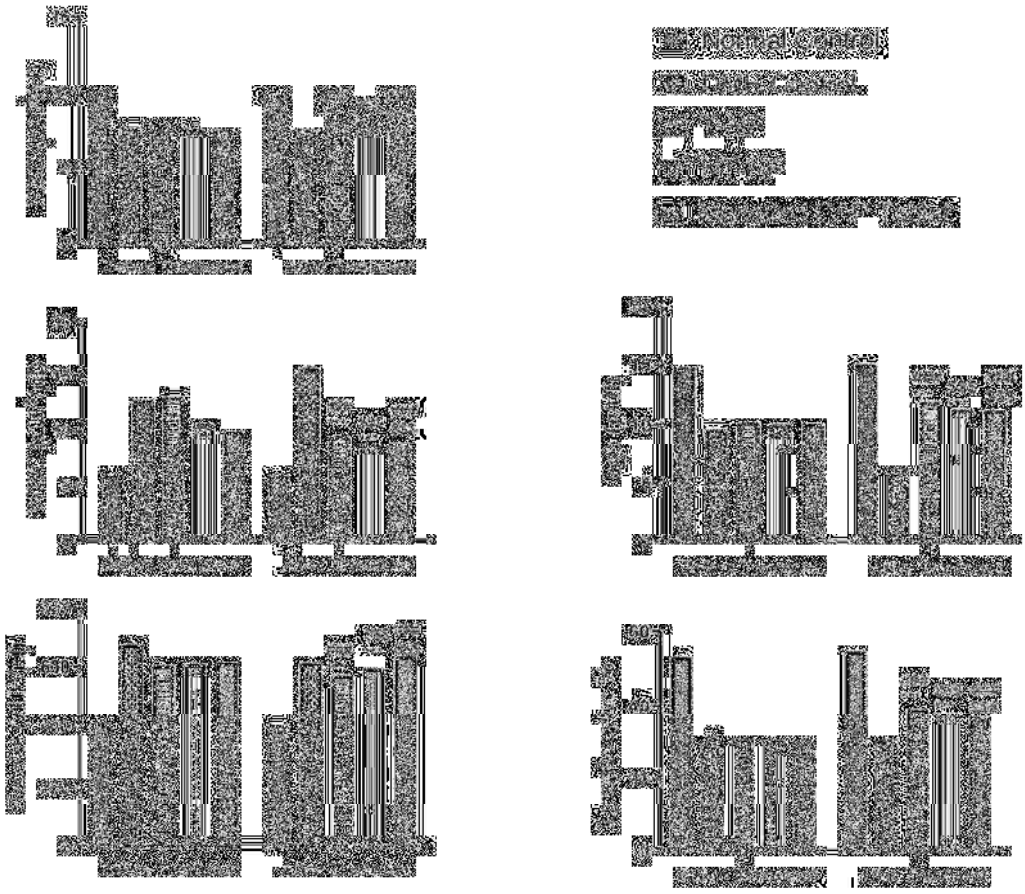

Figure 30: Hematological parameters measured before and after treatment; p^{***} <.001(T-NF *vs* NT-NF), $p^{\#\#\#}$ <.001(T-NF *vs* marketed CAP tablet), p$$$<.001(T-NF *vs* marketed CAP tablet)

4.6 Statistical Evaluation

Experimental results with p-values of <.05 were considered significant. Results are shown as a mean ± SD.

5. DISCUSSION

5.1 CAP and TQ HPLC Method Development

The concomitant identification of TQ and CAP, despite its absence in previous HPLC analyses, necessitated the formulation of a technique to accurately quantify both substances in tandem. Consequently, a pioneering HPLC methodology was devised. The isosbestic point is indicative of the wavelength at which the absorption spectra of two distinct compounds converge, or more precisely, the wavelength at which the molar absorptivity values of the two compounds exhibit parity. The isosbestic point approach is employed for the simultaneous estimation of multiple substances, albeit its application for the estimation of CAP and TQ has not been duly documented. Consequently, the isosbestic point methodology enables the convenient quantification of both CAP and TQ simultaneously, thereby facilitating the subsequent interpretation of the obtained outcomes. To concurrently assess both the critical aggregation concentration (CAP+TQ) a novel RP-HPLC technique was devised, leveraging the concept of isosbestic points. This method has demonstrated commendable precision and reliability in its ability to provide accurate measurements. It has been determined that the values of all validation parameters fall within the permissible range.

5.2 Optimization by point prediction

Based on a meticulously crafted formulation, it meets our criteria for particles of moderate size, possesses a pertinent zero-point charge, and exhibits exceptional efficiency in encapsulating substances, as evidenced by a desirability value approaching unity. This observation underscores the fact that the employed

methodology is both fruitful and highly effective. Ideally, the measure of desirability ought to reside within the numerical range of zero and one. The discovery of a value close to 1 implies the utilization of a robust methodology. Upon conducting an ANOVA on three consecutive responses, denoted as X1 and X2, it was ascertained that the quadratic model effectively captured the essence of the data. This conclusion was derived from the outcomes presented in Table 5. The optimally designed formulation, as assessed based on the criteria of small PS, low PDI, and high EE, has exhibited a preferability value that approaches unity. This suggests that the method's robustness has been effectively utilized through the implementation of a quadratic model via BBD.

5.3 Galactosylation, PNP synthesis, and Eudragit coating

Gal-PLGA, a compound of considerable scientific interest, is meticulously synthesized through a remarkably efficient procedure that involves the covalent attachment of D-galactose units to PLGA. This intricate process imparts hydrophilic properties to the polymer, allowing it to readily dissolve in water under neutral pH conditions. Prior investigations have elucidated that the recently synthesized Gal-PLGA exhibits superior performance concerning hydrosolubility and cell compatibility when compared to PLGA. While previous research has shown that GC exhibits a notable improvement in its ability to target hepatocytes compared to chitosan, this is attributed to the specific interactions between galactose moieties and asialoglycoprotein receptors (76). However, there is a scarcity of studies that investigate the colon-targeting specificity of Gal-PLGA. In recent studies, a multitude of studies have elucidated the potential of galactosylated chitosan (GC) in facilitating the targeted delivery of pharmaceutical agents to activated colonic macrophages,

primarily through the mechanism of galactose receptor-mediated endocytosis. Furthermore, a multitude of scientific investigations have substantiated the notion that galectins, which comprise a group of 15 galactoside-binding proteins found in mammals, exhibit an elevated expression in CRC. These galectins have been found to possess a pivotal function in governing the intricate processes of cancer development, progression, and metastasis. Furthermore, it is worth noting that galectins demonstrate a remarkable propensity for binding to naturally occurring low molecular weight carbohydrates, specifically galactose and lactose. To the utmost extent of our understanding, there exists a dearth of studies documenting the potential of GC as a carrier for CRC targeting, employing the esteemed combination of CAP and TQ. Hydrophilic compounds exhibit suboptimal EE, whereas the double emulsions technique enables the encapsulation of both hydrophobic and hydrophilic pharmaceutical substances. Moreover, this method has proven to yield a more stable synthesis of PNP. The coating agent known as eudragit serves the purpose of safeguarding the NP system against degradation caused by the highly acidic environment of the stomach. Furthermore, it facilitates the controlled release of the drug specifically within the intestinal-colon pathway, thereby enabling precise targeting of the colon. NPs possessing an extended-release profile and an enteric coating have exhibited noteworthy efficacy in effectively delivering their cargo to their designated cellular targets.

5.4 Characterization

5.4.1 Particle size and Entrapment efficiency

In the realm of medication administration, the intricate interplay between cellular absorption, biodistribution, and the delivery process itself necessitates a meticulous examination of NP size, which emerges as a paramount determinant. Particles with dimensions less than 300 nm in size are deemed to be more desirable. Based on the findings of the present investigation, it has been determined that the PNP formulations possessing a particle size below the threshold of 300 nm exhibit the capacity to effectively reach the designated target.

It has been observed that a decrease in Gal-PLGA concentration leads to a reduction in particle size expressed as a percentage of weight per volume. Additionally, it is noted that there is a slight decrease in particle size with increasing PF-127 concentration expressed as a percentage of weight per volume. This phenomenon can potentially be attributed to the fact that a lower concentration of stabilizer diminishes interfacial stability, thereby causing NPs to aggregate when employed in higher concentrations. The presence of C has been observed to exert a direct and consequential negative impact on the functioning of PS, potentially resulting in a decline in its overall performance.

The determination of the impact of a polymer is contingent upon the degree of miscibility exhibited by the drug within the organic phase, as well as the nature of the interaction between the polymer and the drug. Due to the remarkable emulsification properties exhibited by the polymer solution, it possesses the capacity to accommodate the utmost quantity of pharmaceutical substances within its

composition. In a parallel manner, the augmentation of the PF-127 (B) concentration resulted in a corresponding elevation in the percentage of EE. As the concentration of Gal-PLGA (A) was increased, a concomitant increase in the percentage of EE of CAP and TQ was observed. Moreover, the augmentation of C resulted in a notable decline in %EE, primarily attributable to the concomitant diminution in PS.

5.4.2 ZP and PDI

To ascertain the impact of the charge of the negatively charged NPs residing on the surface of a positively charged PNP on both their physical stability and their capacity, an investigation was conducted on the phenomenon known as ZP. Due to the inherent repulsive nature of electric forces between particles of identical charge, it follows that particles possessing high ZP values exhibit remarkable physical stability over extended temporal scales. The ZP of the uncoated NP was determined to be +47.30±0.14. The findings elucidated that the affirmative ZP of CAP-TQ-Gal-PLGANP could be effectively counteracted through the incorporation of Eud S-100, leading to a resultant value of -25.2±0.31. This observation indicates that the presence of a negative charge on Eudragit effectively conceals the positive charge of CAP-TQ-Gal-PLGANP, leading to the formation of Eud-CAP-TQ-Gal-PLGANP.

5.4.3 TEM and SEM study

Upon examination of uncoated NPs, it was observed through TEM that the particles exhibited a spherical morphology, characterized by their smooth and polished surfaces. The potential explanation for the surface roughness observed on the coated NPs may be attributed to the presence of the Eudragit coating. The absence of drug crystals adhering to the surface of the NP may be regarded as an indication of the

effective entrapment of the drug within the NP matrix. Uncoated NPs exhibit a diminished particle size in comparison to their coated counterparts, as substantiated by TEM analysis.

5.4.4 DSC and FTIR

The DSC thermograms of Eud-CAP-TQ-Gal-PLGANP revealed the absence of distinct endothermic peaks associated with the sharp amorphous state of the NP. This observation provides compelling evidence for the entrapment of the drug within the NPs. FTIR spectrum of a composite comprising a pharmaceutical compound and a polymer exhibits negligible discernible changes. This discovery effectively eliminates the potential for any interactions between drugs and polymers.

5.4.5 *In-vitro* drug release

The investigation focused on examining the cumulative percentage of medication release in both coated and uncoated pharmaceutical formulations under different pH conditions. A notable observation can be made regarding the release of medication, wherein over 20% of the administered dosage was discharged within a time frame of 1-2 hours under a pH level of 1.2. This finding suggests that the disintegration of PLGA in acidic environments, brought about by the hydrolysis of ester groups within the polymer chain, exhibited an escalated pace as the pH level increased. This phenomenon was observed specifically in the case of uncoated nanofibers. No discernible traces of medication seepage from the coated NF were observed within 6 hours. Given the propensity of the carboxyl groups within the Eud-S100 polymer to undergo ionization in response to alterations in pH, it has been demonstrated that this particular polymer exhibits remarkable efficacy in facilitating

the targeted delivery of medication to the colon, thereby circumventing the undesirable degradation of said medication within the gastric milieu. Notably, the release of the drug commences at a pH of 7, with a gradual progression resulting in a 20% release after 8 hours. Following 16 hours, the discharge exhibited a consistent pattern, persisting for a maximum span of 24 hours, accounting for 86.4% of the total time.

5.5 Colloidal stability

Following 6 months in storage at a temperature of 40°C, it was observed that the phase separation and visual clarity of the Eud-CAP-TQ-PLGANPs remained unchanged, as depicted in Figure 19. The observed alterations in particle size (PS) during the freezing stage, specifically from 183nm to 181nm, can be considered inconsequential. Furthermore, the %EE consistently remained above 75% and within acceptable limits when stored at temperatures of 4°C and -20°C. However, it is noteworthy that a negligible change in both PS and %EE when stored at 25°C, which suggests a certain degree of instability in these conditions. Based on the findings of stability studies, it has been determined that Eud-CAP-TQ-Gal-PLGANP exhibited a remarkable level of stability under varying temperature conditions, specifically refrigeration at 4°C and freezing at -20°C. Notably, no observable alterations were detected, indicating the robustness of this compound.

5.6 **MTT assay**

Performing the computation of the IC_{50} value. Illustration 20 exhibits the comprehensive array of categorized ratings. As a result of their exceptional performance, the research team has chosen CAP+TQ, NT-NF, and T-NF as the

subjects for further investigation and subsequent comparative analysis. An MTT experiment was conducted on the HT-29 cancer cell lines to ascertain the cellular toxicity of CAP+TQ, NT-NF, and T-NF. The employed targeted nano framework has proven to be efficacious, as exemplified in the visual representation depicted in Figure 20. At a concentration of 3.125µg/mL, the compound T-NF exhibited a cell survival rate of 57%, while both NT-NF and CAP TQ demonstrated comparable efficacy with survival rates of 64% and 75% respectively. At a concentration of 50µg/ml, the viability of T-NF cells decreased to less than 30%, indicating a significant cytotoxic impact of the medication derived from NP. This cytotoxic effect has the potential to enhance the therapeutic efficacy of the treatment. In contrast to non-specific delivery methods, the targeted administration of drugs through a galectin-mediated capacity of T-NF results in enhanced drug accumulation. This is supported by the observed augmentation in cellular toxicity of T-NF specifically in cell lines that overexpress galectin (77).

5.6.1 ROS and MMP

The cellular concentration of ROS serves as a pivotal determinant in discerning the successful intracellular penetration of the drug via NP delivery. The untreated group (NC) exhibited minimal amelioration, with any observed progress being ascribed solely to suboptimal cultural circumstances. The exposure to NP has resulted in a discernible enhancement. Tremendous advancements were observed in the T-NF cohort in contrast to the remaining groups. It is plausible to posit a potential association between the number of NPs internalized by cellular entities and the subsequent escalation in ROS amplification, thereby instigating the process of programmed cell death, known as apoptosis.

When cellular production of matrix metalloproteinase ceases, it serves as an initial indication of the onset of apoptosis. The quantification of MMP depletion within cellular structures was conducted at a concentration of 8µg/mL. Subsequently, the impacts of CAP+TQ, NT-NF, and T-NF were meticulously examined and evaluated. In contrast to the other experimental cohorts, the treated group denoted as T-NF exhibited a noteworthy decrease in green fluorescence after an extended period of incubation, as visually depicted in Figure 22. This observation strongly suggests the occurrence of a collapse in MMP under investigation. It is widely acknowledged that the occurrence of mitochondrial dysfunction gives rise to caspase pathways, thereby triggering apoptotic cell death. This process entails the swift depletion of MMP, expansion of organelles, and the liberation of cytochrome C.

5.6.2 Caspase -3-activity and DAPI assay

One notable biomarker that warrants attention is caspase-3, the protease that is frequently activated in the intricate process of cellular apoptosis. Upon being conjoined with cellular DNA, the aforementioned reagent undergoes luminescence after its activation by caspase within apoptotic cells. In stark juxtaposition to the NT-NF and CAP+TQ cohorts, the empirical evidence presented indicates that the T-NF group exhibited elevated levels of caspase activity. This observation implies that the administration of antioxidants augments the process of apoptosis triggered by the pharmacological intervention.

DAPI labeling was employed to determine the presence or absence of apoptosis induced by T-NF. No discernible modifications were observed in the cellular composition or physical form of the cells that were not subjected to any form of treatment. Nevertheless, subsequent exposure to CAP+TQ resulted in a mere fraction of cells exhibiting chromatin condensation and cellular shrinkage. In the

context of comparing NT-NF and T-NF, it is noteworthy to observe that T-NF exhibited a greater manifestation of nuclear fragmentation, chromatin condensation, and blebbing of the nucleus in association with the process of apoptosis.

5.6.3 Apoptosis assay

When a cellular entity undergoes the process of self-destruction, it exhibits discernible alterations in both its nuclear and cytoplasmic components, characterized by distinct morphological and biochemical modifications. We employed the Annexin V-FITC/PI labeling technique to ascertain cellular viability and discern the preliminary and advanced phases of apoptosis, alongside the occurrence of necrosis. The observed decrease in cellular viability and the elevated occurrence of early and late apoptosis within the targeted group, in comparison to the other treatment groups, suggests the initiation of cellular demise as a result of heightened intracellular absorption and controlled discharge of the drug from the NPs. Remarkably, T-NF exhibited exceptional apoptotic capabilities.

5.7 Rat *in-vivo* efficacy findings

An investigation into acute oral toxicity prompted the exploration of an elevated dosage for administration. The disparity in body weight between the CRC-induced rats and the healthy controls was evident, as was the observation that the CRC-induced rats exhibited reduced consumption of food and water in comparison to both their transgenic and nontransgenic counterparts. The animals within the cohort administered the commercial tablet experienced a reduction in body mass due to the deleterious effects associated with the tablet, thereby diminishing their prospects of survival. The graphical representation in Figure 26 showcases the comparative analysis of survival rates among the five distinct groups. Furthermore, the collected data was juxtaposed with a previous study conducted on the subject of colorectal

cancer using CAP-loaded lipid NP (78). All groups that were induced by DMH exhibited clear indications of the development of ACF. Rats that were administered with DMH exhibited a notable augmentation in the occurrence of ACF specifically within the distal portion of their colon. Upon juxtaposing the cohort of T-NF-treated rodents with their counterparts who received DMH injections alongside other treated groups, a discernible decrease in both the generation and cumulative quantity of ACF was observed. In the experimental cohort, there was a conspicuous absence of any discernible manifestation of ACF formation. Notwithstanding the observed decrease in the abundance of ACF, it is noteworthy that the administered tablet continued to elicit a surge in adverse effects among the animal subjects, including but not limited to gastrointestinal distress, emesis, and cutaneous inflammation. The DMH control group exhibited a notable augmentation in the quantity of white blood cells (WBCs) and platelets. However, a marginal decline was observed in the count of red blood cells (RBCs), lymphocytes, and the concentration of hemoglobin (Hgb). The potential presence of carcinogenic oxidative stress within lymphocytes derived from DMH could potentially elucidate the underlying causation for the observed hematological abnormalities. Following a course of therapy involving the CAP and TQ, it was observed that normal values were either attained or in the process of being achieved. As a consequence of cancer therapy, there is a reduction in the number of lymphocytes observed. Significant enhancements in blood parameters were noted for the NT-NF, T-NF, and commercially treated CAP tablet cohorts, as compared to the DMH control group. The aforementioned findings provide further support to the in-vitro cell line investigations, which have demonstrated that T-NF exhibits a notable capacity to augment oral bioavailability and exert anti-colon cancer effects.

6. SUMMARY

Due to TQ's multitargeting capacity and CAP's promising pharmacological potential, it is an excellent therapeutic candidate for treating CRC. However, significant challenges in designing a formulation were presented by its poor solubility, instability, and oral bioavailability. To improve their efficacy in treating CRC, researchers have considered administering NPs of CAP and TQ together via oral administration. This research aimed to create and study the efficacy of a CAP and TQ-loaded functionalized NF for the management of CRC.

Through galactose receptor-mediated endocytosis, Gal- PLGA can transport medicines to activated colonic macrophages. For CRC treatment, functionalized NF was developed and tested. Numerous studies indicated that galectin is overexpressed in CRC and regulates its development and spread because it has a strong affinity for natural small sugars like galactose, allowing CRC to be targeted. Also, the absorption of Poloxamers (PF-127) onto hydrophobic drug carriers slows their clearance from the bloodstream. In the context of precise and prolonged medication administration, this is of paramount importance. Hydrophilic surfaces with lower surface charge created by the adsorption of Poloxamers onto hydrophobic particles allow for longer circulation in the plasma by preventing the adsorption of opsonins.

To quantitatively assess CAP and TQ in PNPs, an isosbestic point-based R-HPLC method was designed and validated following ICH recommendations. Using a solvent evaporation approach followed by probe sonication, drug-loaded NP was successfully synthesized. To find the optimal PNP we employed a factorial design strategy and analyzed all nine possible iterations with the help of the Design-Expert program. The gathered data was used to test many polynomial models, and the best-fit

model was chosen using several statistical criteria. The Design-Expert program generated contour and response surface plots that graphically displayed the interplay between the explanatory and dependent variables. The highest entrapment effectiveness and smallest particle size led to the selection of the optimized batch of PNP. PS, PDI, and ZP were all measured with a zeta sizer for the PNP. TEM and SEM studies verified the PNP's expected surface shape. FTIR and DSC analyses verified the drug's characterization and its compatibility with various excipients. Gal-PLGA was proven to have formed by HNMR analysis. The Eudragit-S100 coating on the optimized PFPNP served to protect the medicine when it was introduced into an acidic solution. For 6 months, the Eud-CAP-TQ-Gal-PLGANP was stored at 25, 4, and -20°C, where its particle size, PDI, ZP, and drug release were studied.

The MTT assay determined whether or not the targeted NF was cytotoxic to HT-29 cell lines in vitro. The combined CAP+TQ and NT-NF showed lower antitumor activity than T-NF. Both qualitative and quantitative cell uptake studies corroborated the cytotoxicity findings observed in vitro. The nuclear alterations in treated HT9 cells were seen using a DAPI staining test.

According to OECD rules 423, acute oral toxicity was done on T-NF's composition, and the results showed that it was non-harmful to male Wistar rats at the administered dose. Oral administration of the formulated T-NF was found to be safe in the study. Histopathological analysis of treated colon tissues of Wistar rats revealed substantial tumor necrosis following treatment with T-NF, and the anti-cancer investigation showed that oral administration of T-NF into CRC-induced animals resulted in tumor regression. Targeted NF has been proposed as a possible targeted medication delivery strategy via oral administration based on the results of *in vitro* and *in vivo* research.

7. CONCLUSION

In the current research endeavor, a concerted effort was made to enhance the effectiveness of CRC therapy through the utilization of a groundbreaking PNP, in conjunction with CAP and TQ. PNP was effectively formulated and optimized through BBD factorial design. The optimized PNP9 exhibits favorable characteristics such as desirable particle size and enhanced entrapment efficiency. These attributes are attributed to the specific ratio of PF-127 and Gal-PLGA. The process of Galactosylation has proven to be efficacious in producing functionalized PLGA with notable advantages in terms of its ability to target CRC.

The PNP was subjected to optimization techniques to enhance its efficiency, and subsequently coated with Eud-S-100 to provide a protective barrier against the acidic conditions prevalent in the stomach, thereby safeguarding the drug. FTIR and DSC investigations have effectively showcased the encapsulation of CAP and TQ within the PNPs, thereby affirming their successful integration. TEM and SEM examination conducted on the PNP unveiled a distinctive morphology characterized by a spherical configuration. The in vitro drug release analysis conducted for PNP has revealed a biphasic burst release pattern, wherein the release mechanism is predominantly governed by diffusion control throughout 24 h. The coated NPs exhibited controlled drug release at a pH of 7, whereas the uncoated NPs displayed an abrupt drug release under acidic conditions. The results of the MTT and cell uptake experiments demonstrated a notable enhancement in the internalization of T-NF within HT-29 cells when compared to the unbound forms of CAP+ TQ and NT-NF. The results of the qualitative and quantitative analyses of cell uptake have demonstrated that T-NF, as a drug delivery system, exhibits a notable efficacy in

inducing cytotoxic effects specifically in HT-29 cells.

Based on the research conducted on male Wistar rats, the investigation sought to ascertain the safe dosage of the treatment for acute oral toxicity. The histopathological evaluation provided evidence of the biocompatibility of the developed T-NF. This information was further corroborated by the histopathological results score. The *in-vivo* investigation of the anticancer properties of T-NF has revealed promising therapeutic potential in the context of DMH-induced animals. Fundamentally, the application of an intricately crafted PNP system exhibits substantial potential in the domain of averting and managing CRC through the utilization of TQ, which has demonstrated encouraging synergistic outcomes with CAP. Additional investigations utilizing sophisticated preclinical models are imperative to substantiate the effectiveness of this particular formulation for the treatment of the same.

8. BIBLIOGRAPHY

1. Hossain MS, Karuniawati H, Jairoun AA, Urbi Z, Ooi DJ, John A, et al. Colorectal cancer: a review of carcinogenesis, global epidemiology, current challenges, risk factors, preventive and treatment strategies. Cancers. 2022;14(7):1732.
2. Xie YH, Chen YX, Fang JY. Comprehensive review of targeted therapy for colorectal cancer. Signal transduction and targeted therapy. 2020;5(1):22.
3. Rasool M, Malik A, Waquar S, Arooj M, Zahid S, Asif M, et al. New challenges in the use of nanomedicine in cancer therapy. Bioengineered. 2022;13(1):759–73.
4. Adhikari C. Polymer nanoparticles-preparations, applications and future insights: A concise review. Polymer-plastics technology and materials. 2021;60(18):1996–2024.
5. Rizi HAY, Shin DH, Rizi SY. Polymeric nanoparticles in cancer chemotherapy: a narrative review. Iranian journal of public health. 2022;51(2):226.
6. Khan MA, Tania M, Fu S, Fu J. Thymoquinone, as an anticancer molecule: from basic research to clinical investigation. Oncotarget. 2017;8(31):51907.
7. Almajali B, Al-Jamal HAN, Taib WRW, Ismail I, Johan MF, Doolaanea AA, et al. Thymoquinone, as a novel therapeutic candidate of cancers. Pharmaceuticals. 2021;14(4):369.
8. Norwood AA, Tan M, May M, Tucci M, Benghuzzi H. Comparison of potential chemotherapeutic agents, 5-fluoruracil, green tea, and thymoquinone on colon cancer cells. Biomedical sciences instrumentation. 2006;42:350–6.

9. Fatfat M, Fakhoury I, Habli Z, Mismar R, Gali-Muhtasib H. Thymoquinone enhances the anticancer activity of doxorubicin against adult T-cell leukemia in vitro and in vivo through ROS-dependent mechanisms. Life sciences. 2019;232:116628.
10. Jafri SH, Glass J, Shi R, Zhang S, Prince M, Kleiner-Hancock H. Thymoquinone and cisplatin as a therapeutic combination in lung cancer: In vitro and in vivo. Journal of Experimental & Clinical Cancer Research. 2010;29(1):1–11.
11. Odeh F, Ismail SI, Abu-Dahab R, Mahmoud IS, Al Bawab A. Thymoquinone in liposomes: a study of loading efficiency and biological activity towards breast cancer. Drug delivery. 2012;19(8):371–7.
12. Upadhyay P, Sarker S, Ghosh A, Gupta P, Das S, Ahir M, et al. Transferrin-decorated thymoquinone-loaded PEG-PLGA nanoparticles exhibit anticarcinogenic effect in non-small cell lung carcinoma via the modulation of miR-34a and miR-16. Biomaterials science. 2019;7(10):4325–44.
13. Odeh LH, Talib WH, Basheti IA. Synergistic effect of thymoquinone and melatonin against breast cancer implanted in mice. Journal of cancer research and therapeutics. 2018;14(Suppl 2):S324–30.
14. McKendrick J, Coutsouvelis J. Capecitabine: effective oral fluoropyrimidine chemotherapy. Expert Opinion on Pharmacotherapy. 2005;6(7):1231–9.
15. Walko CM, Lindley C. Capecitabine: a review. Clinical therapeutics. 2005;27(1):23–44.
16. Choi DR, Yoon SN, Kim HS, Kim JH, Kim KY, Kim BC, et al. A phase II study of capecitabine and oral leucovorin as a third-line chemotherapy in

patients with metastatic colorectal cancer. Cancer chemotherapy and pharmacology. 2015;75:639–43.

17. Tiwari G, Tiwari R, Wal P, Wal A, Rai AK. Primary and novel approaches for colon targeted drug delivery-A review. International Journal of Drug Delivery. 2010;2(1).
18. Kolte BP. Colon targeted drug delivery system-a novel perspective. Asian journal of biomedical and pharmaceutical sciences. 2012;2(14):21.
19. Basit AW. Advances in colonic drug delivery. Drugs. 2005;65:1991–2007.
20. Banerjee A, Pathak S, Subramanium VD, Dharanivasan G, Murugesan R, Verma RS. Strategies for targeted drug delivery in treatment of colon cancer: current trends and future perspectives. Drug discovery today. 2017;22(8):1224–32.
21. Amidon S, Brown JE, Dave VS. Colon-targeted oral drug delivery systems: design trends and approaches. Aaps Pharmscitech. 2015;16:731–41.
22. Chourasia MK, Jain SK. Design and development of multiparticulate system for targeted drug delivery to colon. Drug delivery. 2004;11(3):201–7.
23. Ghorab DM, Amin MM, Khowessah OM, Tadros MI. Colon-targeted celecoxib-loaded Eudragit® S100-coated poly-ϵ-caprolactone microparticles: Preparation, characterization and in vivo evaluation in rats. Drug delivery. 2011;18(7):523–35.
24. Mehta R, Chawla A, Sharma P, Pawar P. Formulation and in vitro evaluation of Eudragit S-100 coated naproxen matrix tablets for colon-targeted drug delivery system. Journal of advanced pharmaceutical technology & research. 2013;4(1):31.

25. Tsai SW, Yu DS, Tsao SW, Hsu FY. Hyaluronan–cisplatin conjugate nanoparticles embedded in Eudragit S100-coated pectin/alginate microbeads for colon drug delivery. International Journal of Nanomedicine. 2013;2399–407.

26. Thiruppathi R, Mishra S, Ganapathy M, Padmanabhan P, Gulyás B. Nanoparticle functionalization and its potentials for molecular imaging. Advanced Science. 2017;4(3):1600279.

27. Zhang D, Tao L, Zhao H, Yuan H, Lan M. A functional drug delivery platform for targeting and imaging cancer cells based on Pluronic F127. Journal of Biomaterials Science, Polymer Edition. 2015;26(8):468–82.

28. Chung YI, Kim JC, Kim YH, Tae G, Lee SY, Kim K, et al. The effect of surface functionalization of PLGA nanoparticles by heparin-or chitosan-conjugated Pluronic on tumor targeting. Journal of controlled release. 2010;143(3):374–82.

29. Kim JY, Choi WI, Kim YH, Tae G, Lee SY, Kim K, et al. In-vivo tumor targeting of pluronic-based nano-carriers. Journal of Controlled Release. 2010;147(1):109–17.

30. Hu Q, Liang B, Sun Y, Guo XL, Bao YJ, Xie DH, et al. Preparation of bufalin-loaded pluronic polyetherimide nanoparticles, cellular uptake, distribution, and effect on colorectal cancer. International Journal of Nanomedicine. 2014;4035–41.

31. Yang YC, Cai J, Yin J, Zhang J, Wang KL, Zhang ZT. Heparin-functionalized Pluronic nanoparticles to enhance the antitumor efficacy of sorafenib in gastric cancers. Carbohydrate polymers. 2016;136:782–90.

32. Yu J, Qiu H, Yin S, Wang H, Li Y. Polymeric drug delivery system based on pluronics for cancer treatment. Molecules. 2021;26(12):3610.

33. Hosseinzadeh H, Atyabi F, Dinarvand R, Ostad SN. Chitosan–Pluronic nanoparticles as oral delivery of anticancer gemcitabine: preparation and in vitro study. International journal of nanomedicine. 2012;1851–63.

34. Pitto-Barry A, Barry NP. Pluronic® block-copolymers in medicine: from chemical and biological versatility to rationalisation and clinical advances. Polymer Chemistry. 2014;5(10):3291–7.

35. RAIKAR PR, DANDAGI PM. FUNCTIONALIZED POLYMERIC NANOPARTICLES: A NOVEL TARGETED APPROACH FOR ONCOLOGY CARE. Int J App Pharm. 2021;13(6):1–18.

36. Masood F. Polymeric nanoparticles for targeted drug delivery system for cancer therapy. Materials Science and Engineering: C. 2016;60:569–78.

37. Madej M, Kurowska N, Strzalka-Mrozik B. Polymeric nanoparticles—tools in a drug delivery system in selected cancer therapies. Applied Sciences. 2022;12(19):9479.

38. Salari N, Faraji F, Torghabeh FM, Faraji F, Mansouri K, Abam F, et al. Polymer-based drug delivery systems for anticancer drugs: A systematic review. Cancer Treatment and Research Communications. 2022;100605.

39. Rezvantalab S, Drude NI, Moraveji MK, Güvener N, Koons EK, Shi Y, et al. PLGA-based nanoparticles in cancer treatment. Frontiers in pharmacology. 2018;9:1260.

40. Alibolandi M, Amel Farzad S, Mohammadi M, Abnous K, Taghdisi SM, Kalalinia F, et al. Tetrac-decorated chitosan-coated PLGA nanoparticles as a

new platform for targeted delivery of SN38. Artificial cells, nanomedicine, and biotechnology. 2018;46(sup2):1003–14.

41. Ruirui Z, He J, Xu X, Li S, Peng H, Deng Z, et al. PLGA-based drug delivery system for combined therapy of cancer: Research progress. Materials Research Express. 2021;8(12):122002.
42. Nicolas J, Mura S, Brambilla D, Mackiewicz N, Couvreur P. Design, functionalization strategies and biomedical applications of targeted biodegradable/biocompatible polymer-based nanocarriers for drug delivery. Chemical Society Reviews. 2013;42(3):1147–235.
43. Choudhury H, Gorain B, Pandey M, Khurana RK, Kesharwani P. Strategizing biodegradable polymeric nanoparticles to cross the biological barriers for cancer targeting. International journal of pharmaceutics. 2019;565:509–22.
44. Jahan ST, Sadat S, Walliser M, Haddadi A. Targeted therapeutic nanoparticles: an immense promise to fight against cancer. Journal of drug delivery. 2017;2017.
45. Gad A, Kydd J, Piel B, Rai P. Targeting cancer using polymeric nanoparticle mediated combination chemotherapy. International journal of nanomedicine and nanosurgery. 2016;2(3).
46. Parveen S, Sahoo SK. Polymeric nanoparticles for cancer therapy. Journal of drug targeting. 2008;16(2):108–23.
47. Hirsch BR, Zafar SY. Capecitabine in the management of colorectal cancer. Cancer management and research. 2011;79–89.
48. Xue-Hui C, Zhang-Qi F, Qian X, Jiang-Qiang X, Xian-Wen Y, Xi-Tai S. Fabrication and evaluation of SDF-1 loaded galactosylated chitosan

nanoparticles for liver targeting. Materials Research Express. 2017;4(3):035028.

49. Ramzy L, Metwally AA, Nasr M, Awad GA. Novel thymoquinone lipidic core nanocapsules with anisamide-polymethacrylate shell for colon cancer cells overexpressing sigma receptors. Scientific reports. 2020;10(1):10987.
50. Siu FY, Ye S, Lin H, Li S. Galactosylated PLGA nanoparticles for the oral delivery of resveratrol: enhanced bioavailability and in vitro anti-inflammatory activity. International journal of nanomedicine. 2018;4133–44.
51. Wu P, Zhou Q, Zhu H, Zhuang Y, Bao J. Enhanced antitumor efficacy in colon cancer using EGF functionalized PLGA nanoparticles loaded with 5-Fluorouracil and perfluorocarbon. BMC cancer. 2020;20:1–10.
52. Jena G, Niranjan PC, Dixit P. Cytotoxicity and pharmacokinetic studies of PLGA based capecitabine loaded nanoparticles. Indian Journal of Pharmaceutical Education and Research. 2020;54(2):349–56.
53. Rahman Z, Kohli K, Zhang SQ, Khar RK, Ali M, Charoo NA, et al. In-vivo evaluation in rats of colon-specific microspheres containing 5-fluorouracil. Journal of Pharmacy and Pharmacology. 2008;60(5):615–23.
54. Kumar S, Lather V, Pandita D. Stability indicating simplified HPLC method for simultaneous analysis of resveratrol and quercetin in nanoparticles and human plasma. Food chemistry. 2016;197:959–64.
55. Ahmad A, Khan RMA, Alkharfy KM. Development and validation of RP-HPLC method for simultaneous estimation of glibenclamide and thymoquinone in rat plasma and its application to pharmacokinetics. Acta Chromatographica. 2015;27(3):435–48.

56. Ibrahim H, Hamdy AM, Merey HA, Saad AS. Dual-mode gradient HPLC and TLC densitometry methods for the simultaneous determination of paracetamol and methionine in the presence of paracetamol impurities. Journal of AOAC International. 2021;104(4):975–82.

57. Venugopal V, Kumar KJ, Muralidharan S, Parasuraman S, Raj PV, Kumar KV. Optimization and in-vivo evaluation of isradipine nanoparticles using Box-Behnken design surface response methodology. OpenNano. 2016;1:1–15.

58. Hasan-Nasab B, Ebrahimnejad P, Ebrahimi P, Sharifi F, Salili M, Shahlaee F, et al. A promising targeting system to enrich irinotecan antitumor efficacy: Folic acid targeted nanoparticles. Journal of Drug Delivery Science and Technology. 2021;63:102543.

59. Jain A, Kesharwani P, Garg NK, Jain A, Jain SA, Jain AK, et al. Galactose engineered solid lipid nanoparticles for targeted delivery of doxorubicin. Colloids and Surfaces B: Biointerfaces. 2015;134:47–58.

60. Mistry NP, Desai JL, Thakkar HP. Formulation and evaluation of tacrolimus-loaded galactosylated poly (lactic-co-glycolic acid) nanoparticles for liver targeting. Journal of Pharmacy and Pharmacology. 2015;67(10):1337–48.

61. Raish M, Kalam MA, Ahmad A, Shahid M, Ansari MA, Ahad A, et al. Eudragit-Coated Sporopollenin Exine Microcapsules (SEMC) of Phoenix dactylifera L. of 5-Fluorouracil for Colon-Specific Drug Delivery. Pharmaceutics. 2021;13(11):1921.

62. Badran MM, Mady MM, Ghannam MM, Shakeel F. Preparation and characterization of polymeric nanoparticles surface modified with chitosan for target treatment of colorectal cancer. International journal of biological macromolecules. 2017;95:643–9.

63. Anwer MK, Al-Shdefat R, Ezzeldin E, Alshahrani SM, Alshetaili AS, Iqbal M. Preparation, evaluation and bioavailability studies of eudragit coated PLGA nanoparticles for sustained release of eluxadoline for the treatment of irritable bowel syndrome. Frontiers in pharmacology. 2017;8:844.

64. Jeswani G, Chablani L, Gupta U, Sahoo RK, Nakhate KT. Development and optimization of paclitaxel loaded Eudragit/PLGA nanoparticles by simplex lattice mixture design: Exploration of improved hemocompatibility and in vivo kinetics. Biomedicine & Pharmacotherapy. 2021;144:112286.

65. Sunoqrot S, Abujamous L. pH-sensitive polymeric nanoparticles of quercetin as a potential colon cancer-targeted nanomedicine. Journal of Drug Delivery Science and Technology. 2019;52:670–6.

66. Subudhi MB, Jain A, Jain A, Hurkat P, Shilpi S, Gulbake A, et al. Eudragit S100 coated citrus pectin nanoparticles for colon targeting of 5-fluorouracil. Materials. 2015;8(3):832–49.

67. Alshehri S, Imam SS, Rizwanullah M, Fakhri KU, Rizvi MMA, Mahdi W, et al. Effect of chitosan coating on PLGA nanoparticles for oral delivery of thymoquinone: In vitro, ex vivo, and cancer cell line assessments. Coatings. 2020;11(1):6.

68. Li C, Wang Y, Zhang H, Li M, Zhu Z, Xue Y. An investigation on the cytotoxicity and caspase-mediated apoptotic effect of biologically synthesized gold nanoparticles using Cardiospermum halicacabum on AGS gastric carcinoma cells. International journal of nanomedicine. 2019;951–62.

69. Lipnick RL, Cotruvo JA, Hill RN, Bruce RD, Stitzel KA, Walker AP, et al. Comparison of the up-and-down, conventional LD50, and fixed-dose acute toxicity procedures. Food and chemical toxicology. 1995;33(3):223–31.

70. Chivate AN, Salve PS, Doijad RC, Mane AM, Chivate ND. Acute Toxicity Study of Intravenously Administered Capecitabine Resealed Erythrocytes in Mice. Research Journal of Pharmacy and Technology. 2022;15(12):5473–7.
71. Nag S, Das Saha K. Chitosan-decorated PLGA-NPs loaded with tannic acid/vitamin E mitigate colon cancer via the NF-κB/β-Cat/EMT pathway. ACS omega. 2021;6(43):28752–69.
72. Al Moubarak A, El Joumaa M, Slika L, Patra D, Borjac J. Curcumin-Polyallyhydrocarbon nanocapsules potently suppress 1, 2-dimethylhydrazine-induced colorectal cancer in mice by inhibiting Wnt/β-catenin pathway. BioNanoScience. 2021;11:518–25.
73. Jia XD, Han C. Chemoprevention of tea on colorectal cancer induced by dimethylhydrazine in Wistar rats. World Journal of Gastroenterology. 2000;6(5):699.
74. Wang Y, Jin HY, Fang MZ, Wang XF, Chen H, Huang SL, et al. Epigallocatechin gallate inhibits dimethylhydrazine-induced colorectal cancer in rats. World journal of gastroenterology. 2020;26(17):2064.
75. Bekusova VV, Patsanovskii VM, Nozdrachev AD, Trashkov AP, Artemenko MR, Anisimov VN. Metformin prevents hormonal and metabolic disturbances and 1, 2-dimethylhydrazine-induced colon carcinogenesis in non-diabetic rats. Cancer Biology & Medicine. 2017;14(1):100.
76. Zheng D, Duan C, Zhang D, Jia L, Liu G, Liu Y, et al. Galactosylated chitosan nanoparticles for hepatocyte-targeted delivery of oridonin. International Journal of Pharmaceutics. 2012;436(1–2):379–86.

77. Cousin JM, Cloninger MJ. The role of galectin-1 in cancer progression, and synthetic multivalent systems for the study of galectin-1. International journal of molecular sciences. 2016;17(9):1566.

78. Dudhipala N, Puchchakayala G. Capecitabine lipid nanoparticles for anti-colon cancer activity in 1, 2-dimethylhydrazine-induced colon cancer: preparation, cytotoxic, pharmacokinetic, and pathological evaluation. Drug development and industrial pharmacy. 2018;44(10):1572–82.

ANNEXURES

A.ANIMAL ETHICAL CLEARANCE LETTER

KLE College of Pharmacy
A Constituent Unit of
KLE Academy of Higher Education and Research
(Deemed to be University)
DEPARTMENT OF PHARMACOLOGY
JNMC Campus, Nehru Nagar, Belagavi – 590 010, Karnataka, India

BELAGAVI

INSTITUTIONAL ANIMAL ETHICS COMMITTEE
Reg.No.221/Po/Re/S/2000/CPCSEA

CERTIFICATE

Date: 17/03/2021

This is to certify that the project proposal no ...11.... entitled," Pluronic polymer functionalized nanoparticles loaded Capecitabine and Thymoquinone for targeting colorectal cancer: An experimental study" submitted by Dr./ Mr./ Ms., Prasiddhi R. Raikar under the guidance of Prof. (Dr.) P.M. Dandagi has been approved/recommended by the IAEC of KLE College of Pharmacy, Belagavi, Reg.No.221/Po/Re/S/2000/CPCSEA in its meeting dated 13/03/2021, resolution No. 30 has been sanctioned .....71..... Rats/ Mice/ Rabbits/Guinea pig (animals) sex ---male--- under this proposal for a duration of next.....months.

You are hereby informed to strictly adhere to the protocol submitted for approval. Further you are required to keep the account of animals used for the project in specified Performa, Form D.

Authorized by	Name	Signature	Date
Member Secretary:	Dr. N.A. Khatib	Institutional Animal E... KLES's College of Pharmacy, BELGAUM - 590010	17/03/2021
Main Nominee of CPCSEA:	Dr. Vinod Kumar C	CPCSEA Nominee Institutional Animal Ethics Committee KLES's College of Pharmacy, BELGAUM.	17-3-2021

B. PUBLICATIONS AND POSTER CERTIFICATES

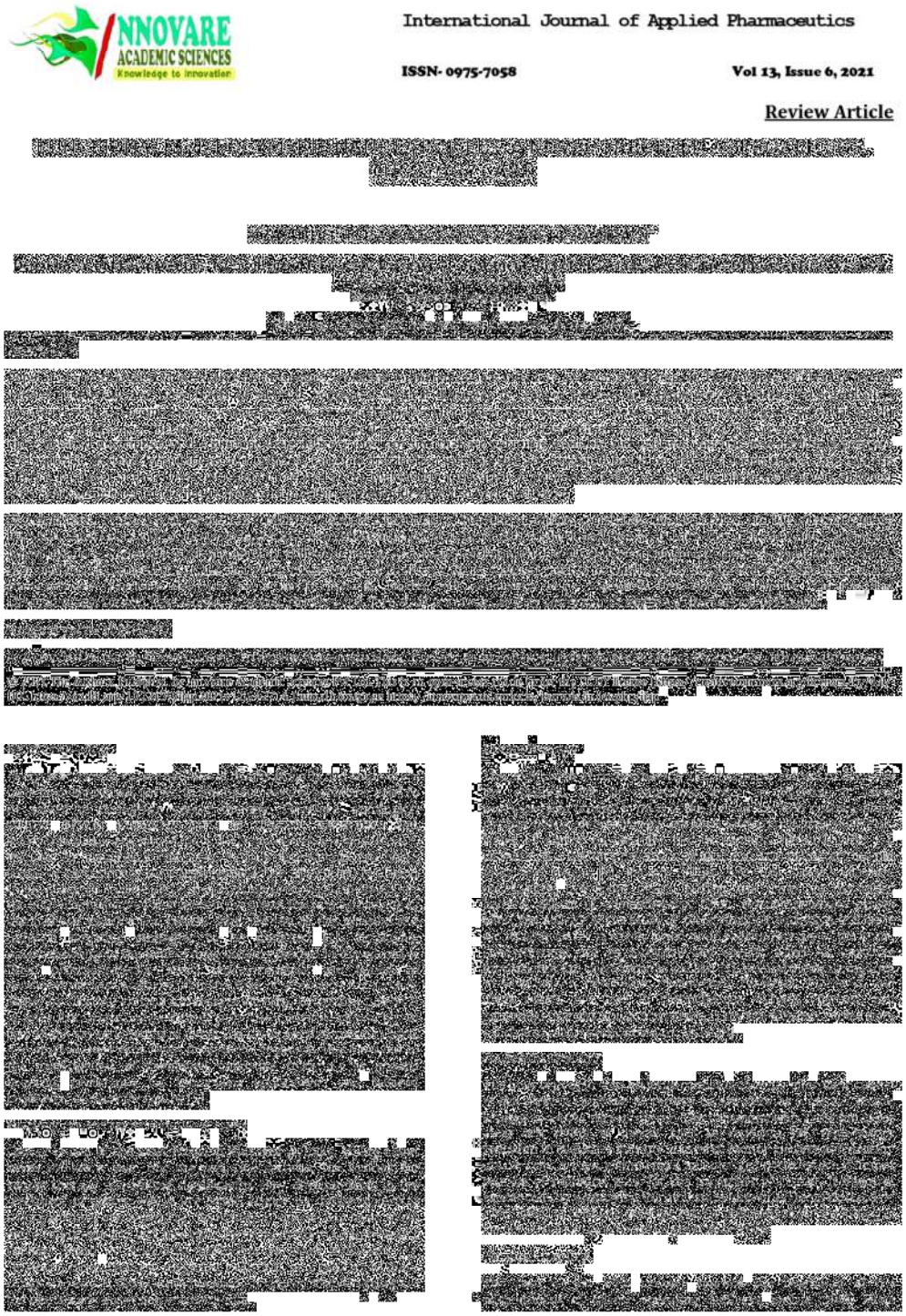

medications, for example, chemotherapy, radiation, or surgery. Many clinical experiments are ongoing to test the use of PDT for different forms of cancer [23]. The only way to be able to use nanoparticles as a photo-sensitizing carrier is to meet *al.* l of the needs of an optimal PDT agent [24].

Laser therapy

Lasers are most widely used for cancers and precancerous development to shrink or kill. The most prevalent application with laser therapy is peripheral disorders, including cancer of the skin of basal cells in the very early stages of multiple cancers, such as non-small cell lung cancer, vulvar, ovarian, penile, and cervical cancer. Laser therapy can also mitigate various signs of cancer, such as bleeding or obstruction. In combination with various other therapies, including surgery, chemotherapy, or radiation therapy, laser therapy can be used. Furthermore, laser treatment can be used to scan the lymph vessels to reduce swelling and minimize the metastasis for tumor cells [25]. Three types of laser are used more

Fig. 1: Biomedical applications of nanotherapeutics

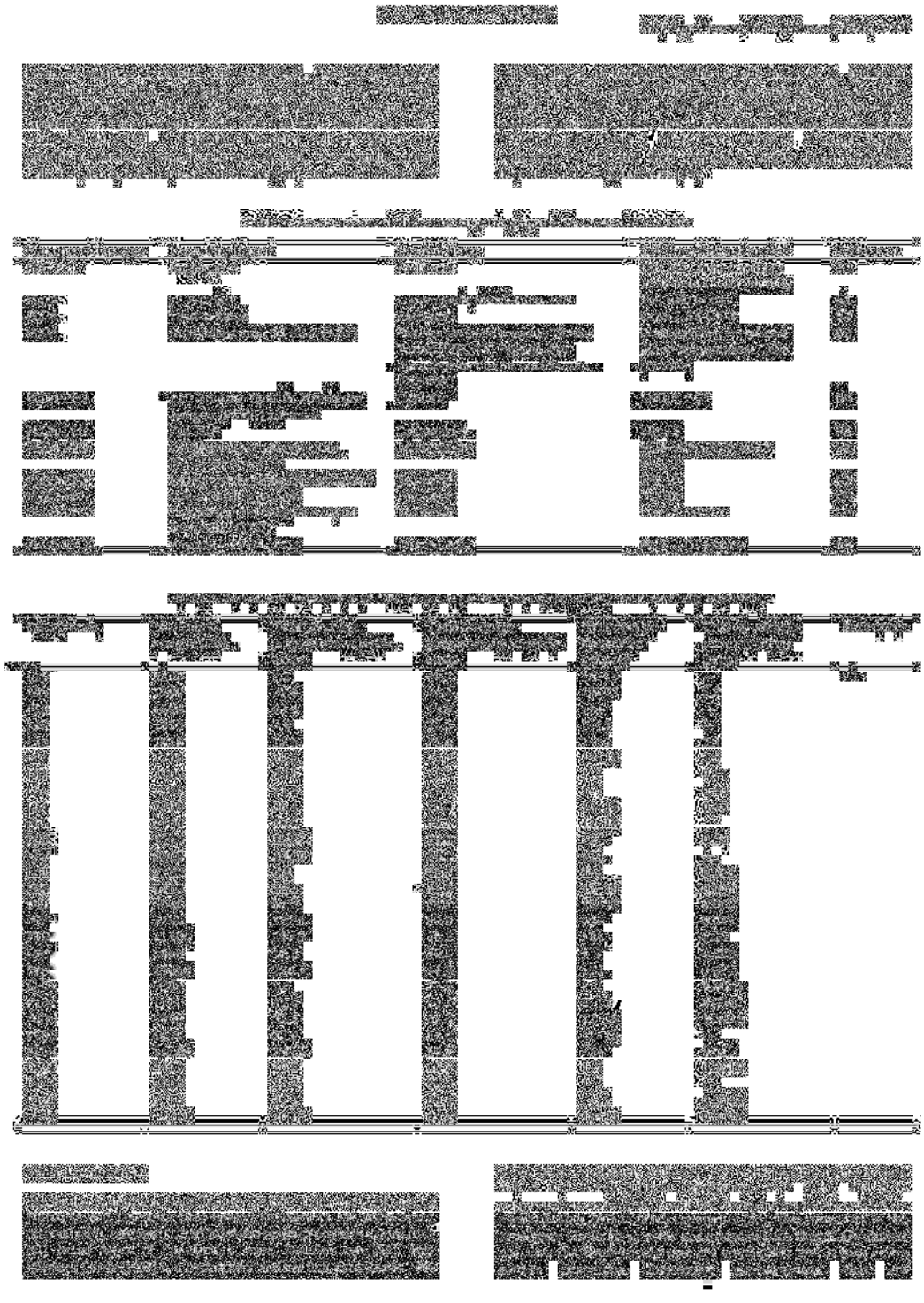

abnormally high pH gradients across organelle membranes by H1-

micellization and de-micellization [91].

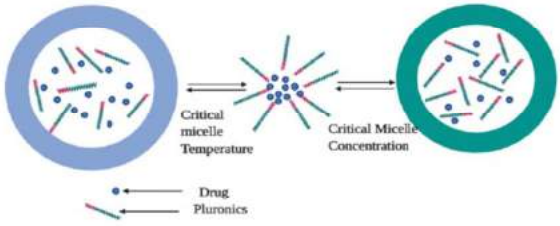

Fig. 3: The development of pluronic micelles in the watery medium according to Pluronics and temperature concentration [82]

hydrophobicity [108-110]. The first depends primarily on the presence of pluronic, hydrophobic blocks to ensure the superior involvement of drug molecules [111, 112].

Tumor-selective drug targeting with pluronic

The transportation of drug transporters in the extracellular region from tumor interstitial to target cells can be increased with high-affinity interactions. This can be achieved by means of ligands, which display selective binding on cancer cellular surface to an upregulated molecular target. This technique increases cell absorption, off-targeting effects and amplifies clinical benefits by withdrawing the target cells from within. Despite their high specificity, anti-compound targeting is limited in large-scale development due to their large molecular sizes, immunogenic, and complexity. Its large size hinders carrier trafficking, particularly in solid tumors [113]. On the other hand, low molecular weight compounds are inexpensive, non-immunogenic, and have superior regulation of the density on the surface of the carrier. Terminal hydroxyl groups of pluronic were used to attack ligands in literature papers [68, 114-116]. The approach involves the immediate binding of ligands to more volatile aldehyde, carboxylic acids, and primary amine terminals or the derivation of hydroxyl groups. The latter can be used to bind molecules sensitive to stimuli and targets. Crosslinkable groups are often inserted into the hydrophilic block to

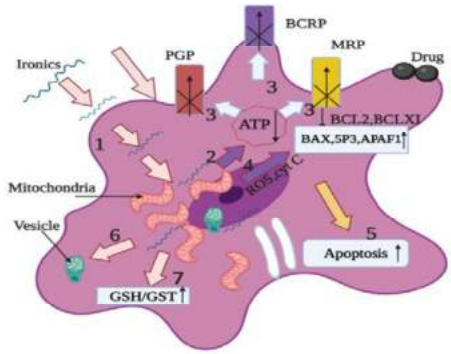

Fig. 4: Effect of pluronics in MDR cancer cells: (1) entrance of

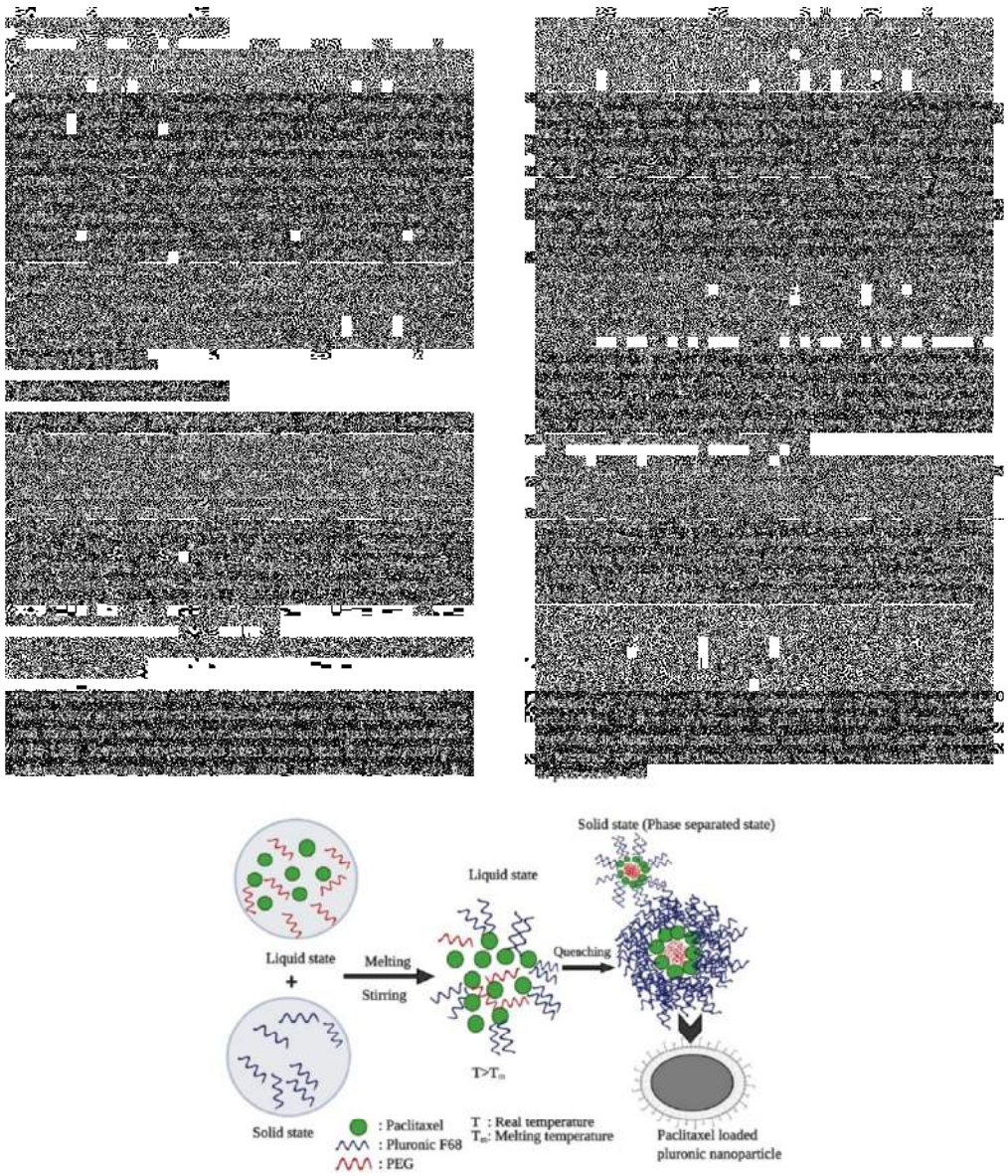

Fig. 5: The formation of Pluronic-based NPs with a core/shell structure. The core is composed of a mixture of PEG (molecular weight: 400)

[redacted]

core/shell NPs [153]. PLGA NPs were developed without the use of a poisonous organic solvent with the liquidized pluronic F-127 as a solvent. As the pluronic F-12, pluronic-coated PLGA NPs with a

and DTX. A pattern of continuous release of both model drugs has been found that the presence of a Pluronic coating on the liposome core surface mediated the release of the model drug.

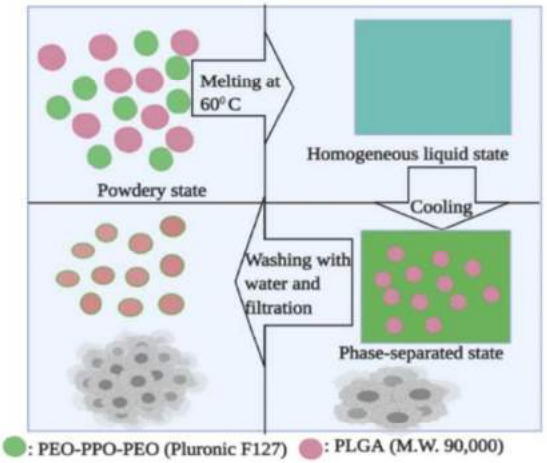

Fig. 6: Temperature-induced phase transition in the melt mixture of PLGA and Pluronics [153]

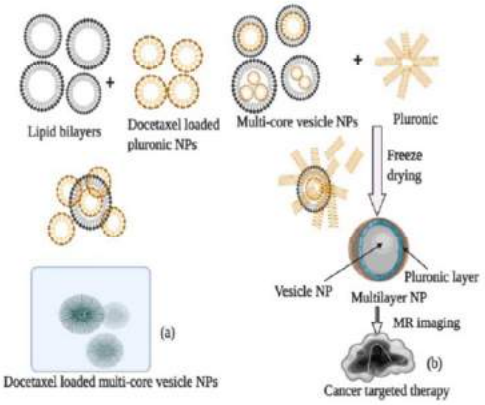

[redacted]

8

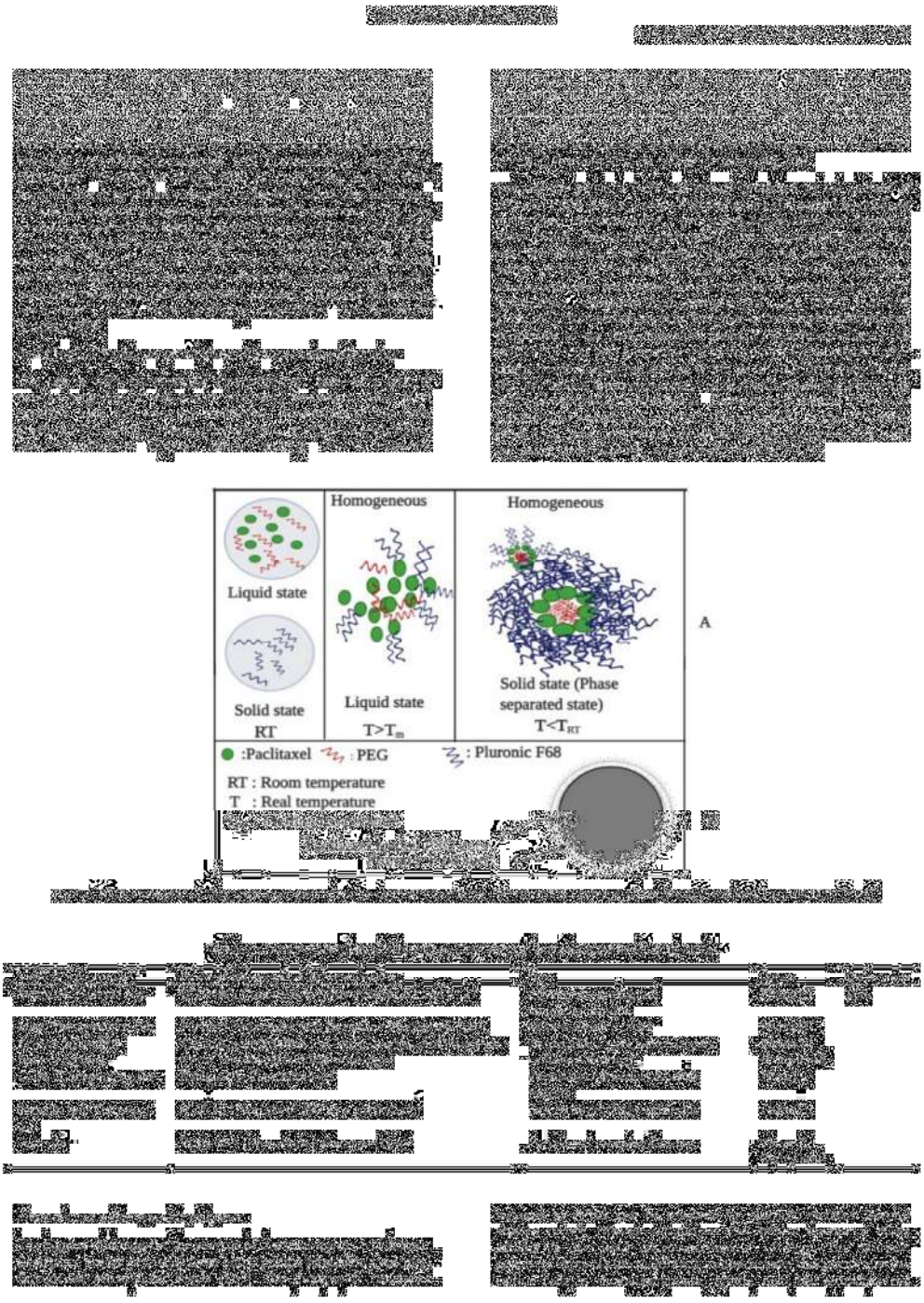
Homogeneous
Homogeneous
Liquid state
Solid state
RT
Liquid state
T>Tm
Solid state (Phase
separated state)
T<TRT
A
:Paclitaxel
: PEG
: Pluronic F68
RT : Room temperature
T : Real temperature

9

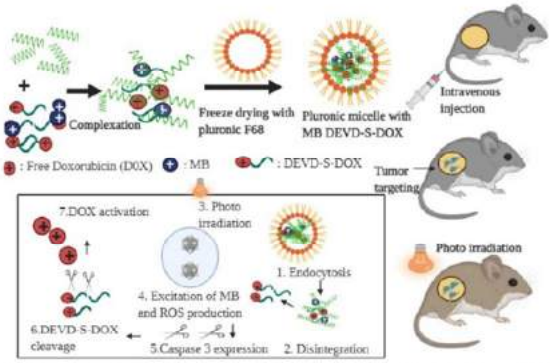

Fig. 9: An illustrative description of chemo-photodynamic combination therapy [76, 119]

10

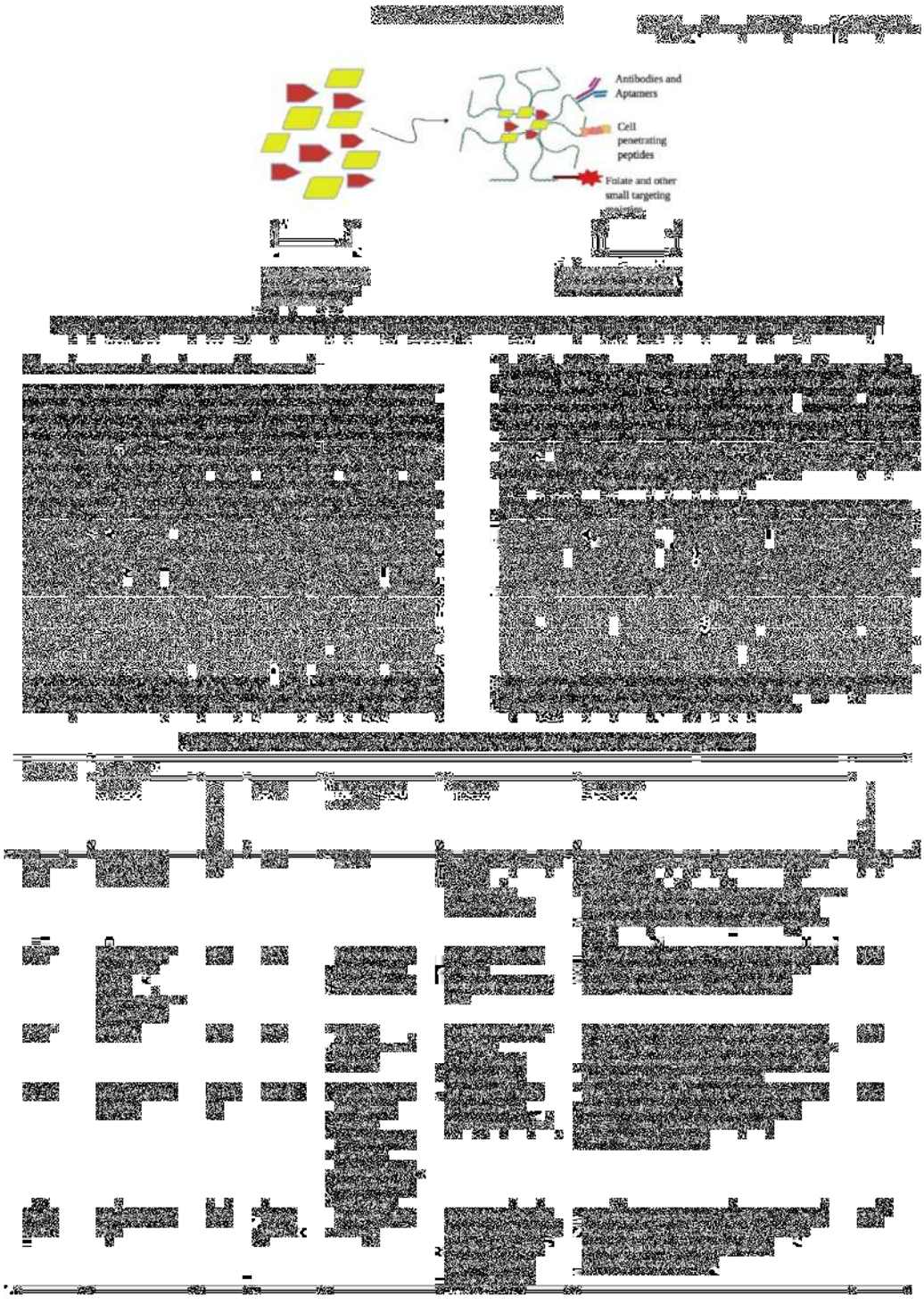
Antibodies and
Aptamers
Cell
penetrating
peptides
Folate and other
small targeting

11

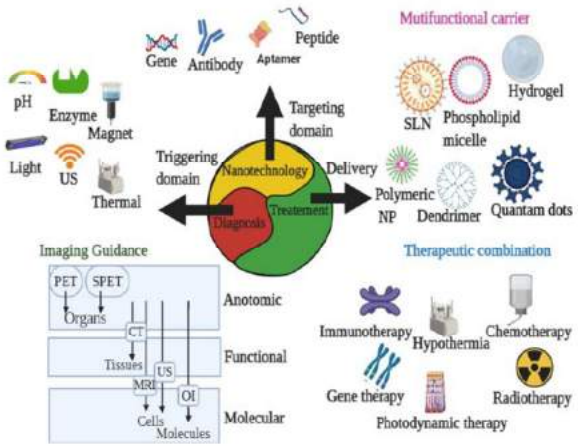

Fig. 11: Multifunctional theranostic and bio imaging nanosystems. PET, positron-electron transmission; SPECT, single-photon emission computed tomography; CT, computed tomography; MRI, magnetic resonance imaging; NPs, nanoparticles; US, ultrasounds; OI, optical imaging [187]

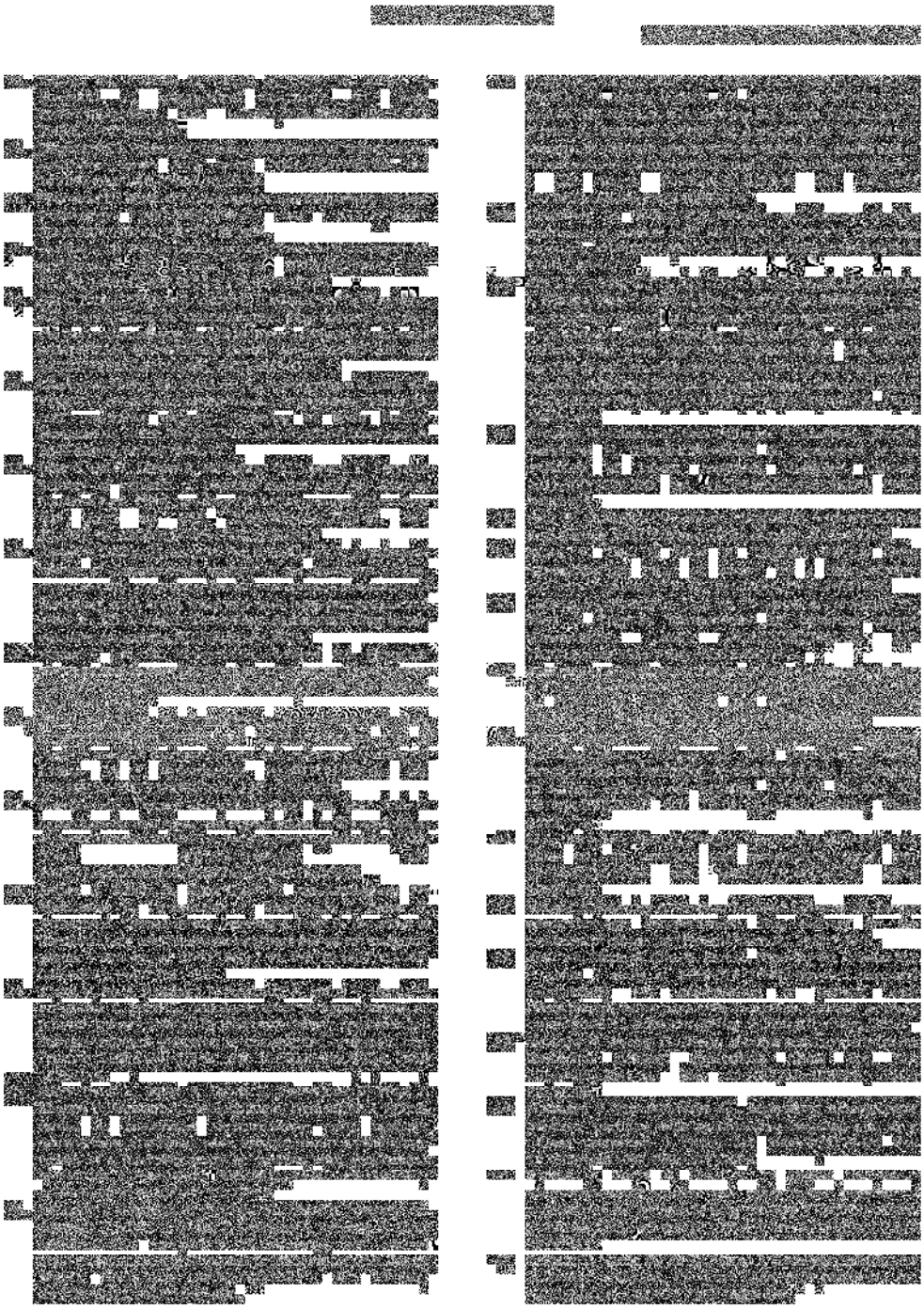

13

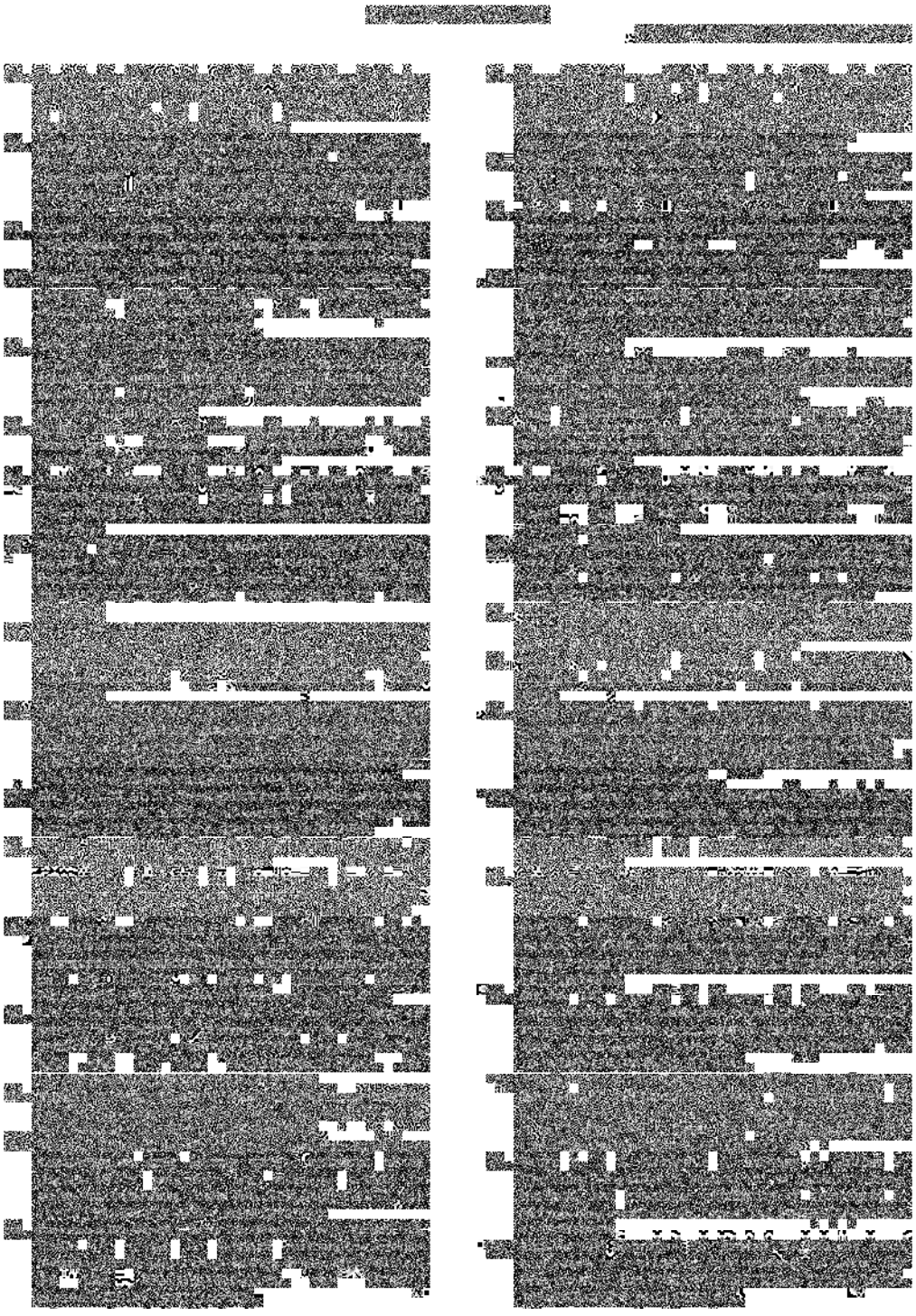

14

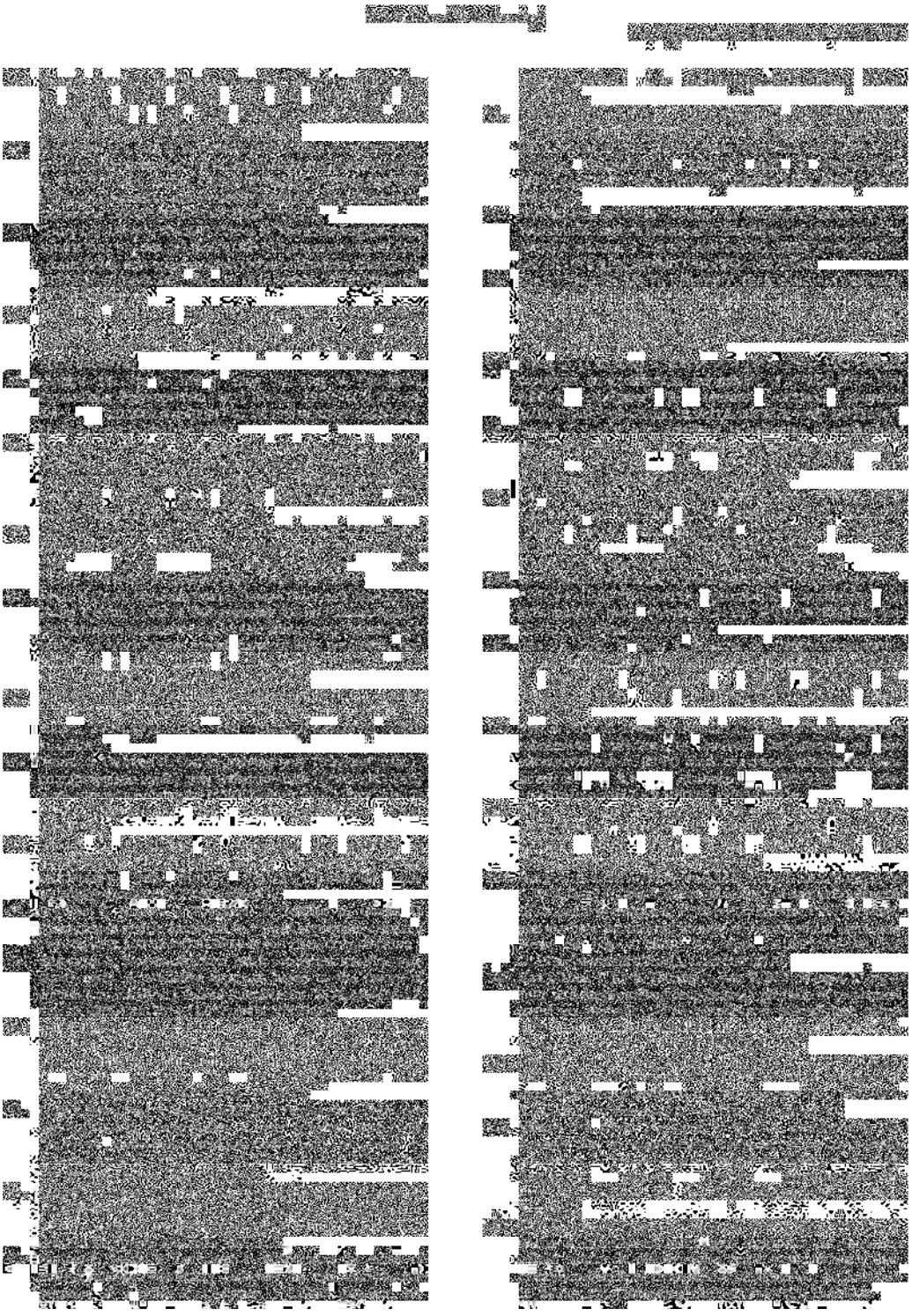

15

16

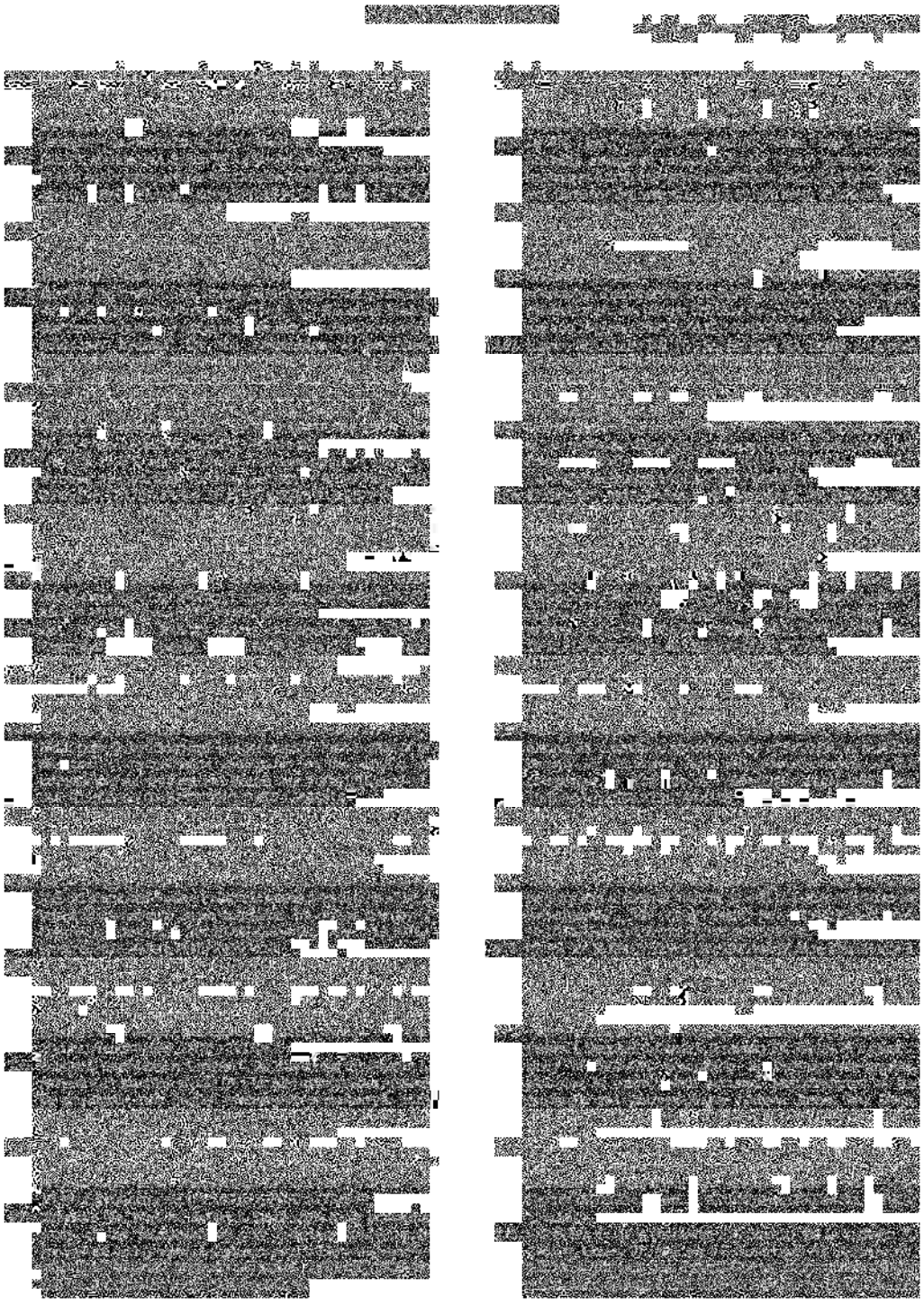

17

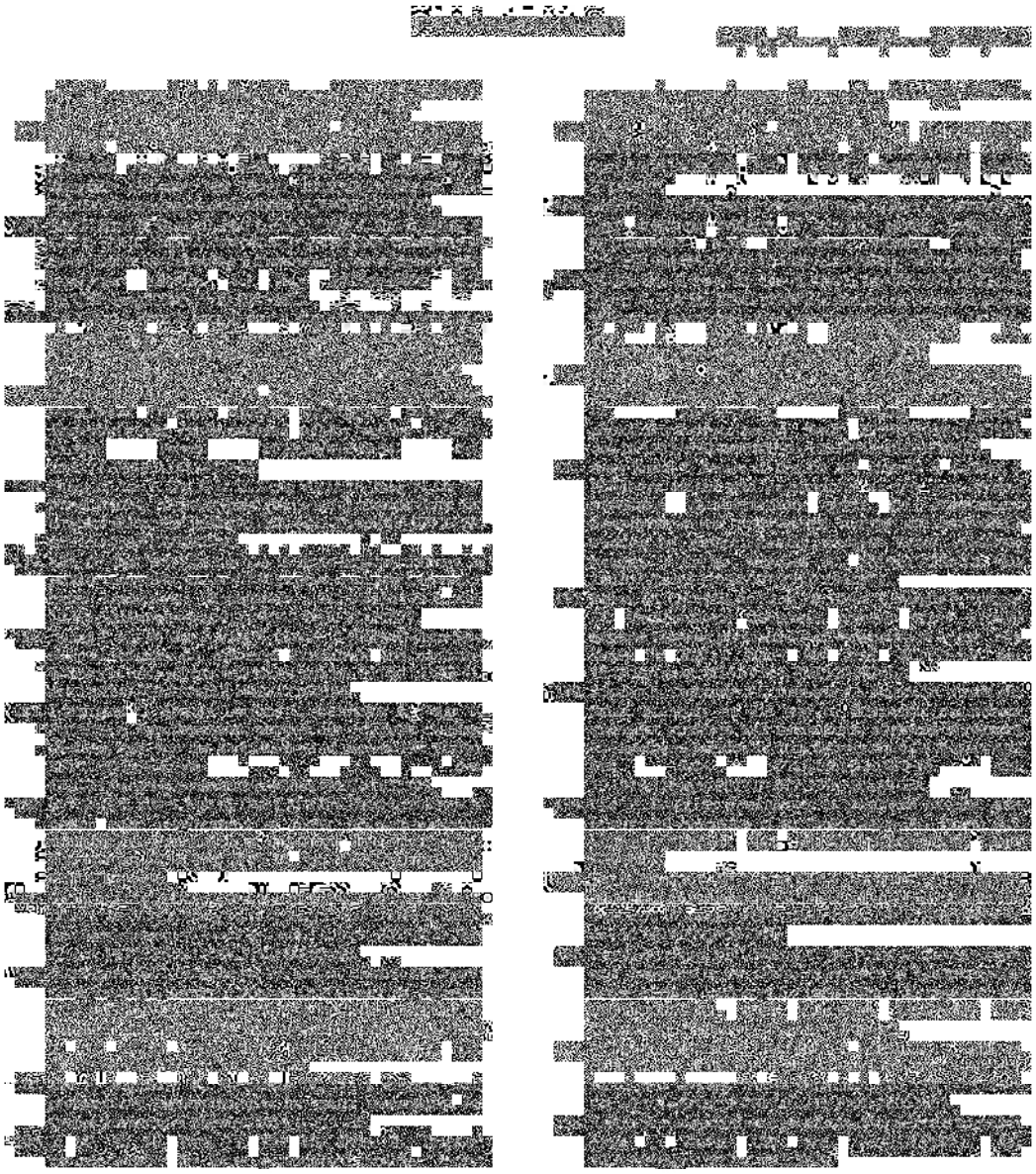

IJPSR (2022), Volume 13, Issue 9 (Research Article)

INTERNATIONAL JOURNAL OF PHARMACEUTICAL SCIENCES AND RESEARCH

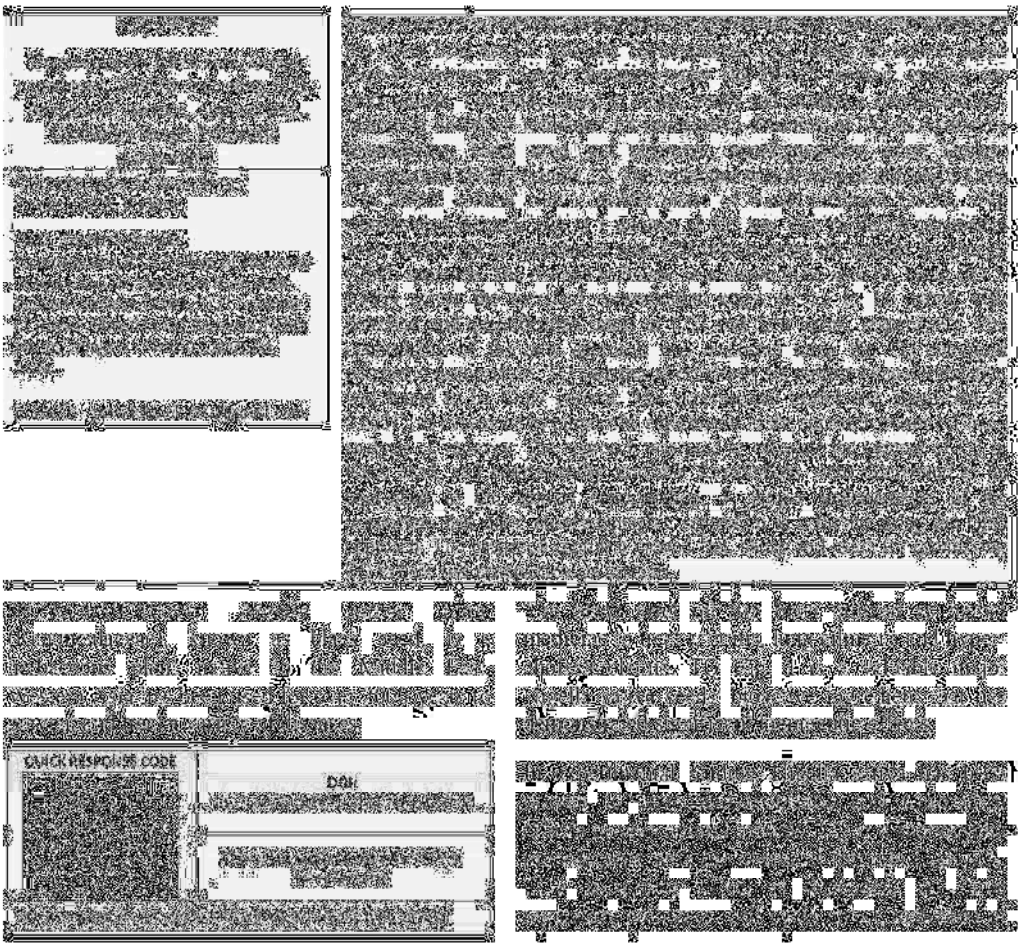

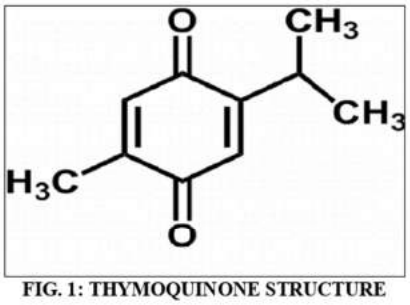

FIG. 1: THYMOQUINONE STRUCTURE

filtering by Millipore Direct-Q®-3 equipment (Molsheim, France).

Instrumentation: The chromatographic process was designed using a Shimadzu Prominence HPLC-20 AT system (Shimadzu, Kyoto, Japan) with LC Solution software and binary pumps (LC-20AD) with a degasser (DGU20A5), UV–Vis detector, auto-sampler (SIL 20AC HT) and column oven (CTO-10AS). The data was interpreted and analyzed using Shimadzu LC solution software (version 1.25). Chromatographic separation and

TQ (10 mg/ml in methanol) were obtained with TQ was achieved **Table 1, Fig. 3**.

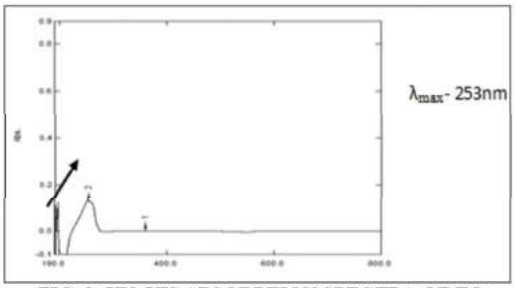

FIG. 2: UV–VIS ABSORPTION SPECTRA OF TQ

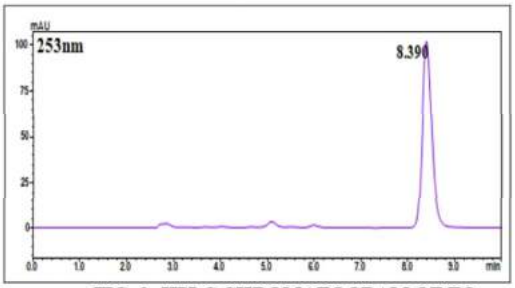

FIG. 3: HPLC CHROMATOGRAM OF TQ

TABLE 1: METHOD DEVELOPMENT PARAMETERS AND CHROMATOGRAPHIC CONDITIONS

Assay for Stress Degradation: Table 2 depicts the

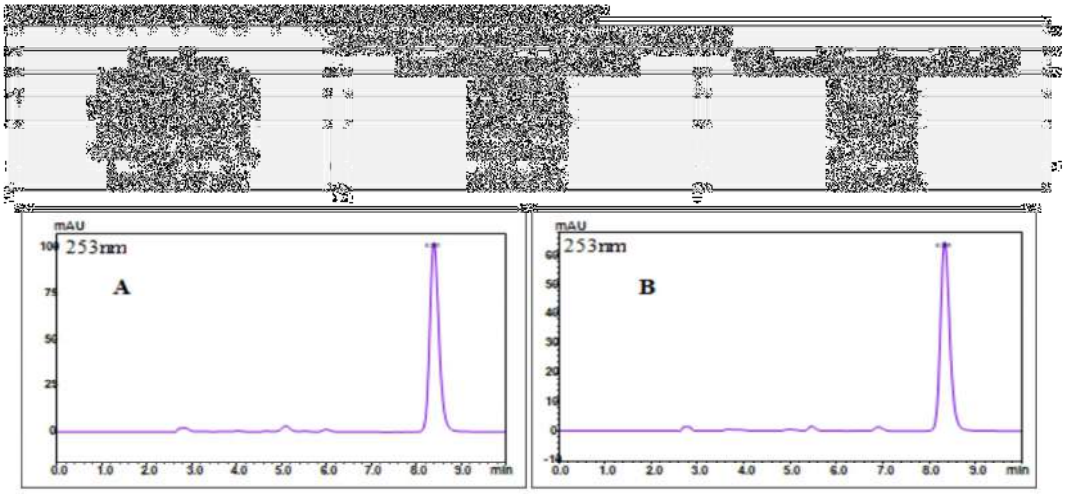

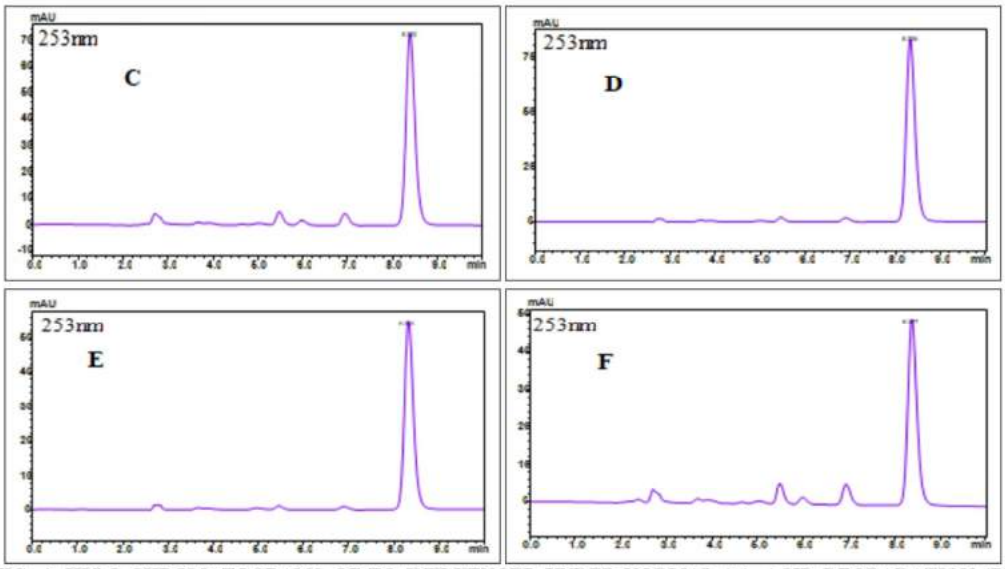
mAU
253nm
C
mAU
253nm
D
mAU
253nm
E
mAU
253nm
F

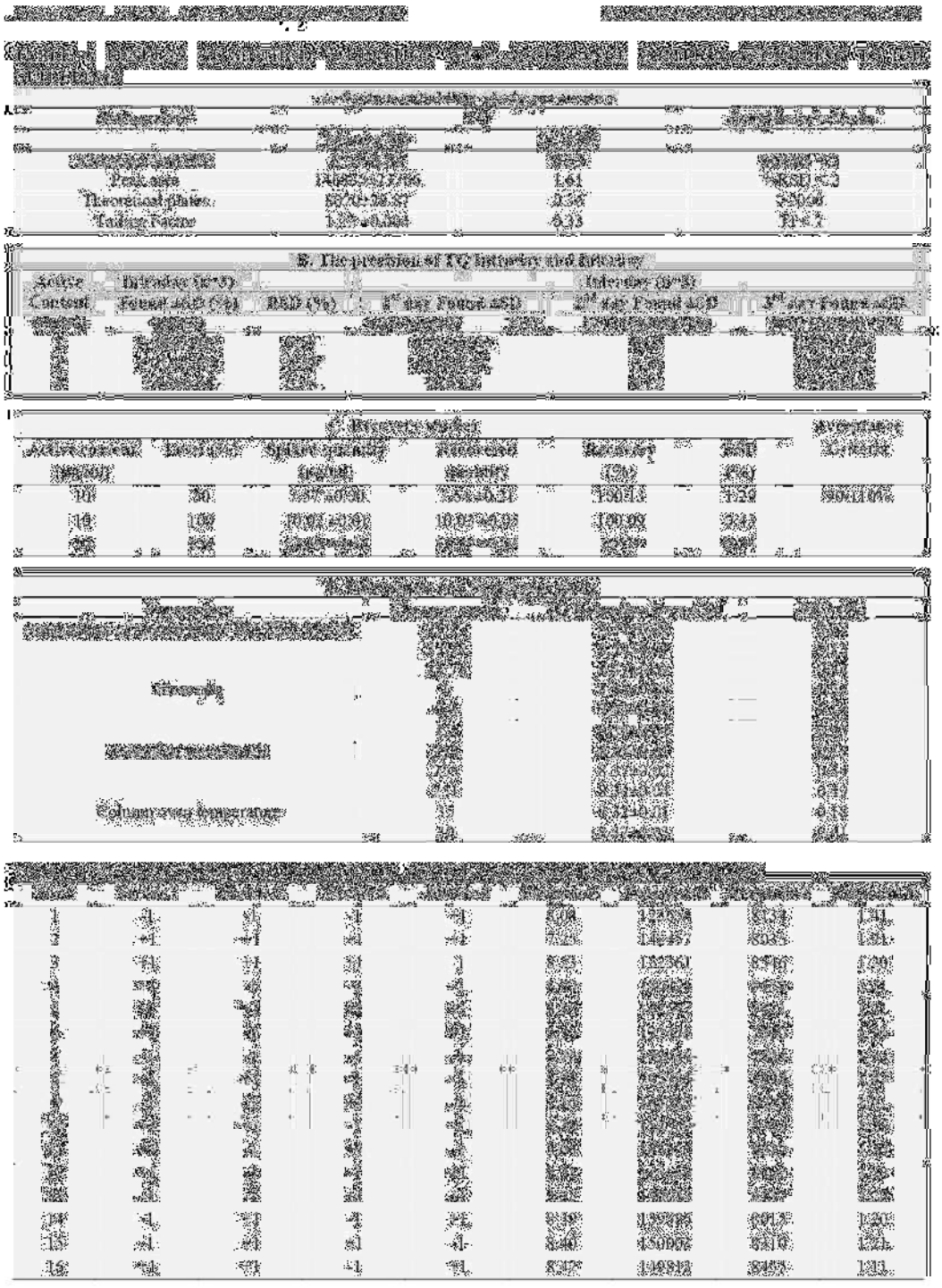

TQ	P value	R- square	Equation in terms of coded factors	Predicted value	Observed value	Relative Error (%)
Theoretical	<0.0001	0.9926				1.96

respectively, which was within the permitted range

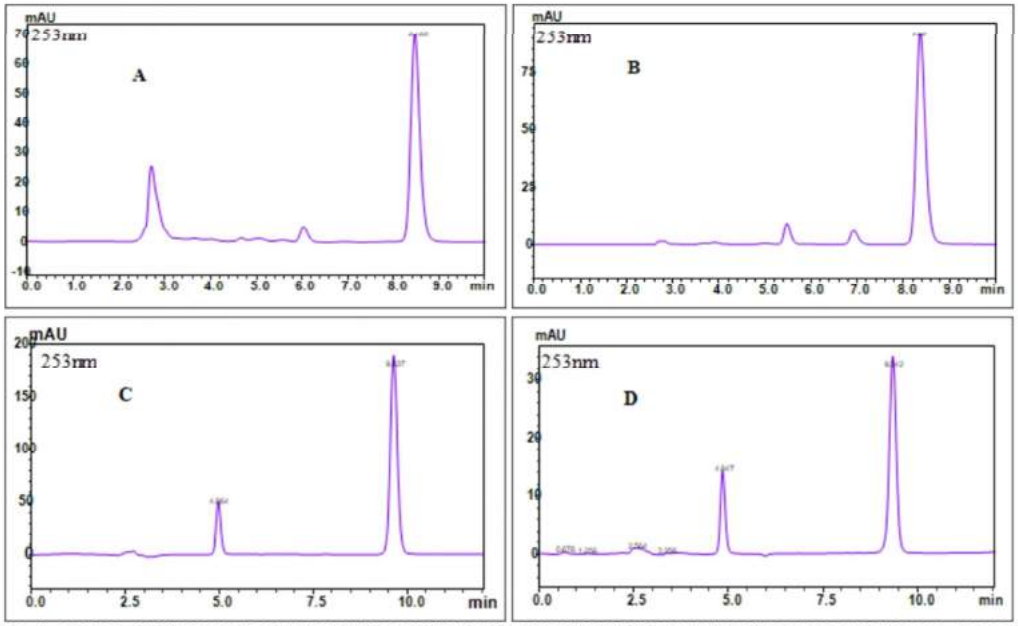

FIG. 5: HPLC CHROMATOGRAM OF TQ OBTAINED IN POLYMERIC NANOFORMULATION (A), BLACK SEEDS (B), BLACK SEED OIL(C), AND BLACK SEED CHURNA (D)

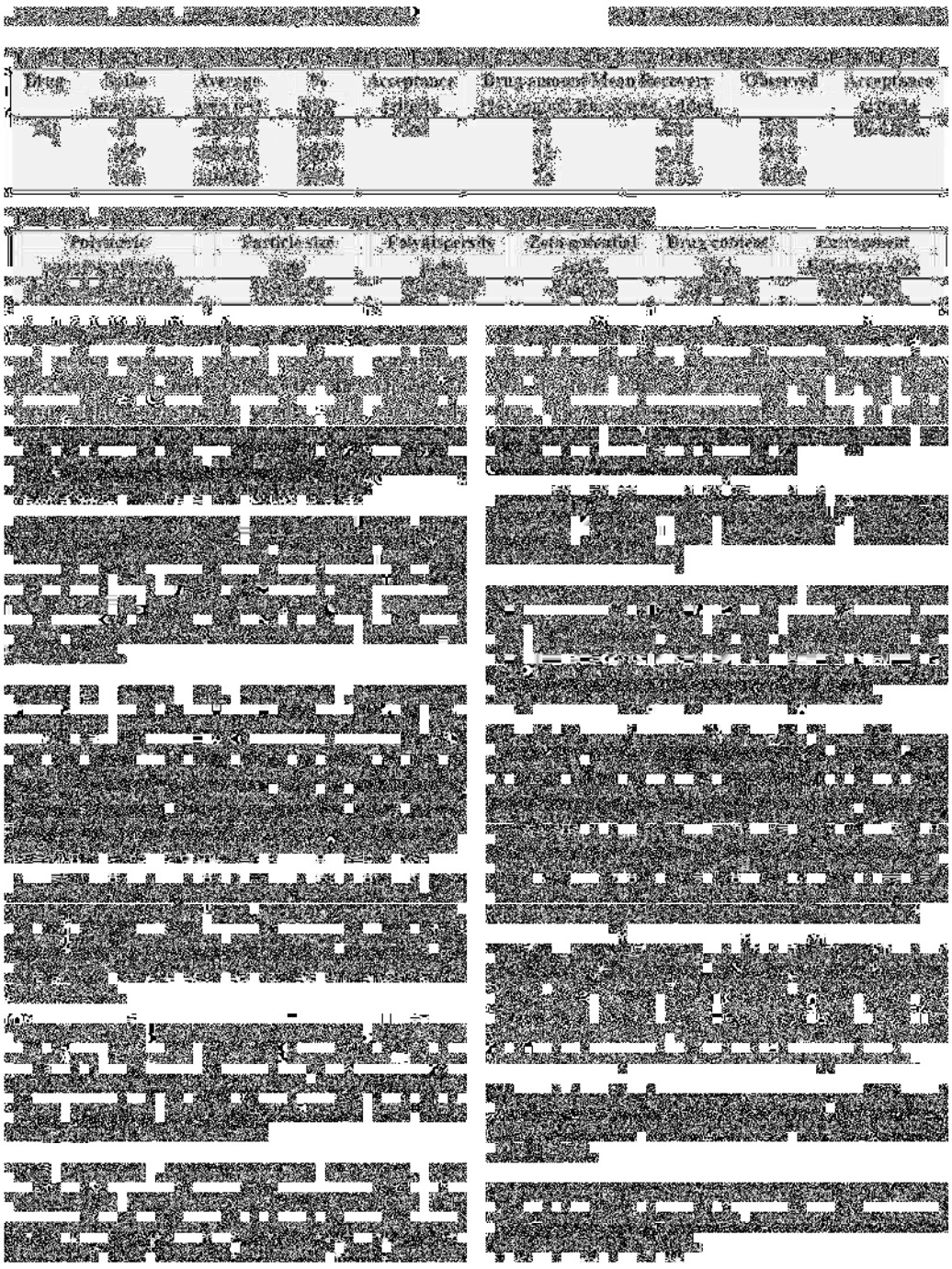

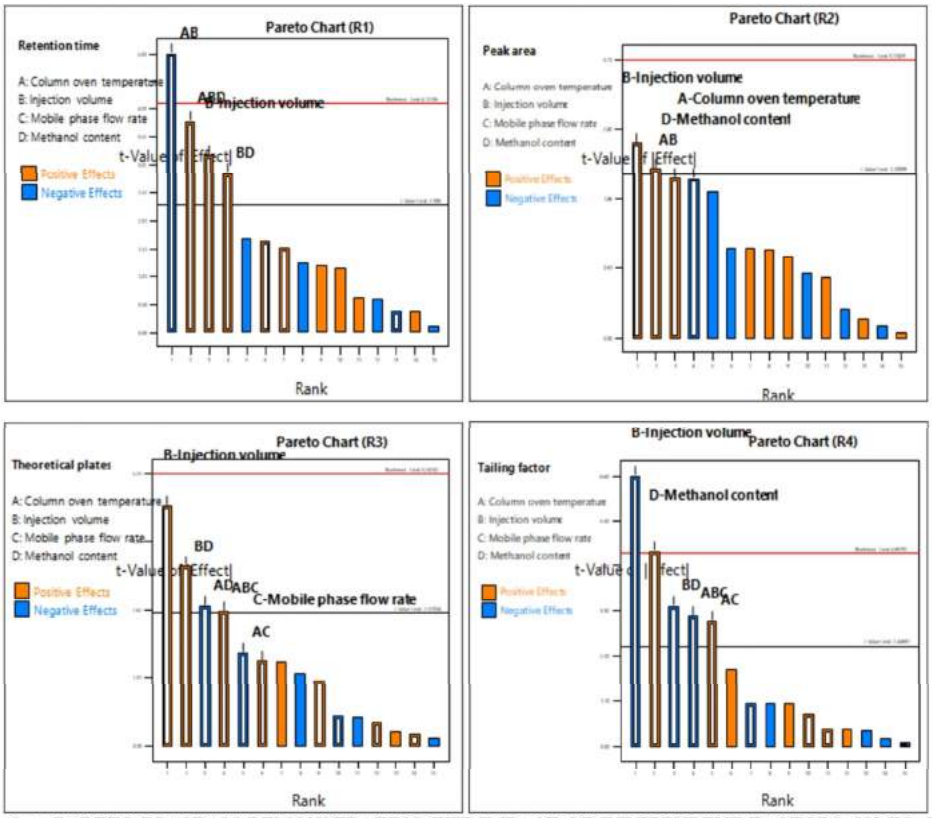

FIG. 6: A PARETO DIAGRAM DEMONSTRATING THE IMPACT OF INDEPENDENT FACTORS ON TQ. THE COLUMN OVEN TEMPERATURE (A), INJECTION VOLUME (L) (B), MOBILE PHASE FLOW RATE (ML/MIN) (C), ACETONITRILE CONTENT (PERCENT) (D), AND INTERACTION EFFECTS ON RETENTION TIME (R1), PEAK AREA (R2), THEORETICAL PLATE NUMBER (R3), AND TAILING FACTOR (R4)

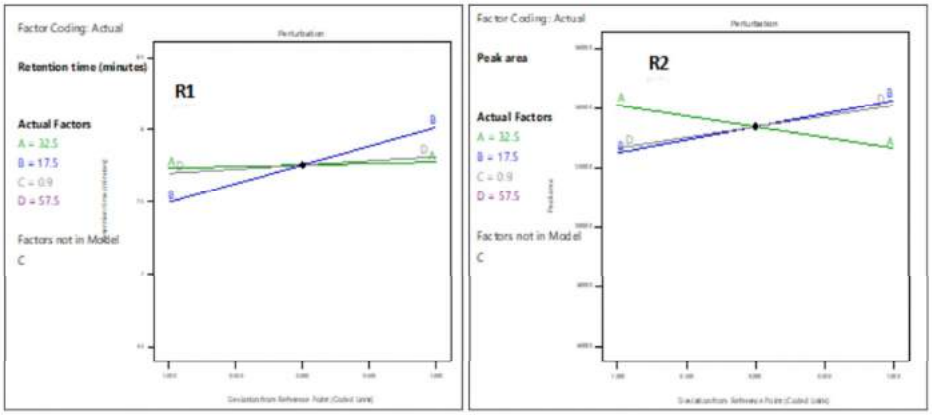

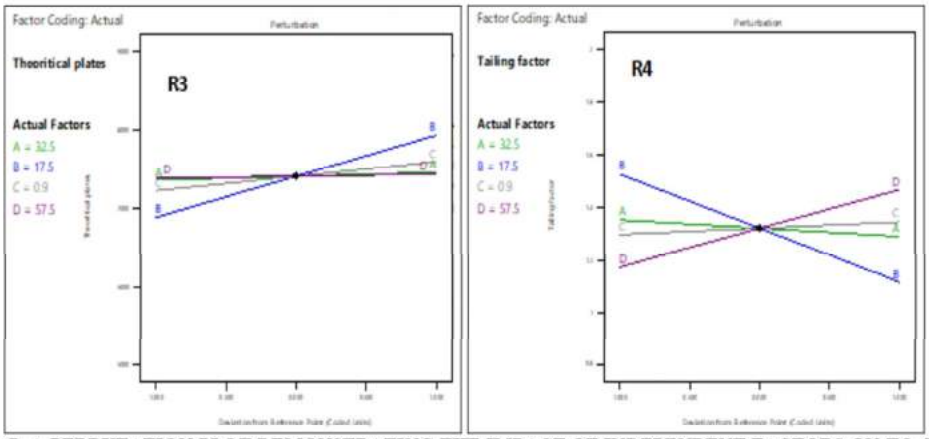

FIG. 7: A PERBUTATION PLOT DEMONSTRATING THE IMPACT OF INDEPENDENT FACTORS ON TQ. THE COLUMN OVEN TEMPERATURE (A), INJECTION VOLUME (L) (B), MOBILE PHASE FLOW RATE (ML/MIN) (C), ACETONITRILE CONTENT (PERCENT) (D), AND INTERACTION EFFECTS ON RETENTION TIME (R1), PEAK AREA (R2), THEORETICAL PLATE NUMBER (R3), AND TAILING FACTOR (R4)

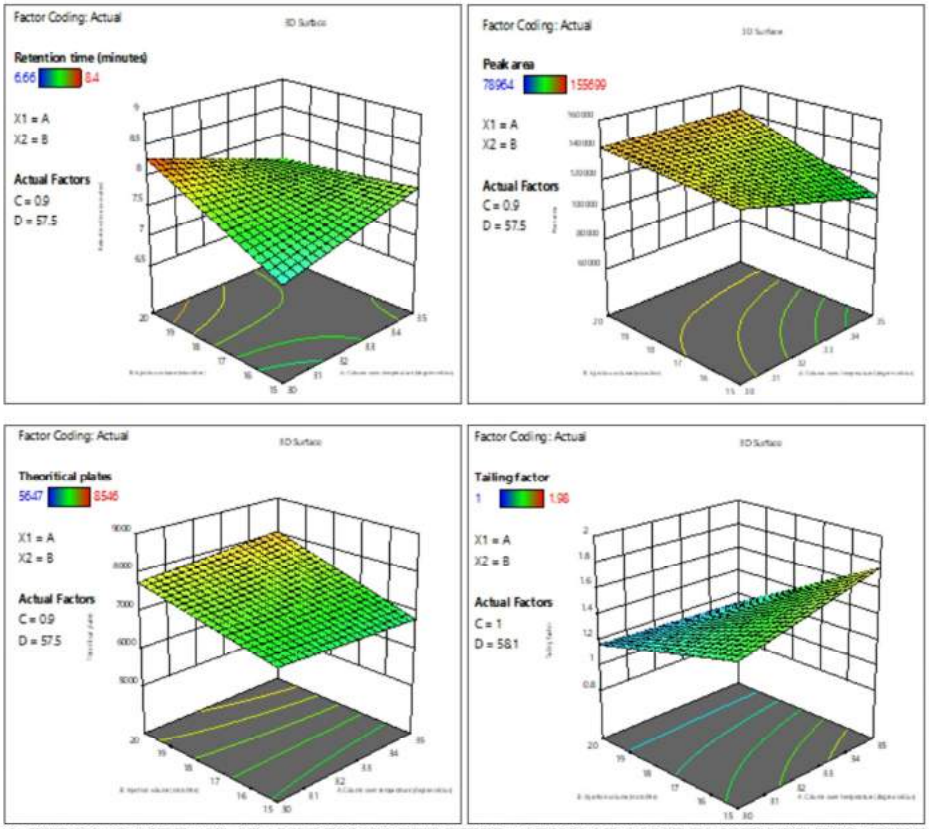

FIG. 8: THE TQ 3D SURFACE GRAPH DEPICTS THE INTERACTION OF COLUMN OVEN TEMPERATURE (A), INJECTION VOLUME (B), MOBILE PHASE FLOW RATE (C), AND PERCENT ACN (D) ON RETENTION TIME (R1), PEAK AREA (R2), THEORETICAL PLATES (R3), AND TAILING FACTOR (R4)

Raikar et al., IJPSR, 2022; Vol. 13(9): 3690-3702. E-ISSN: 0975-8232; P-ISSN: 2320-5148

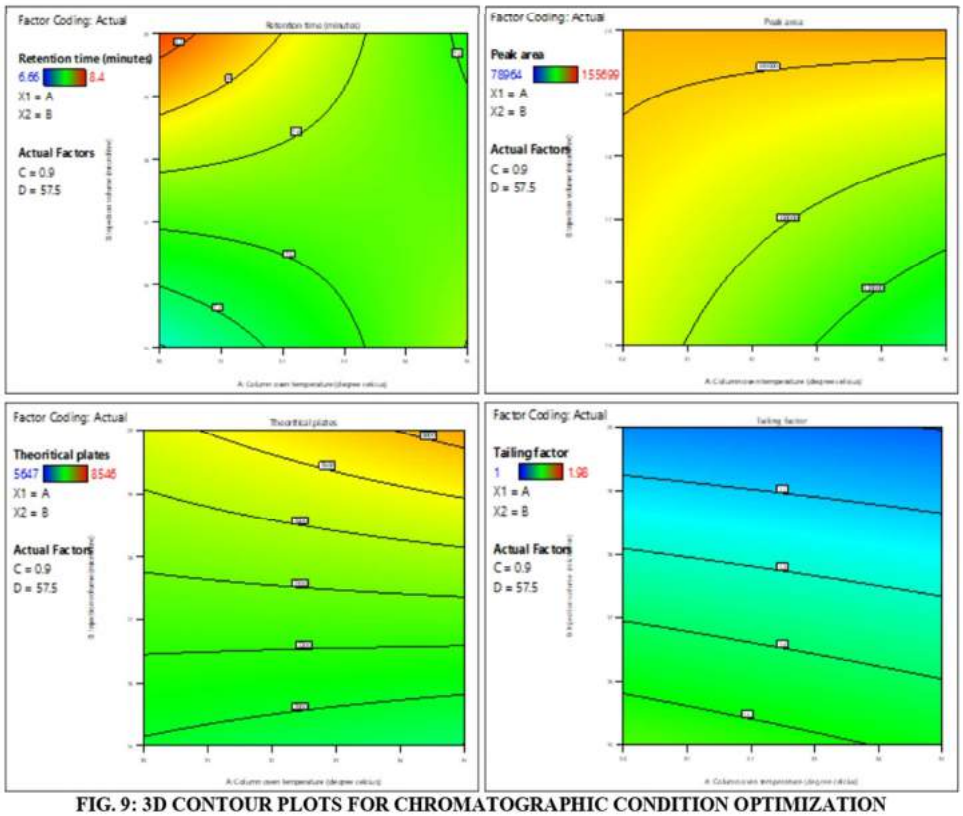

FIG. 9: 3D CONTOUR PLOTS FOR CHROMATOGRAPHIC CONDITION OPTIMIZATION

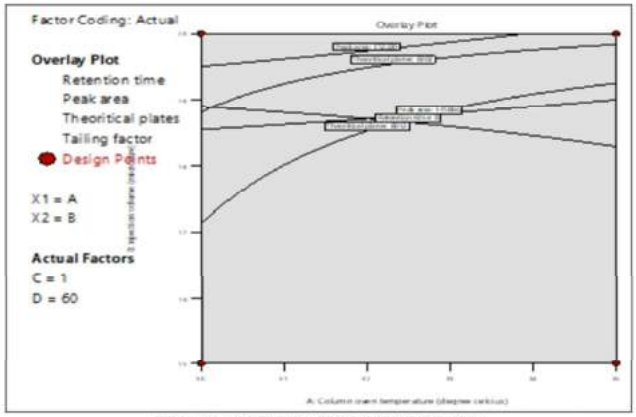

FIG. 10: OVERLAY PLOTS FOR TQ

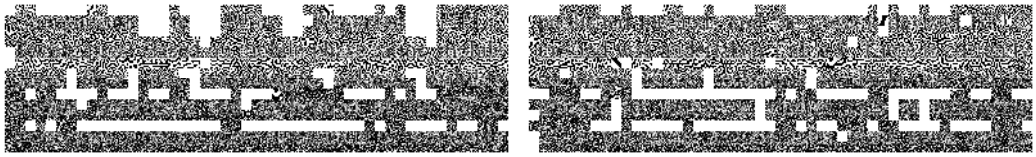

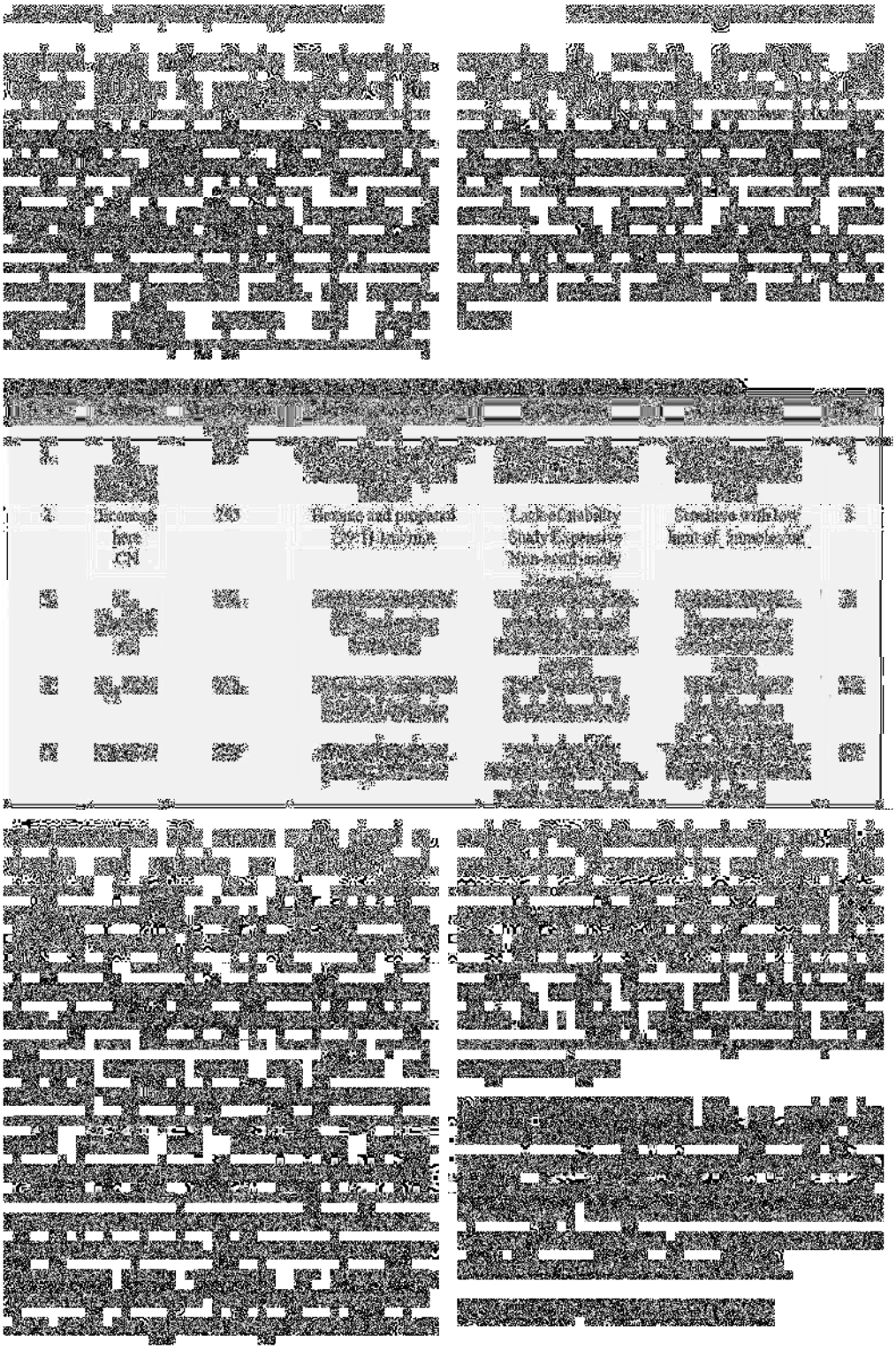

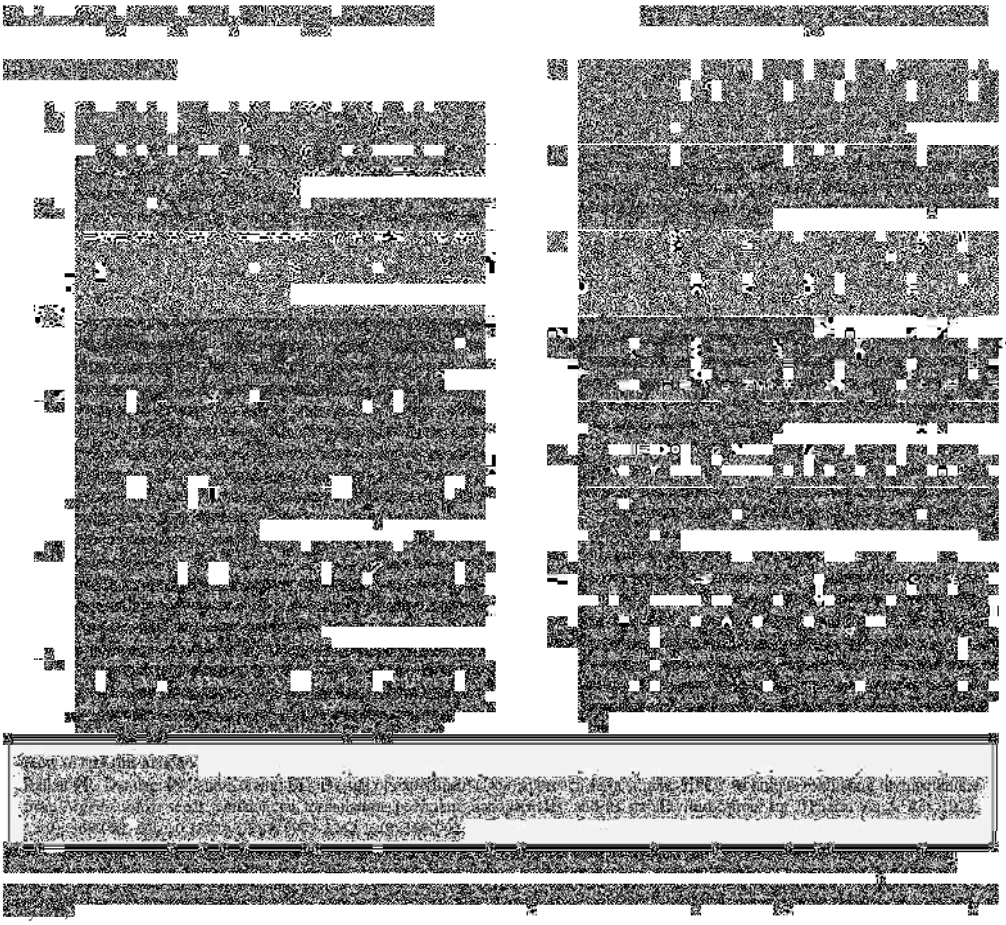

Journal of Chromatographic Science, 2023, 00, 1–11
https://doi.org/10.1093/chromsci/bmad021
Article

OXFORD

[redacted]

Colorectal cancer (CRC) is also known as colon cancer since it affects the colon, large intestine and rectum, among other places. A CRC patient's survival is influenced by recurrence and distant metastases (1). Chemotherapy is still the most [redacted] concentrations in cancer tissue, but this comes at the cost of enormous contamination of the rest of the body and it fails due to its lack of specificity, which generates toxicological issues that lead to side effects and medication resistance (2). Thus, CRC therapy has relied on biodegradable polymeric nanoparticles as well as organometallic and carbon-based compounds to address these challenges (3). They might be used to encapsulate medicines, preserve therapeutic compounds and provide several benefits over bulk materials. For example, nanoparticles can transport hydrophilic and hydrophobic drugs with the same level of efficacy and stability. They also have a large drug-carrying capacity and controlled release capabilities, as well as the ability to deliver both hydrophilic and hydrophobic drugs (4).

Thymoquinone (TQ), a key component of *Nigella sativa* seeds' volatile oil, is used in traditional and folk medicine for its anti-inflammatory and antioxidant effects (5). Because TQ chemosensitizes colon cancer cells and has a synergistic impact with most anticancer medicines, it was chosen for use in biodegradable polymeric nanoformulation to combat colon cancer (6, 7). Figure 1 displays the TQ and capecitabine (CAP) structures.

The validation section determines the suitability of a high-performance liquid chromatography (HPLC) method. Specificity, linearity, accuracy, precision, limits of detection (LODs) and limits of quantitation (LOQs) are the main components of new method validation, according to ICH guidelines (8, 9). The method for analyzing drugs in nanoformulation should be sufficiently robust, sensitive and precise; thus, the design of experiment has been used in this method to study the effect of factors individually and in combination. The design of experiments (DOE) is based on experimental design principles, mathematical equations or models and factor outcomes. This study focuses on the DOE optimization, development and validation of a new analytical method (10). The DoE method is widely used to implement quality by design (QbD) in both academic and commercial settings. Understanding the

product and process is essential to ensuring quality in the finished product in QbD (11). Analytical QbD is a risk-based scientific paradigm for developing analytical methods that aim to achieve enhanced method performance, high robustness, ruggedness and flexibility for continuous improvement (12). For QbD, HPLC methods, robustness and ruggedness should be tested earlier in the development stage to ensure the method's efficiency over the product's lifetime (13). Otherwise, it can take a significant amount of time and effort to

[redacted]

experimental designs known as factorial designs are typically very economical in that they provide a great deal of useful information from a limited number of experiments. In a factorial design, the effects of each experimental factor and how they interact with one another is looked into concerning the response(s) (14).

When it comes to evaluating medication formulations, the analytical approach is crucial. A precise, accurate and effective analytical approach is essential for a better evaluation of formulations. Earlier spectrophotometric methods have been used to estimate CAP and TQ separately in analytical and bio-analytical samples (15–19). The simultaneous detection of TQ and CAP, however, has never been documented using an HPLC method. However, a method that can determine the stability of CAP and TQ in the nanoparticulate system has yet to be published. This work, therefore, intended to create a simple, precise and sensitive reverse-phase RP-HPLC technique for measuring CAP and TQ in biodegradable polymeric nanoformulation and to verify it by the ICH Q2 R1 criteria (20). The design of experiments is used to explore the impacts of variables independently and in combination since an analytical approach must be sensitive and precise. An experimental design is based on mathematical equations and models that take into account a wide range of possible influences on an experiment (21).

Materials and Methods

[redacted]

Acetonitrile (ACN) and methanol were bought from Merck, Mumbai, India, and were of HPLC grade. The nylon filtration membrane was purchased from Jay Distributors (Mumbai, India). Throughout the research, analytical-grade chemicals

[redacted]

Bath Sonicator (Bransonic Ultrasonic Corporation, USA). There is a direct-Q3 Millipore Corporation water-purifying system that uses Milli-Q water (Millex HV®, Millipore, USA). An experiment was validated using Design-Expert® software, version 13 (Stat-Ease, Inc., Minneapolis, USA).

Chromatographic conditions

We examined the impact on the separation of CAP and TQ of several mobile-phase compositions and found that a combi-

[redacted]

mode. and was run for a total of 12 min. For simultaneous estimation, the isosbestic point of active pharmaceutical ingredients (API) 271 nm was utilized and the column was kept at 30°C throughout (22).

Preparation of API standard solutions

The standard stock solution (1000 μg/mL) was made by weighing 10 ± 0.1 mg of drug samples and dissolving it in methanol (10 mL) for 5 min using a bath sonicator. Dilutions of the drugs standard stock solution in the prepared mobile phase resulted in working standard solutions ranging from 0.25 to 16 μg/mL (23, 24).

HPLC technique development and optimization

Different mobile-phase ratios, flow rates and column oven temperatures were used to create a technique for the simultaneous measurement of CAP and TQ. Several mobile-phase compositions were used to improve the drug's retention time (Rt) and theoretical plate count (N), as well as to reduce the tailing factor (Tf). A peak area, Rt, N and Tf were evaluated to optimize the methods of separation for CAP and TQ (25, 26).

The stability of CAP and TQ was assessed by force degradation studies

CAP and TQ were subjected to forced degradation testing by

[redacted]

condition: APIs solutions kept under normal circumstances for zero time and APIs solutions that were to be degraded for 1 h (27).

[redacted]

Oxidative degradation

It took 1 h for the hydrogen peroxide–induced force degradation to take place after mixing 2 mL of 3% w/v H_2O_2 solution with 1 mL of CDS (1 mg/mL ± 0.1 mg) in the dark at room temperature. Afterward, the materials were diluted with methanol and examined using HPLC.

Photolytic degradation

Validation studies

For different parameters, the improved technique was validated per the ICH requirements (28, 29).

System suitability

The linear regression and correlation coefficients may be calculated from the peak area vs. concentration graph. The

solutions of CAP and TQ (10 μg/mL) had been spiked in triplicates with known quantities of the CDS at low, medium and high concentrations.

LOD and LOQ

The following formula was used to determine LOD and LOQ based on the standard deviation (σ) from the *y*-intercept and slope mean (S) of the calibration plot (30):

$LOD = 3.3(\sigma/S)$ and $LOQ = 10(\sigma/S)$, respectively.

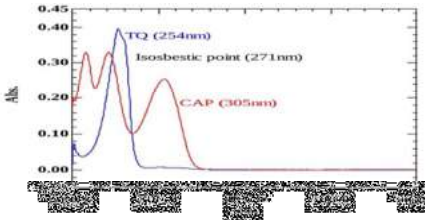

experimental model was used to calculate Rf, peak area, *N*, and Tf (with two levels and four factors). To find chromatographic reactions, DoE software analyzed 16 runs with two levels of 1 and +1. The analysis of variance (ANOVA) model was used to determine the influence of independent variables (31).

Quantification of CAP and TQ in nanoformulation: application of the developed method

polydispersity index of the prepared polymeric nanoparticles were determined using Nanotrac (32).

$$\text{Encapsulation efficiency (EE)} = \frac{\text{Total drug} - \text{Free drug}}{\text{Total drug}} \times 100$$

of H_2O and ACN, H_2O with MeoH (aqueous: organic) and varied ratios were tried. CAP and TQ were analyzed at both λmax and the isosbestic point (Figure 2). It was decided to optimize MeoH, ACN and H_2O at a ratio of 30:35:30 %v/v as it produced superior outcomes. *N*, Tf and Peak areas were examined and the results are presented in Table I and Figure 3.

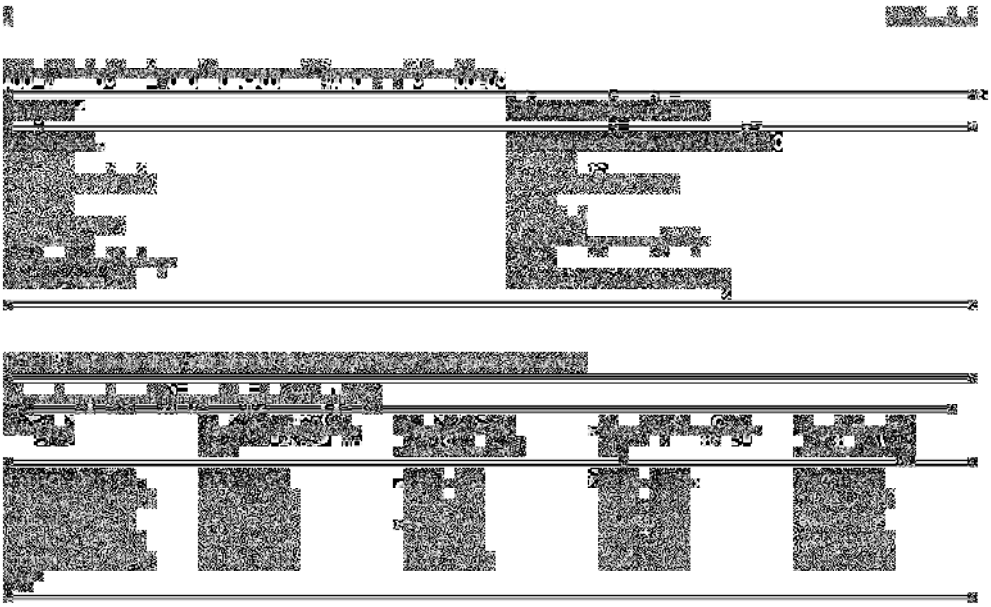

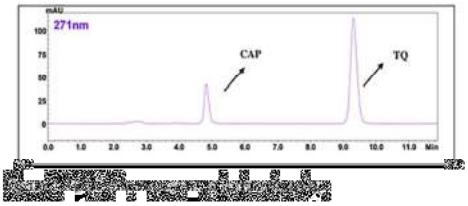

Forced degradation studies

The findings of the force degradation investigations are shown in Table II. CAP degraded by 18.67 ± 0.16% when exposed to sunlight but remained stable under acidic, alkaline, thermal and oxidative circumstances with a mean percent recovery of 94.8 ± 0.82%, 92.67 ± 0.96%, 97.41 ± 0.02% and 90.15 ± 0.52%, respectively. According to mean percent

degradation was seen in TQ under oxidative and photolytic degradation. According to Figure 4, deteriorated samples had chromatograms different from the unstressed sample.

Validation of the optimized method

System suitability

To characterize system suitability data, the percent standard deviations of RT, peak area, *N* and Tf were employed. Acceptable values were found for all parameters (Table IIIA).

Linearity

In the standard calibration plot for CAP and TQ, concentration was found to be linear between 0.25 and 16 μg/mL.

Results are depicted in Table IIIB.

Accuracy

This study revealed that CAP and TQ had a mean percentage recovery range of 97.26–100.58% and 99.86–99.82% high recovery, respectively. This suggests that the established technique is highly accurate (Table IIIC).

the acceptance criteria and showed the method was precise (Supplementary Table I).

LOD and LOQ

The LOD for CAP and TQ was 0.05 and 0.12 μg/mL, respectively, at the isosbestic point, and the LOQ for CAP

Robustness study

Findings demonstrated that the retention duration was unchanged, confirming the robustness of the devised HPLC technique (Supplementary Table II). The impacts of independent factors such as mobile-phase composition, wavelength, flow rate and column oven temperature on different responses (RT, peak area, Tf10 percent and *N*) was indicated in Supplementary Tables III and IV. Table IV shows the polynomial equation for each response. To examine the impact of independent variables on the chromatographic results, the program supplied perturbation plots interactions and Pareto charts as seen in Figures 5 and 6. DoE program computed the R^2 coefficient, *P*-value and relative errors.

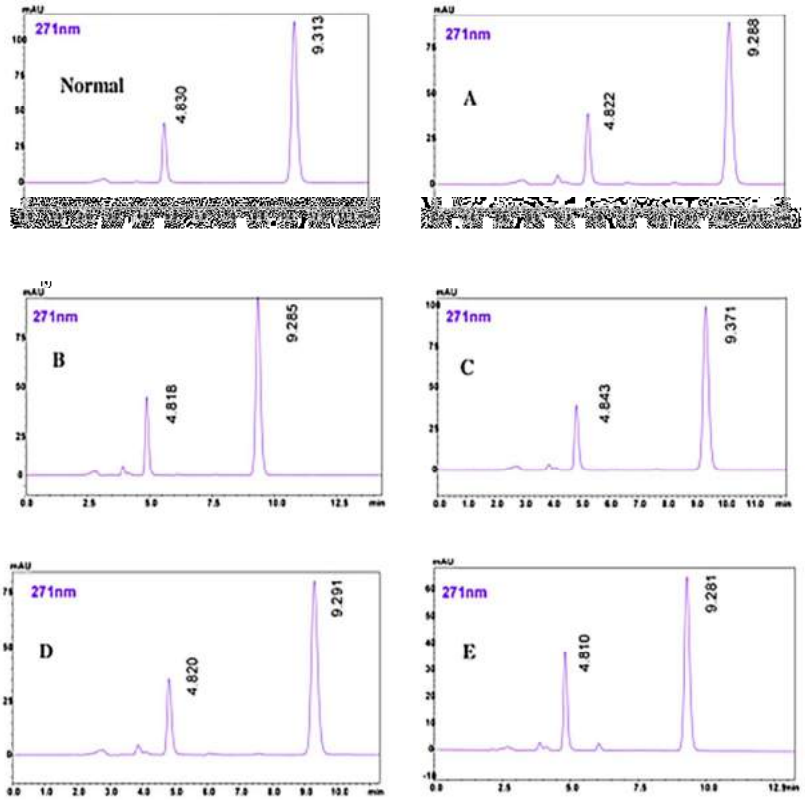

Figure 4. HPLC chromatograms of CAP and TQ that have been forcefully degraded under normal acid degradation (A), alkali degradation (B), thermal

The encapsulation efficiency (EE) of CAP and TQ in polymeric nanoparticles was estimated by using the newly developed HPLC-RP technique. Figure 7 shows intense peaks of CAP and TQ in the HPLC chromatogram of polymeric nanoparticles. CAP had a mean percent EE of 90.18%, while TQ showed 90.12% EE. For the drug estimate from polymeric nanoparticles, the accuracy and precision values are shown in Table V. In this study, the mean percent recoveries for CAP and TQ were between 98.49% and 104.09%, and the RSD % was less than 2.0. On the other hand, the mean particle size and PDI of the polymeric nanoparticles were determined using a particle size analyzer. The overall drug content was

and physiological fluids using an HPLC method. However, TQ and CAP have never been detected together previously using an HPLC method. For validation, in an isocratic mode, a modified mobile phase composed of methanol:ACN:water (35:30:35) %v/v was employed to separate the compounds with enhanced retention time. CAP and TQ were eluted in 4.87 and 9.43 min, respectively. Since we used water instead of acetic acid and ammonium acetate in the mobile phase, our approach is superior to the preceding method in this respect (7, 22). Stressed and unstressed samples were used in forced degradation tests to determine the true degradation peak heights of both analytes. CAP and TQ were less

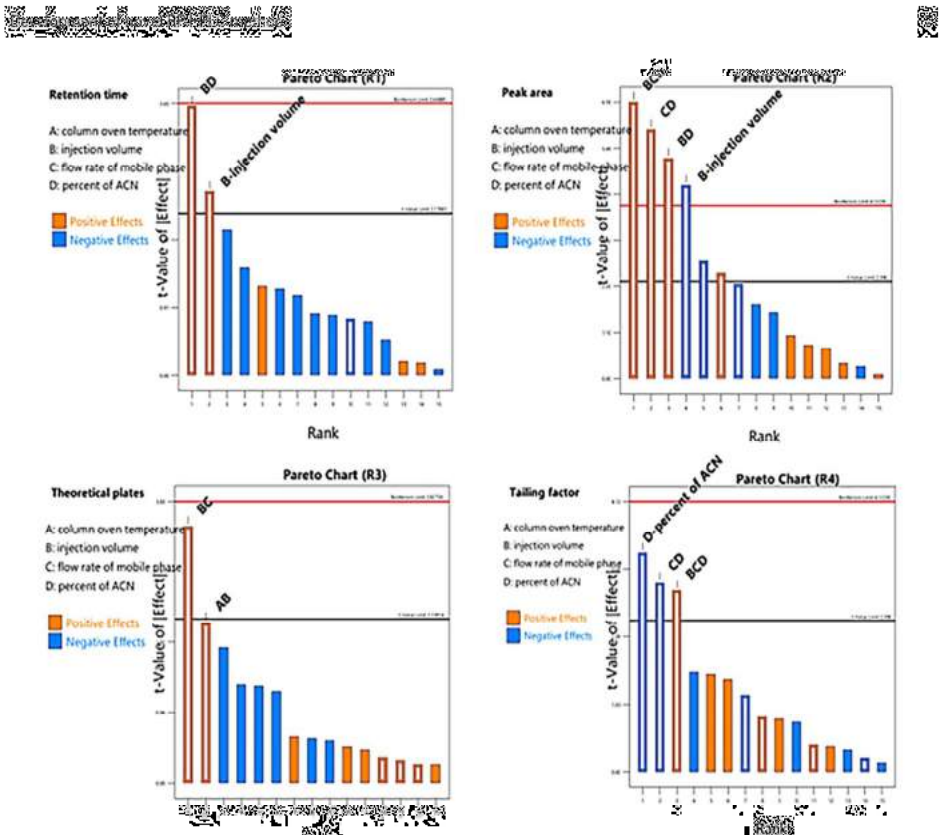

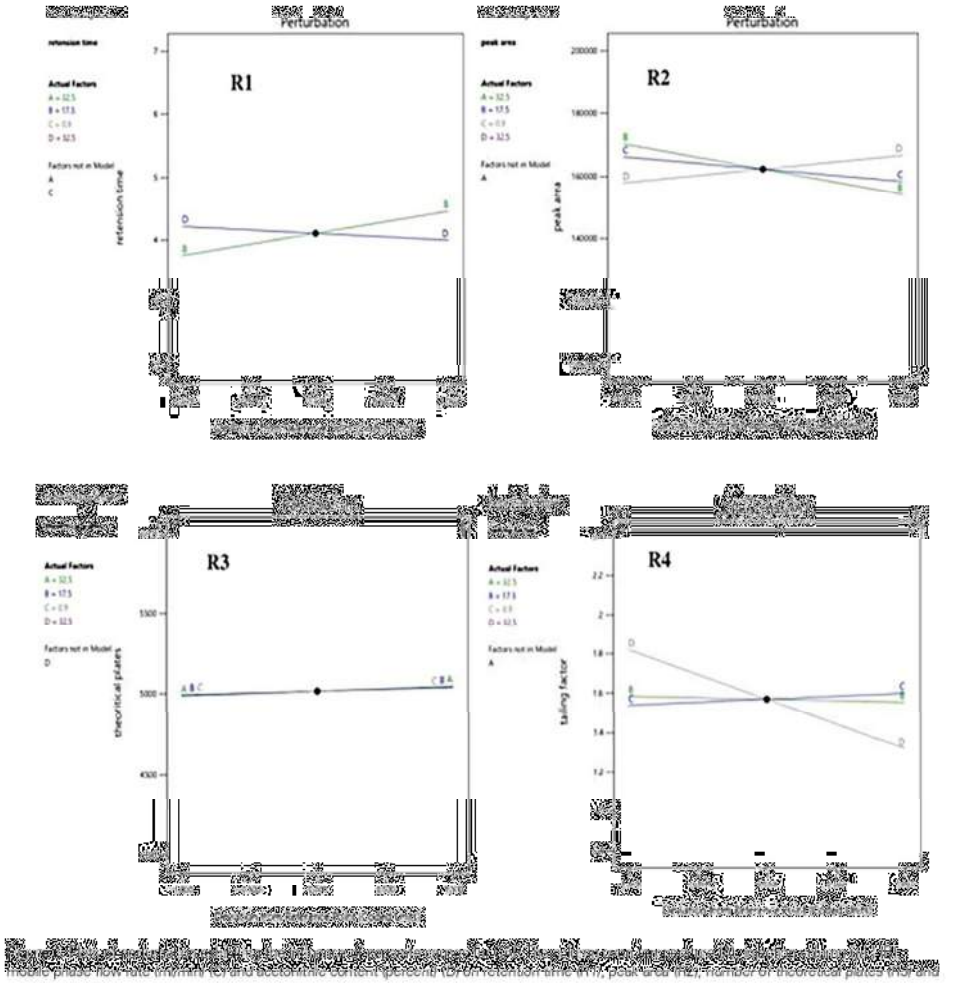

tailing factor (R4).

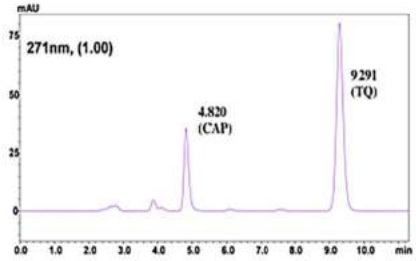

element. For CAP a slight change in the injection volume (B) and a major change in the percent ACN concentration (D) has a substantial impact on retention time, according to the perturbation chart. According to Figures 5 and 6, there was a decrease in Rt with an increase in D was observed. For TQ only, a change in B showed a major positive change in the Rt time (Supplementary Figures S1 and S2). Changes in B, the mobile-phase flow rate (C) and D have a substantial impact on the peak area of CAP whereas raising B resulted in the decline of the peak area and D showed a positive impact. For TQ, D showed a negative impact on peak area and a positive impact on Tf. Column oven temperature (A) had no effect on peak area and shows a reduction in *N* with an increase in B and C for CAP, whereas, for TQ, variations in D and C showed a major effect on peak area and tailing factor and remained unaffected by B.

Tf showed a positive effect for TQ. Statistically significant quadratic effects of variables and responses were identified in robustness experiments using DoE software. The link between a response variable and predictor variables was examined

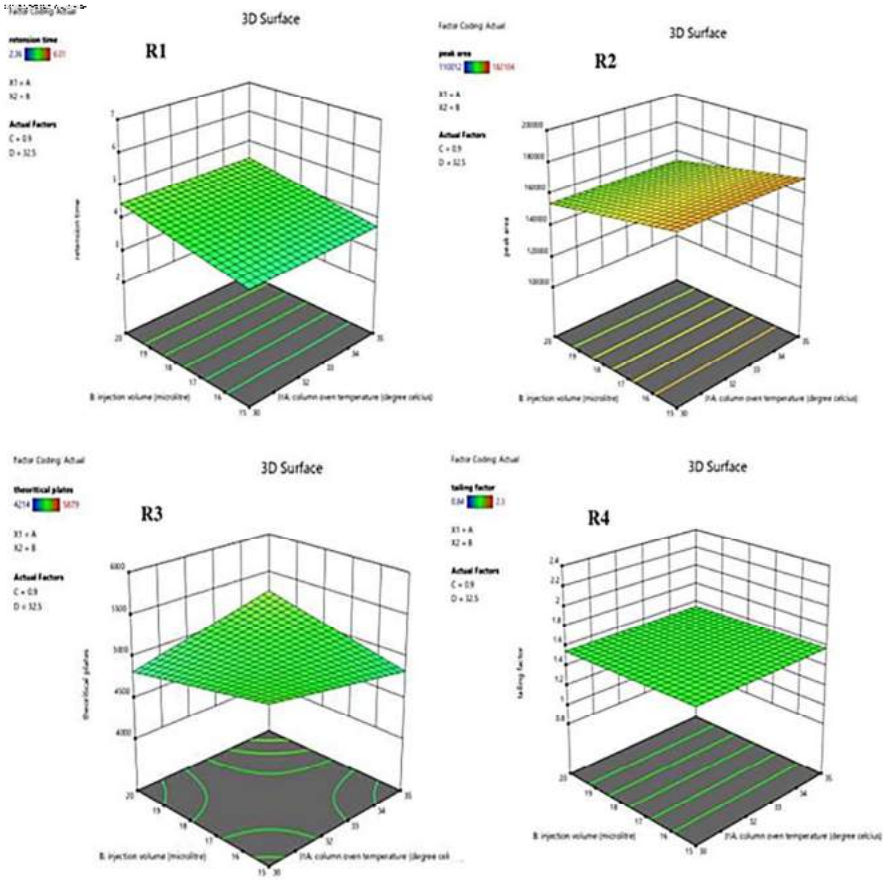

Figure 8. The 3D surface graph for CAP showing the interaction between column oven temperature (A), injection volume (B), mobile-phase flow rate (C) and % ACN (D) on retention time (R1), peak area (R2), theoretical plates (R3) and tailing factor (R4).

using a 3D Surface Plot for both CAP and TQ (Figure 8) (Supplementary Figures S3–S5). Overlay plots demonstrated data dependability by comparing a simulation-based data set to actual data from fielded products (Figure 9). DoE runs were statistically significant with R^2 near 1 and low percent relative error. The desirability ratings near one suggest that the approach is extremely reliable even when the components are out of whack (Supplementary Figure S6). Because of this, it may be used in any laboratory regularly. Using the solvent evaporation method, CAP and TQ-loaded biodegradable polymeric nanoparticles were produced, and their drug content was measured. Excipients in formulations did not

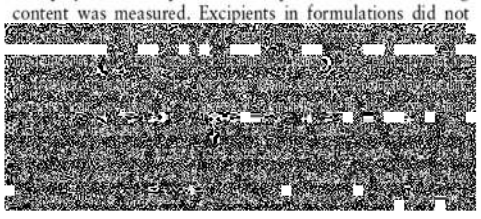

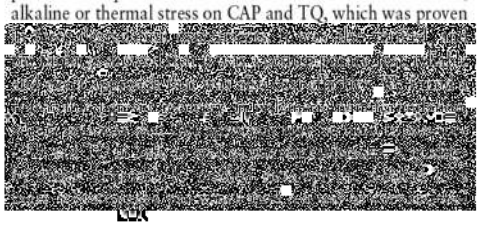

both in bulk and in nanoformulation by using the proposed method.

Conclusion

To create and refine an RP-HPLC-based analytical technique for the quantitative estimation of CAP and TQ, a 2^4 factorial design was employed. As a result of the ANOVA, the effects of independent variables were analyzed and recorded using perturbation plots and Pareto charts. There was no acidic, alkaline or thermal stress on CAP and TQ, which was proven

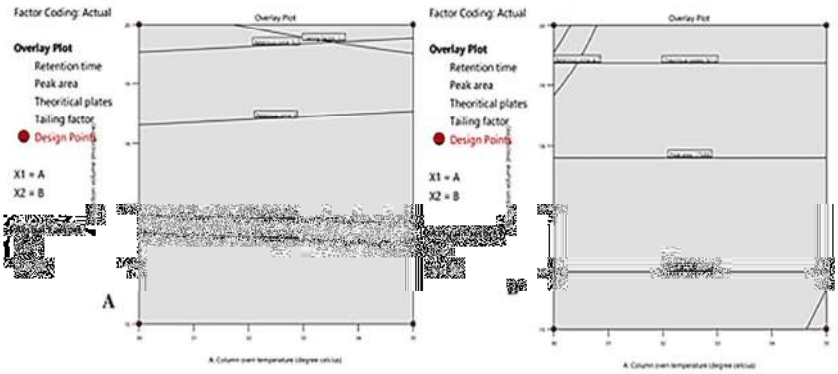

Figure 9. Overlay plots for TQ (A) and CAP (B).

approach due to the emphasis on risk assessment and management. Understanding dependent variables, diverse factors and their interaction effects on the replies were efficiently studied as a key component of QbD.

Acknowledgments

The authors are grateful for the infrastructural and financial assistance provided by the KLE Academy of Higher Education and Research, KLE College of Pharmacy, Belagavi, and KLE's Dr Prabhakar Kore Basic Science Research Centre.

Supplementary data

Supplementary data are available at *Journal of Chromatographic Science* online.

Funding

None

Conflict of interest statement. No competing interest by the authors to declare.

References

1. Rawla, P., Sunkara, T., Barsouk, A.; Epidemiology of colorectal cancer: Incidence, mortality, survival, and risk factors; *Przeglad Gastroenterol.*, (2019); **14**(2): 89.
2. Krasteva, N., Georgieva, M.; Promising therapeutic strategies for colorectal cancer treatment based on nanomaterials; *Pharmaceutics.*, (2022); **14**(6): 1213.
3. Brar, B., Ranjan, K., Palria, A., Kumar, R., Ghosh, M., Sihag, S., *et al.*; Nanotechnology in colorectal cancer for precision diagnosis and therapy; *Front. Nanotechnol.*, (2021); **3**: 699266.
4. Liu, Z., Robinson, J.T., Sun, X., Dai, H.; PEGylated Nanographene oxide for delivery of water-insoluble cancer drugs; *J. Am. Chem. Soc.*, (2008); **130**: 10876–10877.
5. Ghanavi, Z., Velayati, Ú.A., Farnia, P., Naji, A.M., Kalatehjari, S.; Extraction and purification of anticancer thymoquinone from seeds of Nigella sativa by preparative high-performance liquid chromatography; *J. Med. Plants –Prod*, (2020); **9**(Special): 73–79.
6. Habib, N., Choudhry, S.H.P.L.C.; Quantification of Thymoquinone extracted from Nigella sativa L.(Ranunculaceae) seeds and antibacterial activity of its extracts against bacillus species; *Evid. Based Complementary Altern. Med.*, (2021); **2021**: 1–11.
7. Jayaseelan, S., Bajivali, S.K., Ramesh, U., Sekar, V., Perumal, P.; Bioanalytical method development and validation of Capecitabine by RP-HPLC method; *Int. J. Chem. Tech. Res*, (2010); **2**: 2086–2090.
8. Ye, C., Liu, J., Ren, F., Okafo, N.; Design of experiment and data analysis by JMPÒ (SAS institute) in analytical method validation; *J. Pharmaceut. Biomed.*, (2000); **23**: 581–589.
9. EMA. The international conference on harmonization ICH technical requirements for registration of pharmaceuticals for human use on pharmaceutical quality system Q10. (2008) (accessed October 7, 2021).
10. Kumar, L., Reddy, S., Manuguli, R., Pai, G.; Full factorial design for optimization, development and validation of HPLC method to determine valsartan in nanoparticles; *Saudi Pharmaceutical Journal.*, (2015); **23**: 249–555.
11. Patel, K.Y., Dedania, Z.R., Dedania, R.R., *et al.*; QbD approach to HPLC method development and validation of ceftriaxone sodium; *Futur J Pharm Sci.*, (2021); **7**: 141.
12. Borman, P., Nethercote, P., Chatfield, M., Thompson, D., Truman, K.; The application of quality by design to analytical methods; *Pharm Tech.*, (2007); **31**: 142–152.
13. Schweitzer, M., Pohl, M., Hanna, B.M., Nethercote, P., Borman, P., Hansen, G., *et al.*; Implications and opportunities of applying QbD principles to analytical measurements; *Pharm Tech.*, (2010); **34**: 52–59.
14. Bhatt, D., Rane, S.; QbD approach to analytical RP-HPLC method development and its validation; *Int. J. Pharm. Pharm. Sci.*, (2011); **3**: 79–187.
15. Harini, U., Pawar, A.; Validated UV and visible spectrophotometric method for the estimation of Capecitabine–a cancer drug; *Der Pharmacia Lettre*, (2016); **8**(13): 11–16.
16. Ravisankar, P., Devala Rao, G., Naveen Kumar, M., Krishna Chaitanya, M.; An improved RP-HPLC method for the quantitative determination of Capecitabine in bulk and pharmaceutical tablet dosage form; *Pharmacia. Lettre*, (2013); **5**: 249–260.
17. Karajgi, S.R., Somashekhar, M., Chincholi, P., Deginal, L.S., Bhouramma, M., Mirji, P., *et al.*; Novel validated method for the estimation of Capecitabine in pharmaceutical dosage forms by first order derivative spectrophotometry; *Res. J. Pharm. Technol.*, (2021); **14**(10): 5238–5241.
18. Aboul-Enein, H.Y., Abou-Basha, L.I.; Simple HPLC method for the determination of Thymoquinone in black seed oil (Nigella sativa Linn); *J. Liq. Chromatogr. Relat. Technol.*, (1995); **18**(5): 895–902.
19. Taleuzzaman, M., Imam, S.S., Gilani, S.J.; Quantitative determination of thymoquinone in Nigella sativa and its Nano formulation using validated stability indicating HPTLC Densiometric method; *Int. Curr. Pharm. J.*, (2017); **6**(10): 53–60.

20. ICH. Validation of analytical procedures: text and methodology Q2 (R1) (2005) (accessed October 7, 2021).
21. Ganorkar, S.B., Shirkhedkar, A.A.; Design of Experiments in liquid chromatography (HPLC) analysis of pharmaceuticals: Analytics, applications, implications and future prospects; *Rev. Anal. Chem.*, (2017); **36**(3): 20160025.
22. Bhatia, M.S., Raut, J.N., Barve, A.C., Patil, P.S., Jadhav, S.D.; HPLC assay method development and validation for quantification of Capecitabine in tablets and forced degradation samples; *Marmara Pharm. J.*, (2017); **21**(3): 660–668.
23. Mondal, S., Narendra, R., Ghosh, D., Ganapaty, S.; Development and validation of RP-HPLC and UV spectrophotometric methods for the quantification of Capecitabine. In *International Conference on Harmonization guidelines Q2 (R1)*; (2016); **17**, p. 25.
24. Kurangi, B., Jalalpure, S.; A validated stability-indicating RP-HPLC method for Piperine estimation in black pepper; *Marketed Formulation and Nanoparticles; Ijper*, (2020); **54**(3): 677–686.
25. Ahmad, A., Khan, R.M.A., Alkharfy, K.M.; Development and validation of RP-HPLC method for simultaneous estimation of Glibenclamide and Thymoquinone in rat plasma and its application to pharmacokinetics; *Acta Chromatographica*, (2015); **27**(3): 435–448.
26. Barth, H.; Chromatography fundamentals, part V: Theoretical plates: Significance, properties, and uses. In *LCGC north America Chiral separations by chromatography online*, 1st ed, Chapter 4 ed. Intellisphere, LLC, NJ, USA, (2018), pp. 830–835.
27. Kumar, S., Lather, V., Pandita, D.; Stability indicating simplified HPLC method for simultaneous analysis of resveratrol and quercetin in nanoparticles and human plasma; *Food Chemistry*, (2016); **197**: 959–964.
28. Tirumalasetty, N., Ramchandran, D.; New stability indicating method development and validation of Capecitabine and docetaxel in bulk and pharmaceutical dosage form by using RP-HPLC; *Int. J. Appl. Pharm.*, (2021); **13**: 177–182.
29. Little, T.; *Method validation essentials, limit of blank, limit of detection, and limit of quantitation*. BioPharm International, Iselin, NJ 08830, (2015).
30. Christian, J.R., Patel, K.G.; Validation and experimental design assisted robustness testing of RPLC method for the simultaneous analysis of Brinzolamide and Brimonidine tartrate in an ophthalmic dosage form; *Indian J. Pharm. Sci.*, (2016); 78(5): 631–640.
31. Khaledi, S., Jafari, S., Hamidi, S., Molavi, O., Davaran, S.; Preparation and characterization of PLGA-PEG-PLGA polymeric nanoparticles for co-delivery of 5-fluorouracil and Chrysin; *J. Biomater. Sci. Polym. Ed.*, (2020); **31**(9): 1107–1126.
32. Sun, S.-B., Liu, P., Shao, F.-M., Miao, Q.-L.; Formulation and evaluation of PLGA nanoparticles loaded Capecitabine for prostate cancer; *Int. J. Clin. Exp. Med.*, (2015); **8**(10): 19670.

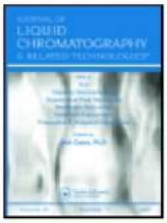

Taylor & Francis

Journal of Liquid Chromatography & Related Technologies

ISSN: (Print) (Online) Journal homepage: https://www.tandfonline.com/loi/ljlc20

[redacted]

Published online: 01 Mar 2023.

Submit your article to this journal

View related articles

View Crossmark data

[redacted]

JOURNAL OF LIQUID CHROMATOGRAPHY & RELATED TECHNOLOGIES
https://doi.org/10.1080/10826076.2023.2183867

An HP-TLC densitometric method and fingerprinting for estimating capecitabine and thymoquinone simultaneously and its application in nanoscience using Box–Behnken design

Prasiddhi Raikar[a,b], P. M. Dandagi[a], and Amruta Balekundri[a]

[a]KLE's College of Pharmacy, KLE Academy of Higher Education and Research (KLE University), Belagavi, India; [b]KAHER's Dr. Prabhakar Kore Basic Science Research Center [BSRC], KLE Academy of Higher Education and Research (KLE University), Belagavi, India

ABSTRACT

World Health Organization estimates that 10% of medications are of inferior quality, thus dangerous to human health. One way to avoid such a problem is to create an adequate, economical, and competitive analytical system. As a result, the study's goal is to create a High-Performance Thin Layer Chromatography (HP-TLC) method for determining capecitabine (CAP) and thymoquinone (TQ) simultaneously. To the best of our knowledge, no such method for determining CAP and TQ simultaneously exists today. The method was created by implementing an analytical quality-by-design approach based on the Box–Behnken design (BBD) to optimize the chromatographic conditions and a combination of factors such as toluene volume (A), solvent front (B), and chamber saturation time (C), all of which were likely to affect the R_f of CAP and TQ, respectively, later validated using TLC-silica coated plate 60 F_{254}. The validated parameters were within an acceptable range, according to ICH guidelines. BBD design revealed that the volume of toluene and solvent front had a greater effect on all of the responses studied and thus needs to be controlled. The developed method of the analysis was found to be facile, dependable, expeditious, cost-effective, and could be used to quantify CAP and TQ in Nanoformulation.

KEYWORDS

Box–Behnken design; capecitabine; densitometry; HP-TLC; nanoformulation; thymoquinone

GRAPHICAL ABSTRACT

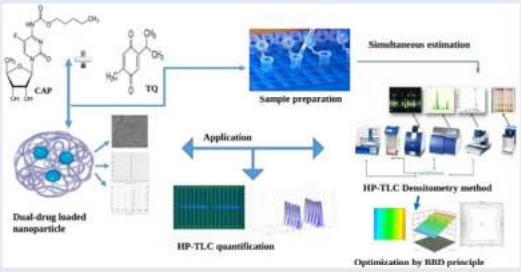

RESEARCH HIGHLIGHTS

- To determine both the drugs in nanoformulation, an accelerated and expeditious densiometric HP-TLC method was developed and validated.
- Particle size, zeta potential, entrapment efficiency (EE), Scanning Electron Microscopy (SEM), and Transmission Electron Microscopy (TEM) analysis were all performed on the prepared nanoformulation.
- According to ICH guidelines, the developed method has been tested for linearity, range, detection limit, quantification limit, precision, and robustness.
- A review of the literature reveals that there are several methods for determining CAP and TQ individually but no HP-TLC method has been reported for simultaneous estimation of CAP and TQ in the combined dosage form.
- Changes in mobile phase volume and changes in chamber saturation duration showed percent RSD-within the 2% criterion, confirming the robustness of the developed method.

CONTACT Prasiddhi Raikar prasiddhiraikar07@gmail.com KLE's College of Pharmacy, KLE Academy of Higher Education and Research (KLE University), Belagavi, Karnataka, India

Introduction

Colorectal cancer (CRC), which arises from the inner wall of the colorectal epithelium, is the third-most-common malignant tumor affecting people worldwide despite diagnosis and treatment. Colorectal adenomas and invasive adenocarcinomas develop as a result of a series of genetic and epigenetic changes in the normal colonic epithelium. New screening methods with higher accuracy are required to reduce the mortality burden of colorectal cancer. Medication resistance limits the use of cytotoxic medication, which has negative side effects.[1] Nanoparticle-based formulations may help to detect cancer earlier and overcome limitations such as hydrophobic nature, poor biodistribution, and thus low therapeutic index.

[redacted]

pletely absorbed after oral administration and acts on 5flurouracil metabolism within human cancer cells.[2]

Thymoquinone (TQ) is a naturally occurring bioactive constituent derived from Nigella sativa black seed oil. Thymoquinone, the plant's main constituent, has antitumor, anti-inflammatory, analgesic, antihypertensive, antidiabetic, antiulcerogenic, respiratory stimulation, antibacterial, and antifungal properties.[3] Thymoquinone is thought to induce apoptosis in tumor cells by suppressing the NF-jB and may be useful as an adjunct to standard chemotherapeutics.[4] However, synergistic combination co-delivery leads to improved target selectivity, minimizing drug resistance with overall therapeutic benefit.[5] As a result, the primary goal of

[redacted]

methods for determining CAP and TQ individually (Figure 1), but no HP-TLC method has been reported for simultaneous estimation of CAP and TQ in the combined dosage form, which is the research gap to be studied. As a result, the study's purpose was to create a facile and robust HP-TLC method for estimating CAP and TQ in nanoformulation. This two-drug combination might have a synergistic effect on metabolism and pharmacokinetics. When compared to other analytical methods for determining drugs in polymeric nanoparticles, HP-TLC methods are best as the samples can be analyzed quickly and at a low cost. The developed HP-TLC method may have several benefits in terms of cost, accuracy, and analysis run time. Therefore, to ensure medication quality, the newly validated method can be used in laboratory tasks to estimate medicines that contain CAP and TQ simultaneously as active ingredients. The specific method was optimized and validated following ICH guidelines.[6] These findings prompted the development of an HP-TLC method for determining CAP and TQ in very low concentrations.

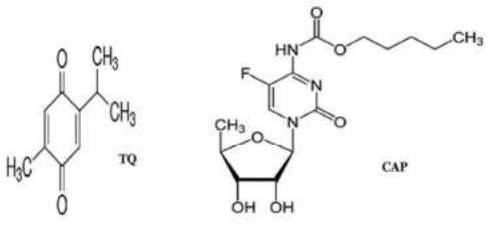

Figure 1. Structures of TQ and CAP.

Materials and methods

Materials

Sigma Aldrich provided CAP (95%) and TQ (95%). Merck in Mumbai, India, supplied the Toluene and Methanol. Poly

[redacted]

throughout the study.

Instrumentation

Camag® TLC scanner with linomat 5 (Switzerland) and vision CATS version 3 software (Camag, Switzerland) were used. The following specifications were taken into account: slit dimensions of 4 mm and 0.45 mm, a scanning speed of 20 mm/s, deuterium lamp as a radiation source, absorbance mode as scan mode, and chromatogram and integrated peak area as output. TLC tank (26.5 cm height, 27 cm width, and 7 cm diameter; Camag, Switzerland), 20 × 10 cm pre-coated silica gel aluminum plates (60 F_{254}, 0.1 mm thickness; E. Merck, Darmstadt, Germany), and TLC Hamilton® glass

[redacted]

a maximum speed of 5000 rpm (Sigma 3-30K, Spin control Comfort, Germany), and a sonicator (Bransonic ultrasonic corporation, USA) were used.

Synthesis of dual drug-loaded PLGA NPs

An innovative simple thin-film hydration method was used to create CAP and TQ-loaded PLGA NPs. In a clean and dry round bottom flask, the drug, PLGA, and Pluronic were dissolved in 20 mL of acetonitrile (ACN). The organic solvent was then removed using a rotator evaporator.[7] After solvent evaporation, the thin film was hydrated with phosphate buffer (pH 7.4). Filtration through Whatman® filter paper No 41 (pore size of 20–25 µm) removed the non-encapsulated drug.

Nanoparticle characterization

Zeta potential, mean particle size, and size morphology

The size and zeta potential were determined using the Malvern Instruments Zetasizer (UK). SEM and HR-TEM analysis were used to image and confirm the size of the PLGA nanoparticles, as well as to better understand their morphology.

% Drug loading capacity (DLC) and % encapsulation efficiency (EE)

PLGA-NPs were diluted with 1.0 mL of ACN, then bath sonicated for 10 min before being centrifuged at 5000 rpm for 10 min.[8] RP-HPLC Shimadzu Prominence HPLC-20 AT system (Shimadzu, Kyoto, Japan) was used to analyze the supernatant solution. The following equation was used to calculate % EE and % DLC.[9]

$$\%\ encapsulation\ efficiency = \frac{Amount\ of\ drug\ loaded\ in\ NPs}{Amount\ of\ initial\ drug\ taken} \times 100$$

$$\%\ Drug\ loading = \frac{Amount\ of\ drug\ loaded\ in\ NPs}{Total\ amount\ of\ NPs} \times 100$$

Preparation of standard solutions and samples

The standard was 10 mg of CAP and TQ each, and the sample was CAP and TQ-loaded PLGA NPs. Both were precisely weighed before being transferred into two separate volumetric flasks of 10 mL each, with methanol serving as the solvent. To achieve complete drug dissolution, for 15 min solutions were placed in an ultrasonic bath and then filtered through a 45 µm membrane before analysis. Working solutions were prepared from stock by diluting with methanol to achieve a working standard of 10 µg/mL of std drugs and drug-loaded NPs as samples.[10]

Method development using HP-TLC chromatography

Reference standard solutions of CAP and TQ in various concentrations were made and spotted as bands on a 60 F_{254}, plate using a Camag Linomat 5 sample applicator with a bandwidth of 8 mm and a micro syringe. For plate development, a twin trough glass chamber was used. Before developing the plate in the chamber, the mobile phase was

pletely dry, it is analyzed using the TLC scanner 4 and the chromatograms were used to interpret the results.[11] UV-Range Scanners are used to identify the spectra.

Chromatographic conditions optimization making use of BBD

A multivariate approach with an experimental design is used to investigate the concurrent variation effect of the factors on the responses. Response surface design is the best experimental design approach for modeling and optimization. BBD was used in the current study to optimize the method's chromatographic conditions BBD was selected. Because of

well as at least one center point run. Preliminary experiments were used to select the key factors for optimization. The preliminary study discovered that changes in various chromatographic conditions, such as toluene volume, solvent front, and chamber saturation time, affect the R_f value of compounds. As a result, these variables were identified as critical parameters influencing the R_f values of the markers. The optimization factors chosen were mobile phase composition (volume of toluene) (A), solvent front (B), and chamber saturation time (C). As shown in Table 1, the R_f value of CAP and TQ were chosen as responses. These three factors, A, B, and C, had nominal values of 7 mL, 80 mm, and 20 min, respectively. In this context, the volume of toluene (A) was kept between 6 and 8 mL. Similarly, the minimum and maximum solvent front (B) values were set to 75 and 85 mm, respectively. Similarly, the minimum and maximum levels for chamber saturation time were set to 15 and 25 min, respectively.[12]

Validation of analytical methods

The analytical methodology was validated following ICH Q2 (R1). Linearity, Precision, range, detection limit, robustness, and quantification limit were all validated.[13,14]

Linearity and range

The standard's range is determined by experimenting with various concentrations of samples; the range chosen is determined by the reference's linearity curve. The wavelength is chosen to perform the parameters at the chosen wavelength.

Precision

The method's system precision was determined by performing intra-day where the same procedure is carried out three

measurements, which according to ICH guidelines should be < 2%.

Specificity

The nanoformulation and standard are applied to the plate and allowed to develop in the specificity parameter. The chromatograms from the developed plates are scanned and compared for overlapping and the R_f value.

Limit of detection

The following formula is used to calculate LOD based on the slope calculated using linearity and standard deviation.

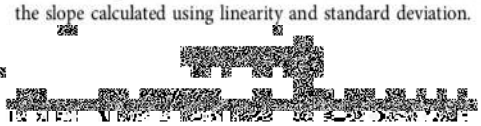

Table 1. Design matrix for the Box–Behnken concept.

Run	Factor 1 A: Volume of toluene (mL)	Factor 2 B: Solvent front (mm)	Factor 3 C: Saturation chamber time (min)	Response 1 R_f of CAP	Response 2 R_f of TQ
1	7	80	25	0.52	0.85
17	8	75	25	0.54	0.83

Limit of quantification

The formula used to find the LOQ parameter is calculated in the same way that it is influenced by the slope and standard deviation. $LOQ = 10 \times \frac{\sigma}{S}$.

Robustness

Minor changes in chromatographic conditions such as altering mobile phase ratio, composition, and duration of chamber saturation were used to evaluate the method.

Quantification

To quantify the CAP and TQ-loaded PLGA NPs, a stock solution with a concentration of 10 µg/mL with 3 L volume was prepared and the procedure was repeated three times.

Results

Nanoparticle characterization

Thin-film hydration was used to develop dual drug-loaded PLGA NPs. Mean particle size and zeta potential were found to be 200 nm and −30.12 mv respectively. The results of the characterization are shown in supplementary table 1 and supplementary figure 1.

Method development

Spectra were obtained after scanning the standards. Following several trials, the HP-TLC method was developed with the solvent system. After many trials, the mobile phase was finalized to toluene: methanol in the ratio 7.5:2.5 v/v, which demonstrated improved separation of the sample, reference, and spectra; as shown in Figure 2.

Chromatographic conditions optimization using BBD

BBD was chosen because of its flexibility, and it can be used to optimize HPTLC separation by better understanding the factor's main and interaction effects. The toluene volume (A), solvent front (B), and chamber saturation time were chosen as optimization factors (C). As responses, the R_f values of the CAP and TQ respectively were chosen. The p-value of the model is less than 0.05, demonstrating that the effect of factors is significant for responses (retention factor of CAP and TQ). As shown in Table 2, all of these parameters were within acceptable limits in the current study.

For a better understanding of the results, the predicted models are presented as perturbation plots (Figure 3) which show how the response changes as each factor move away from its defined reference value, while all other factors remain constant. A contour plot was used to examine the relationship between a response variable and predictor and a desirability rating near 1 indicates that the approach is extremely reliable (Supplementary Figure 2). 3D plots showing the effect of A, B, and C on Response 1 and Response 2 are provided in Supplementary Figure 3. The results of optimization using graphical and numerical methods are the same, indicating that the optimized method based on the BBD principle is accurate (Figure 4). Predicted response models and statistical parameters with the lowest predicted residual error sum of squares (PRESS) value are shown in Table 3. As a result, it can be used in any laboratory regularly. Hence, toluene: methanol 7.5:2.5 (v/v) was found to be a satisfactory mobile phase, with the solvent front 80 mm and chamber saturation time of 20 min as optimized chromatographic conditions.

Method validation

Linearity and range

The linearity was found to be in the 1–7 ng/band range, with a coefficient of correlation of 0.95 for CAP and 0.99 for TQ with a coefficient of variation of 0.08% and 0.01% respectively, as shown in Figure 5 and supplementary figure 4.

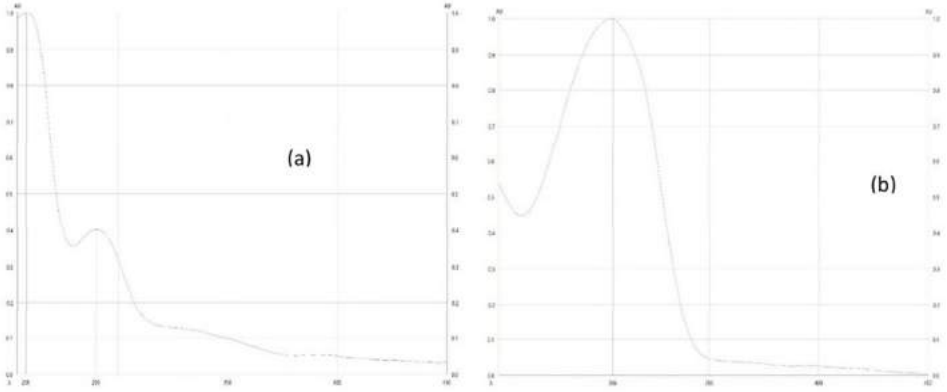

Figure 2. Spectra of (a) thymoquinone and (b) capecitabine.

Table 2. ANOVA table for Response 1 and Response 2.

Source	Sum of squares	df	Mean squares	*F*-value	*p*-Value	
Response 1						
Model	0.0047	3	0.0016	7.56	0.0035	Significant
A-volume of toluene	0.0022	1	0.0222	10.67	0.0061	Not significant
B-solvent front	0.0008	1	0.0008	3.88	0.0705	
[redacted]						
Lack of fit	0.0023	10	0.0002	1.46	0.4193	Not significant
Pure error	0.0005	3	0.0002			

Limit of detection and quantification

LOD for CAP and TQ was determined to be 0.01788 µg/band and 0.03952 µg/band respectively. After applying the formula, LOQ for CAP and TQ was determined to be 0.05419 µg/band and 0.11917 µg/band respectively.

Precision

The developed method's repeatability and intermediate precision (Table 4) were given in terms of the peak area's relative standard deviation.

Specificity

Track I-std TQ, Track II-std CAP, Track III, and IV-Nanoformulation, Track V-mobile phase, and Track VI-solvent were used for the specificity parameters application. Following the application of the specificity parameter, it was discovered that the drug standard and the nanoparticles had a similar R_f value and overlapping position. The chromatograms for the standard and dual drug-loaded polymeric nanoparticles are shown in Figure 6.

Robustness

Following the execution of this parameter, it was discovered that alterations in the composition of the mobile phase showed percent RSD of 0.3998% and 0.2331% for CAP and TQ respectively. Changes in mobile phase volume and changes in chamber saturation duration showed percent RSD—within the 2% criterion, confirming the robustness of the developed method (Table 5 and Figure 7). Track I used TQ, track II used CAP, and tracks III and IV used CAP and TQ-loaded nanoformulation. The R_f values for CAP and TQ were discovered to be 0.52 and 0.86, respectively, and the same data could be reproduced in the CAP and TQ-loaded nanoformulation.

Quantification

The quantification of the drug-loaded PLGA NPs was done in triplicate. Table 6 displays the information. The obtained results' mean and standard deviation were also computed.

Discussion

The thin-film rehydration method is one of the most effective methods for producing PLGA NPs. The nanoparticles

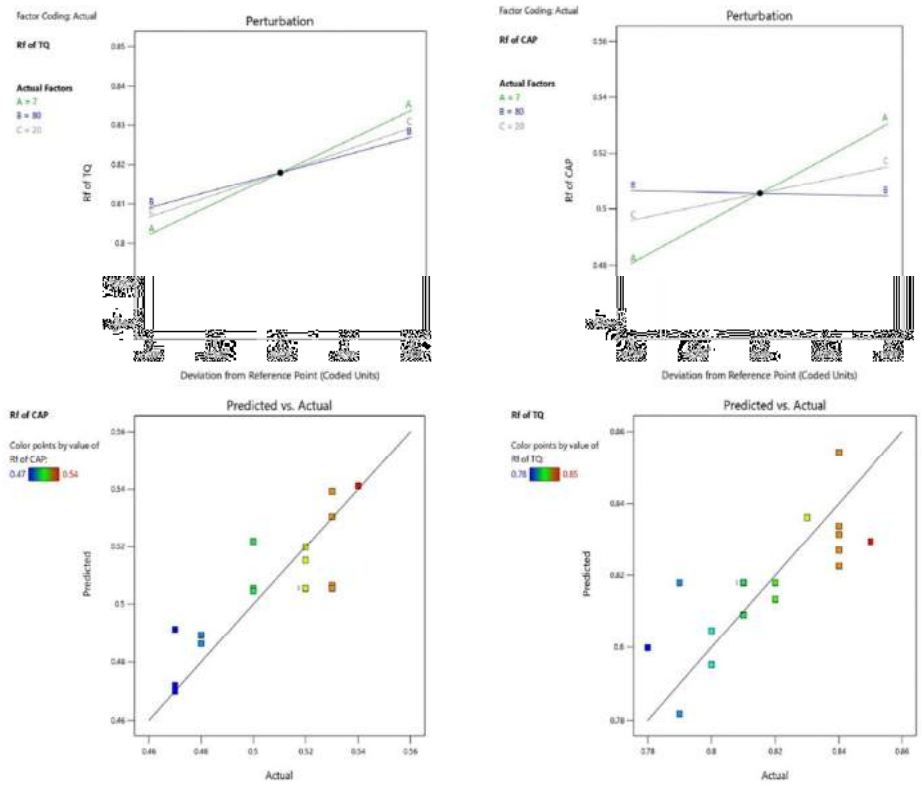

Figure 3. Perturbation and prediction graphs showing the effect of each factor A, B, and C on Response 1 (R_f value of CAP) and Response 2 (R_f value of TQ).

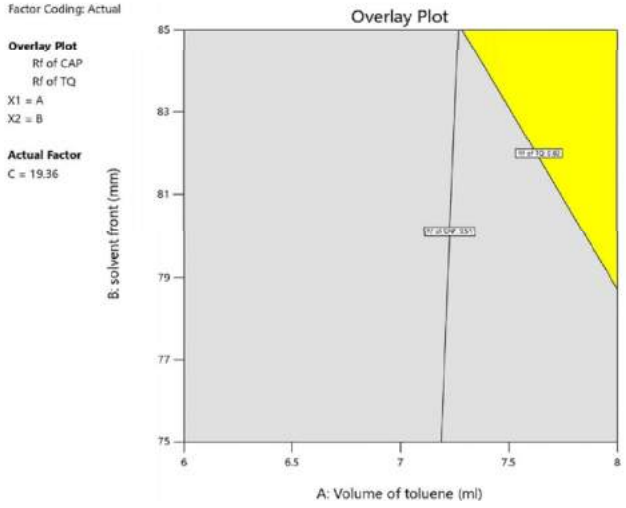

Figure 4. Graphical optimization using overlay plot.

Table 3. ANOVA yielded predicted response models and statistical parameters.

Response	Polynomial equation	Model	*p*-Value	PRESS	Coeffient of variation (% CV)	Standard deviation
Response 1 (R_f of CAP)	$+0.5056 + 0.0249A - 0.0010B + 0.0097C$	Linear	0.0008	0.0047	2.89	0.01
Response 2 (R_f of TQ)	$0.8180 + 0.0158A + 0.0090B + 0.0114C$	Linear	0.0035	0.0047	1.77	0.01

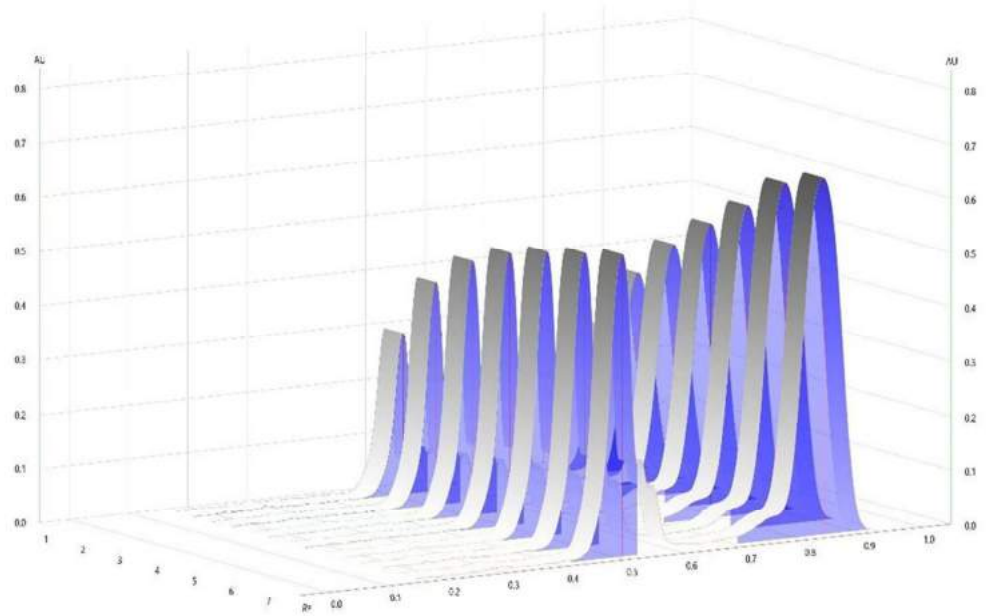

Figure 5. Linearity graph for CAP and TQ.

Table 4. Intraday and Interday precision study.

Drug	Peak area	R_f value
Intraday precision		
CAP	0.0192	0.5210

are stabilized in aqueous media using amphiphilic surfactant molecules. All experiments were carried out in a randomized order to reduce the effects of uncontrolled variables, which could introduce bias into the measurements. Furthermore,

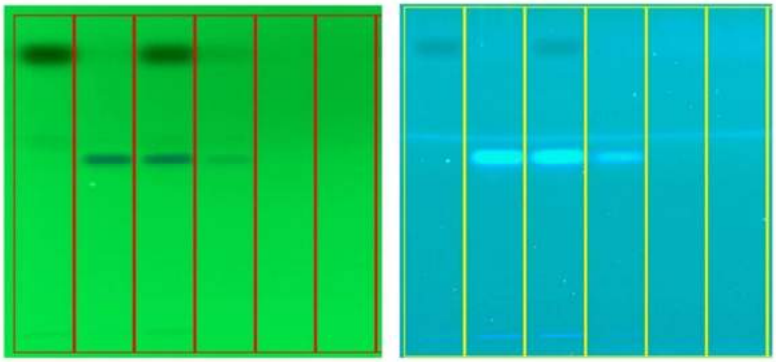

Figure 6. Specificity plates.

Table 5. Robustness study.

		Chromatography-incorporated modifications	
		R_f value	
Factors	Level	CAP	TQ
Mobile phase composition (Toluene: methanol)	±0.1 mL		
7.6	+0.1	0.523	0.856
20	0	0.523	0.862
16	−20	0.518	0.860
% RSD		0.5078	0.2325

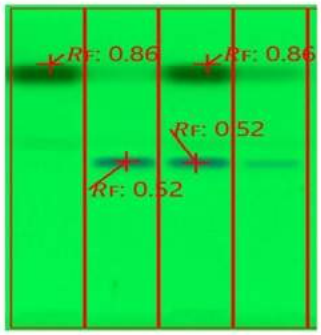

Figure 7. R_f values for validated method.

Table 6. Drug-loaded PLGA NPs quantification.

	Quantification	
Trials	CAP (µg/mL)	TQ (µg/mL)
1	98.720	82.250
2	98.740	82.210
3	98.740	82.260
Mean ± SD	98.733 ± 0.011	82.240 ± 0.026

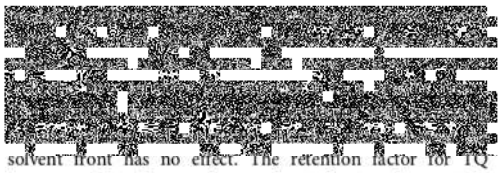

solvent front has no effect. The retention factor for TQ increases with toluene volume, solvent front, and saturation chamber time.

At 254 nm, the method was developed and the chosen mobile phase was validated for the following parameters. Linearity, precision, range, robustness, the limit of detection, and the limit of quantification were all used to validate the newly developed method, adhering to the ICH Q2(R1) guidelines and according to the results, all of the parameters were found to be within the range and were correctly validated.

Conclusion

The volume of toluene, solvent front, and chamber saturation time were all optimized at the same time using BBD response surface design tools, implementing quality by design principles and it was discovered that the volume of toluene and chamber saturation time had the greatest effect on all of the responses studied and thus needs to be controlled. According to the acceptance criteria for chromato-

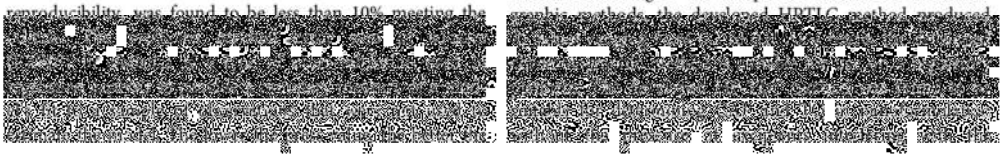

results. The method is also robust, specific, simple, easy, and precise, according to statistical data obtained during validation. It is concluded that using an experimental design-making approach is a flexible procedure capable of reducing the number of experiments. As a result, this HP-TLC method offers several advantages in terms of analysis run time, precision, cost, and robustness. Hence, the newly validated method can be used in laboratory tasks for medicines containing CAP and TQ as active ingredients to ensure medication quality.

Acknowledgments

The authors would also like to thank the director of the Analytical Laboratory at KAHER's BSRC in Belagavi, Karnataka, India, for providing the facilities needed to complete this study.

Disclosure statement

No potential conflict of interest was reported by the author(s).

ORCID

Prasiddhi Raikar http://orcid.org/0000-0002-3057-5126

References

[1] Al-Joufi, F. A.; Setia, A.; Salem-Bekhit, M. M.; Sahu, R. K.; Alqahtani, F. Y.; Widyowati, R.; Aleanizy, F. S. Molecular Pathogenesis of Colorectal Cancer with an Emphasis on Recent Advances in Biomarkers, as Well as Nanotechnology-Based Diagnostic and Therapeutic Approaches. *Nanomaterials* **2022**, *12*, 169. DOI: 10.3390/nano12010169.

[2] Walko, C. M.; Lindley, C. Capecitabine: A Review. *Clin. Ther.* **2005**, *27*, 23–44. DOI: 10.1016/j.clinthera.2005.01.005.

[3] Khader, M.; Eckl, P. M. Thymoquinone: An Emerging Natural Drug with a Wide Range of Medical Applications. *Iran. J. Basic Med. Sci.* **2014**, *17*, 950. DOI: 10.3390/nu14245240.

[4] Ahmad, A.; Husain, A.; Mujeeb, M.; Khan, S. A.; Najmi, A. K.; Siddique, N. A.; Damanhouri, Z. A.; Anwar, F. *A Review on Therapeutic Potential of Nigella Sativa: A Miracle Herb. Asian Pac. J. Trop. Biomed.* **2013**, *3*, 337–352. DOI: 10.1016/S2221-1691(13)60075-1.

[5] Lehár, J.; Krueger, A. S.; Avery, W.; Heilbut, A. M.; Johansen, L. M.; Price, E. R.; Rickles, R. J.; Short, G. F.; Staunton, J. E.; Jin, X.; et al. Synergistic Drug Combinations Tend to Improve Therapeutically Relevant Selectivity. *Nat. Biotechnol.* **2009**, *27*, 659–666. DOI: 10.1093/jaoacint/qsab021.

[6] Attimarad, M.; Ahmed, K. M.; Aldhubaib, B. E.; Harsha, S. High-Performance Thin Layer Chromatography: A Powerful Analytical Technique in Pharmaceutical Drug Discovery. *Pharm. Methods* **2011**, *2*, 71–75. DOI: 10.4103/2229-4708.84436.

[7] Salama, A. H.; Mahmoud, A. A.; Kamel, R. A Novel Method for Preparing Surface-Modified Fluocinolone Acetonide Loaded PLGA Nanoparticles for Ocular Use: In Vitro and in Vivo Evaluations. *AAPS Pharmscitech* **2016**, *17*, 1159–1172. DOI: 10.1208/s12249-015-0448-0.

[8] Kumbhar, P. S.; Diwate, S. K.; Mali, U. G.; Shinde, T. U.; Disouza, J. I.; Manjappa, A. S. Development and Validation of RP-HPLC Method for Simultaneous Estimation of Docetaxel and Ritonavir in PLGA Nanoparticles. *Annales Pharmaceutiques Françaises* **2020**, *78*, 398–407. DOI: 10.10016/J.pharma.20020.07.0004.

[9] Amini, Y.; Amel Jamehdar, S.; Sadri, K.; Zare, S.; Musavi, D.; Tafaghodi, M. Different Methods to Determine the Encapsulation Efficiency of Protein in PLGA Nanoparticles. *Biomed. Mater. Eng.* **2017**, *28*, 613–620. DOI: 10.3233/BME-171705.

[10] Ibrahim, H.; Hamdy, A. M.; Merey, H. A.; Saad, A. S. Dual-Mode Gradient HPLC and TLC Densitometry Methods for the Simultaneous Determination of Paracetamol and Methionine in the Presence of Paracetamol Impurities. *J. AOAC Int.* **2021**, *104*, 975–982. DOI: 10.1093/jaoacint/qsab021.

[11] Sharma, T.; Khurana, R. K.; Borges, B.; Kaur, R.; Katare, O. P.; Singh, B. An HPTLC Densitometric Method for Simultaneous Quantification of Sorafenib Tosylate and Chrysin: Analytical Method Development, Validation and Applications. *Microchem. J.* **2021**, *162*, 105821. DOI: 10.1016/j.microc.2020.

[12] Prajapati, P.; Shah, H.; Shah, S. A. Implementation of QRM and DoE-Based Quality by Design Approach to VEER Chromatography Method for Simultaneous Estimation of Multiple Combined Dosage Forms of Paracetamol. *J. Pharm. Innov.* **2020**, *1*,1–17. DOI: 10.1007/s12247-020-09490-w.

[13] Kelani, K. M.; Hegazy, M. A.; Hassan, A. M.; Tantawy, M. A. A Green TLC Densitometric Method for the Simultaneous Detection and Quantification of Naphazoline HCl, Pheniramine Maleate along with Three Official Impurities. *BMC Chem.* **2022**, *16*, 1–11. DOI: 10.1186/s13065-022-00819-9.

[14] Kudatarkar, N.; Jalalpure, S.; Balekundri, A.; Kurangi, B. Analytical Method Development and Validation for Estimation of Chrysin in Chrysin Loaded Phytosomes Using High Performance Thin Layer Chromatography. *J. Liq. Chromatogr. Relat. Technol.* **2022**, *56*, 1–6. DOI: 10.1080/10826076.2022.2038196.

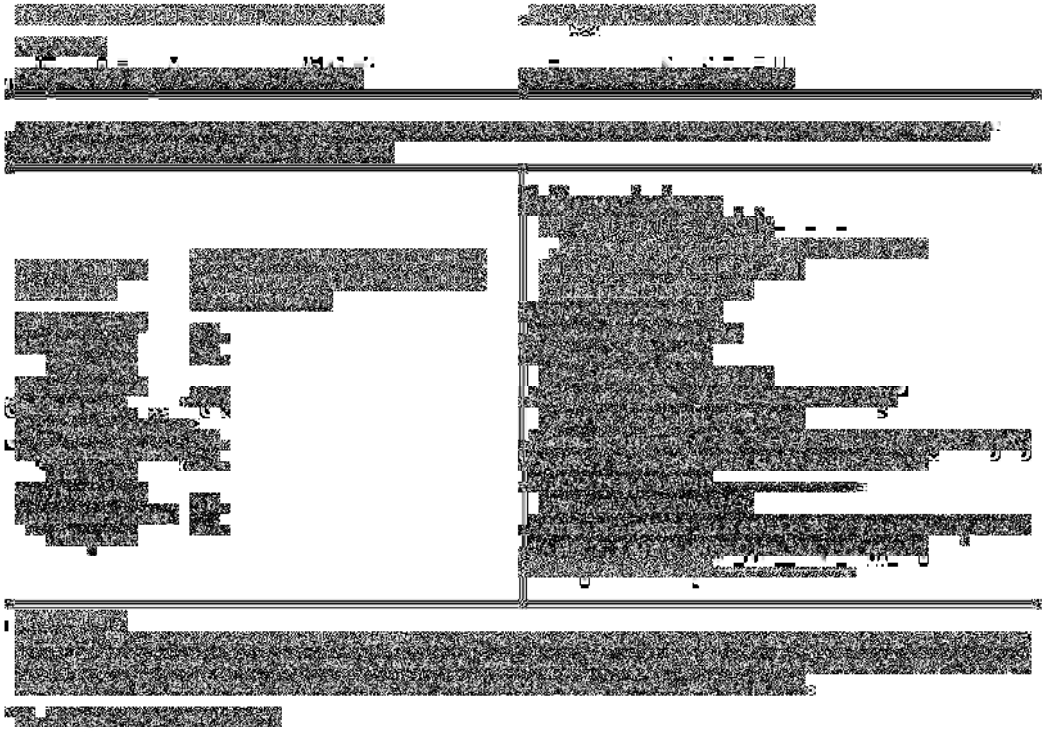

Indira Bahuuddeshiya Shikshan Sanstha, Buldana's

Dr. Rajendra Gode Institute of Pharmacy,

University-Mardi Road, Amravati (444602)

Certificate

This is to be certified that Miss. Prasiddhi Raikar From KLE college of Pharmacy, Belagavi, Presented a poster on topic Functionalized Polymeric Nanoparticles: A Novel Targeted Approach for Oncology Care in Two Days (Virtual) International Conference on, RECENT ADVANCES IN DRUG DISCOVERY (QSAR Modeling, Molecular Docking, Molecular Simulation) held at Dr. Rajendra Gode Institute of Pharmacy, Amravati on 15th and 16th Dec. 2021.

Prof. Rahul D. Jawarkar	Dr. Snehal S. Manekar	Dr. Ravindra L. Bakal
ORGANIZING SECRETARY	CO-CONVENOR	CONVENOR

International Virtual Conference on Biomaterial-Based Therapeutics, Engineering and Medicine

BIOTEM-2021

Organized by

Departments of Biotechnology, Biomedical Engineering and Chemical Engineering, **Manipal Institute of Technology, MAHE**

Under the aegis of

Society for Biomaterials & Artificial Organs India (SBAOI) and **Society for Tissue Engineering and Regenerative Medicine India (STERMI)**

Co-organized by

The American Ceramic Society (ACerS)

CERTIFICATE

This is to certify that

Prasiddhi Ratnakar Raikar

has participated and presented a poster in the

International Virtual Conference on Biomaterial-Based Therapeutics, Engineering and Medicine

held from December 17 - 20, 2021

Bikramjit Basu
President, SBAOI

Dr. Bharath Raja Guru
Convener, BIOTEM-2021

Graduate School of Pharmacy

Gujarat Technological University

&

Society of Pharmacognosy

Formerly Indian Society of Pharmacognosy

ESTD - 2007

CERTIFICATE NO.: GSPICON21OP029

CERTIFICATE OF PARTICIPATION

THIS CERTIFICATE IS BEING AWARDED TO

DR./MR./MS. **MS. PRASIDDHI RATNAKAR RAIKAR**

HAS SUCCESSFULLY PRESENTED A POSTER / ORAL ENTITLED

Formulation and evaluation of PLGA coated polymeric nanoparticles of Thymoquinone targeting colon cancer

DURING

25TH NATIONAL CONVENTION OF SOCIETY OF PHARMACOGNOSY & INTERNATIONAL CONFERENCE ON "NEW HORIZONS OF NATURAL PRODUCTS AND AYUSH REMEDIES" DURING NOVEMBER 27-28, 2021.

MS. JIGNA VADALIA	DR. SANJAY CHAUHAN	DR. UMESH PATIL	PROF. (DR.) NAVIN SHETH
Organizing Secretary, Loc & Asst. Prof., GSP- GTU	Chairman, Loc & Director GSP-GTU	General Secretory Society Of Pharmacognosy	Vice Chancellor Gtu & President Society Of Pharmacognosy